5

Inhibition of Nitric Oxide Synthase Gene Expression: *In vivo* Imaging Approaches of Nitric Oxide with Multimodal Imaging

Rakesh Sharma[1,2]
[1]*Center of Nanomagnetics and Biotechnology, Florida State University, Tallahassee, FL*
[2]*Amity Institute of Nanotechnology, Amity University, NOIDA, U.P. India*

1. Introduction

Nitric oxide is an uncharged free radical abundant in nanomolar quantities and detected by measuring nitric oxide synthase (NOS). Nitric oxide is a gas highly reactive, short lived free radical generated enzymatically by NOS involved in diverse physiological (neurotransmission, immune system) and pathophysiological (tumor progression) mechanisms. Nitric oxide is a biological mediator for its role as EDRF (endothelial-derived relaxing factor) responsible for the regulation of blood vessel relaxation and blood pressure maintenance [Labet et al. 2009]. In recent years, inhibition of NOS gene expression has become a scientific interest to measure NO in tissues and synthetic NOS/NO inhibitors have revolutionized molecular imaging of tissues. Present chapter presents a journey from major mechanistic concepts to the detection of NO, NOS and their multimodal bioimaging applications with limitations.

- Several genes involve in NOS enzyme for its synthase activity (NOS1, NOS2A, NOS3); oxidoreductase activity (NOS1, NOS2A, NOS3, NQO1); as positive regulators(HSP90AB1 or HSPCB, INS); as negative regulators (DNCL1, GLA, IL10);other AKT1, ARG2, DDAH2, DNCL1, EGFR, GCH1, GCHFR genes
- NO diffuses freely across cell membranes. It is short lived but combines with metallic aromatic ‘spin traps' to make stable compounds. NO acts in a paracrine or autocrine manner influencing only cells near its point of synthesis.
- NO is synthesized within cells by a flavocytochrome enzyme NO synthase (NOS). The human contains 3 different NO synthases:
- nNOS (NOS-1) is found in neurons (hence the "n"); iNOS (inducible NOS-2), triggered by inflammatory cytokines found in macrophages; and eNOS (NOS-3): constitutively distributed in the vascular endothelium lining the lumen of blood vessels, lung, and platelets (called constitutive NOS or *c*NOS) [Perrier, et al. 2009]. All types of NOS produce NO from arginine with the aid of molecular oxygen and NADPH as shown in following redox reaction and Figure 1. Inhibition of NOS gene expression in cells may detect NO [Nie et al.2008; Terashima et al. 2010].
- NADH-diphorase stain the NOS expression to detect NO in tissues
- NO is generated in vascular endothelium cells (NO plays role in the regulation of vascular tone), peripheral and central neurons (NO acts as synaptic neuronal

messenger) by three isoforms of NO synthase, endothelial, neuronal, and inducible form [Perrier, et al. 2009, Claudette, et al. 2005]. Detection and in vivo monitoring of NO is very difficult. Spin traps, fluorescent dyes, chemi/bioluminescent sensors detect and image NO by ESR,NMR,PET,US,and optical methods.

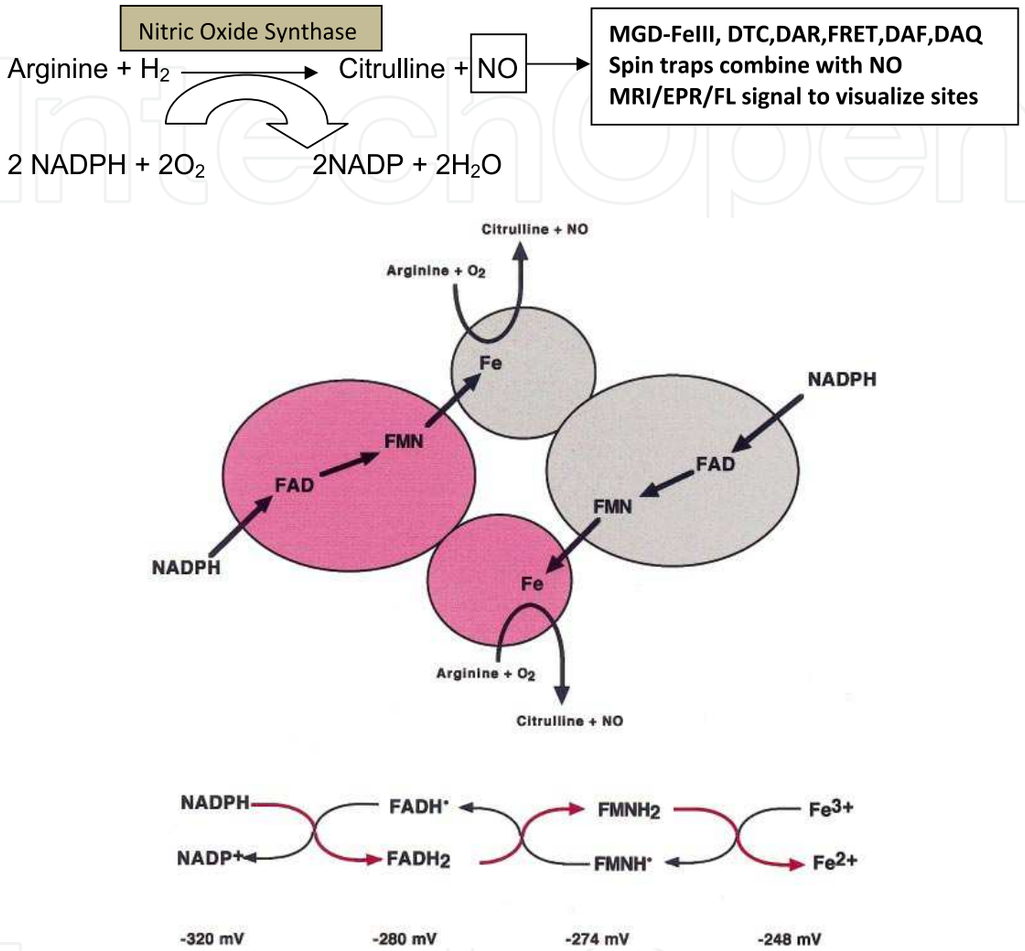

Fig. 1. Redox potentials and direction of electron flow in nNOS enzyme action are shown. The electron flow in the NOS dimer goes via NADPH→FAD→FMN in the reductase of one monomer to the haem iron in the oxygenase domain of a separate monomer. The redox potentials are poised thermodynamically to make this occur. The potentials for the two-electron oxidation of NADPH and the one-electron oxidations of $FADH_2$, $FMNH_2$ and ferric haem are illustrated at the bottom of the Scheme, with the red arrows indicating the direction of electron flow. Note that given the variety of redox couples and the closeness of the $FADH_2$ and $FMNH_2$ potentials the detailed picture is more complex than that illustrated. For example the $FMNH^+$/FMN couple has a redox potential of -49 mV and is likely to donate electrons to the high-potential ferric superoxide species to form the ferryl intermediate. Reduction of the FMN back to $FMNH^+$ would then require an electron from $FMNH^+$. Adapted from Alderton, et al. 2001.

- Mapping the distribution of NO generation or formation of stable spin-trapping species at different locations in tissues or organs by *in vivo* perfusion (**3D visualization of NO**

structural-functional or conformational dynamics as switch OFF and ON) may allow us to understand the real physiological function of NO gas or ionic form under different tissue physiological conditions [Thatte et al. 2009]. Using *in vivo* nitric oxide direct detection by stabilizing NO with suitable spin-trapping reagents is a challenge to estimate the *in vivo* NO concentration by MRI techniques [Hong et al. 2009; Sari-Sarraf, et al. 2009; Liu, et al. 2009; Ny et al. 2008; Fujii, et al, 2007; Vandsburger, et al.2007; Samouilov et al. 2007; Flögel, et al. 2007; Bobko, et al. 2005; Day, et al. 2005; Waller, et al. 2005; Sirmatel, et al. 2007; Itoh, et al. 2004; Berliner, et al. 2004; Haga,et al. 2003; Li, et al. 2003; Hsiao, et al. 2008; Kuppusamy, et al. 2001; Fichtlscherer, et al. 2000; Fujii,et al.1999; Fujii, et al. 2002].

- Other nitric oxide bioimaging technique is flourimetry using fluorescent biomarkers in EPR spectroscopy [Kojima, et al.2001; Fuji, et al.1997; Yoshimura, et al. 1996]. Our immediate focus is to highlight the existing multimodal mechanisms of NO sensitive MRI/EPR signal generation using NOS enzyme expression inhibitors and biosensors to map cellular events.

1.1 Nitric oxide as a second messenger in cellular signaling

Nitric oxide signal transduction through induced-nitric-oxide modifications relies on the system of Cys-based posttranslational modifications. Accordingly, S-nitrosylation of proteins plays an essential role in downstream cascades (Do et al., 1996). Nitric oxide exerts an ubiquitous influence on cellular signaling in large part by means of S-nitrosylation/denitrosylation of protein cysteine residues. S-NO undergo a regulated post-translational protein modification specific to NO-derived effects. These NO-dependent modifications influence protein activity, protein-protein interactions, and protein location. S-nitrosylation thus serves as the prototypical redox-based signal (Janssen-Heininger et al., 2008). S-Nitrosylation has been implicated in transmitting signals downstream of all classes of receptors, including G-protein-coupled receptor (GPCR), receptor tyrosine kinase, tumor necrosis factor, Toll-receptors, and glutaminergic receptors, acting locally within subcellular signaling domains as well conveying signals from the cell surface to intracellular compartments, including the mitochondria and the nucleus (Janssen-Heininger et al., 2008). Cell signaling through S-nitrosylation is useful tool in signaling transduction for:

1. Temporal regulation of response through a rapid and controlled stimulation;
2. The existence of motifs within proteins that provides S-nitrosylation specificity;
3. Colocalization of target proteins with a source of NO;
4. Reversibility of protein S-nitrosylation;
5. Enzymatic control of S-nitrosylation through the action of S-nitrosoglutathione reductase (Janssen-Heininger et al., 2008).

1.2 Why inhibition of NOS expression as bioimaging of NO technique

Mapping the distribution of NO generation at different locations in different tissues and organs by *in vivo* perfusion reveals the physiological function of NO (gas or ionic form) in different tissue physiological conditions [Thatte, et al.2009]. Major nitric oxide imaging techniques utilize mapping NO in tissue using NO specific imaging contrast agents sensitive to fluorescence, magnetic resonance and electron spin resonance. Imaging *in vivo* physical properties of tissue cells such as cell calcium signaling and NO-biomarker is new way by proton magnetic resonance techniques to achieve nanomolar range of nitric oxide mapping

without any toxic effects[Thatte, et al.2009, Hong et al.2009]. Fluorescent nitric oxide cheletropic traps are currently available choices in nitric oxide imaging but all of these have pitfalls of causing neurotoxicity [Reif et al.2009]. In this chapter, we display evidence of the NO sensitive fluorescent probes as cell calcium signaling indicator and possibility of NO specific perfusion MRI tool to visualize physiological nanomolar dynamics of NO in living cells and tissues up to the detection limit of 0.1 nM. The cell signaling indicators such as intracellular calcium revealed that ~1 nM of NO was enough to detect apoptosis events such as caspase 3 activation [Li et al.2009].

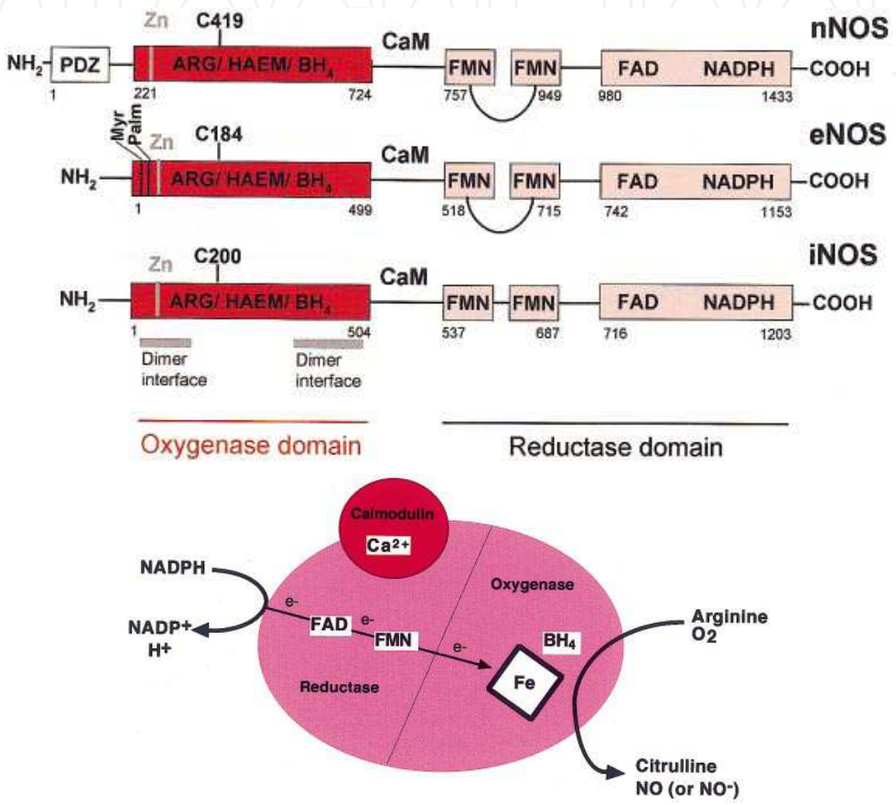

Fig. 2. Domain structure of human nNOS, eNOS and iNOS(on left), Overall reaction catalysed and cofactors of NOS(on right). Adapted from Alderton, et al. 2001.

1.2.1 Feasibility of NOS expression inhibitors as imaging Contrast Agents

NO is a gaseous and highly active neuronal messenger, short lived free radical generated enzymatically by NOS in the brain[Perrier et al.2009]. NOS is a flavocytochrome that is constitutively distributed in the vascular endothelium, brain, lung, and platelets (called constitutive NOS or *c*NOS), but is also found as an inducible form (called inducible NOS or *i*NOS) in many cells and organs, triggered by several factors such as inflammatory cytokines [Claudette et al.2009]. However, NOS is abundant in three isoforms cNOS, iNOS, eNOS as shown in Figure 2. NOS undergo dimerization in presence of BH4 or heme or arginine binding sites. Different roles of flabin, heme, pterin cofactors in NOS are described in detail [Alderton, et al. 2001, Matter et a. 2004]. Authors reviewed NOS activity regulation by calmodulin, phosphorylation, protein inhibitors of NOS(PIN), heat shock protein 90(Hsp 90),

myristoylation, palmitoylation, caveolin, at different domain located in NOS or spilce variants: nNOSβ and nNOSγ, nNOSμ, nNOS-2, iNOS/eNOS splice variants. However, cross-activities of all three isoforms of NOS and their dependence on calcium, common locations have put challenge to specificity and gave way to a new way of specific NO/NOS inhibitor compounds. In recent years, NOS gene expression and its regulation have got attention for two reasons:

- NOS gene expression can be stained, imaged for multimodal molecular imaging
- The NOS inhibitors inhibit NOS as potent anti-inflammatory agents in recent years.
- Visualization of NOS inhibition is believed to serve as in vivo or in vitro biomarkers of the proinflammatory status of NOS inhibitors or in vivo proinflammation bioimaging of tissues.

Some examples of NOS ihibitors are given below.

1.2.2 NOS Inhibitors

NOS inhibition occurs at arginine site, tetrahydrobiopterin site, pteridine site, and heme domain by partially selective or highly selective inhibitors [Alderton, et al. 2001, Matter et a. 2004]. Excellent information of binding site interactions of NOS with relationships at different sites is available [Alderton, et al. 2001, Matter et al. 2004]. To understand better the NOS inhibitor structural-activity relationship, X-Ray analysis, 3D QUSAR, comparative molecular field analysis (CoMFA) analysis, GRID/PCA interpretations have enhanced the scope of NOS in pharmacology as shown in Figures 3,4,5 [Matter et al.2004]. There are array of NOS inhibitors described in the literature as drug testing tools. Table 1 shows efficacy of some of these in inhibiting the three human NOS isoforms.. Of these the most widely used have been l-NMMA, l-NNA and its methyl ester prodrug (NG-nitro-l-arginine methyl ester, `l-NAME' and aminoguanidine. However, inhibitors show pitfalls on selectivity to NOS, types of interactions with iNOS and nNOS isoforms. **Selective** NOS inhibitors may be selective in the physiological range (l-arginine concentration etc). Inhibitor agents with 10-50-fold selectivity are useful as `partially selective inhibitors.

inhibitor	IC50 (μM)			Selectivity (fold)		
	iNOS	nNOS	eNOS	iNOS vs nNOS	iNOS vs eNOS	nNOS vs eNOS
L-NNA*	3.1	0.29	0.35	0.09	0.11	1.2
L-NMMA	6.6	4.9	3.5	0.7	0.5	0.7
7-NI*	9.7	8.3	11.8	0.9	1.2	1.4
ARL17477*	0.33	0.07	1.6	0.2	5	23.
Aminoguanidine*	31	170	330	5.5	11	1.9
L-NIL	1.6	37	49	23.	49.	1.3
1400W	0.23.	7.3	1000	32.	4000*.	130*
GW273629	8.0.	630	1000	78.	125*.	1.6*
GW274150	1.4.	145	466	104.	333	3.2

The data shown are for inhibition of the human NOS isoforms in the presence of 30 μM L-arginine at 37 °C over 15 min after a 15 min pre-incubation with inhibitor under turnover. The data serves as progressive inhibitory mechanisms for the NOS assay. Data are from Young et al. 2000.

Table 1. Selectivity of inhibitors of NOSs is compared for different inhibitors

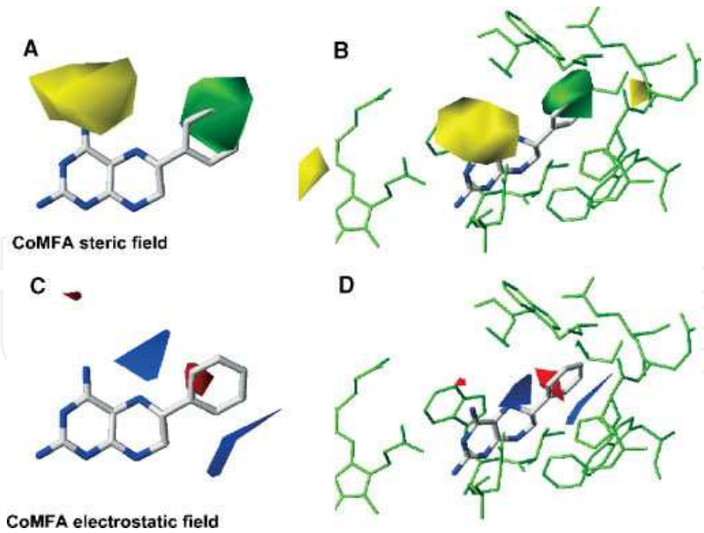

Fig. 3. Contour maps for NOS-I comparative molecular field analysis (CoMFA) analysis with a 4-amino-pteridine inhibitor.A: Steric contour map, green contours indicate sterically favored regions, yellow contours indicate unfavored areas. B: Samethan, A: with NOS-I binding site. C: Electrostatic contour map, blue contours refer to regions, where negatively charged substituents are unfavorable, red contours indicate regions, where negatively charged substituents are favorable. D: Same as C with NOS-I binding site. Reproduced with permission from Matter et al. 2004.

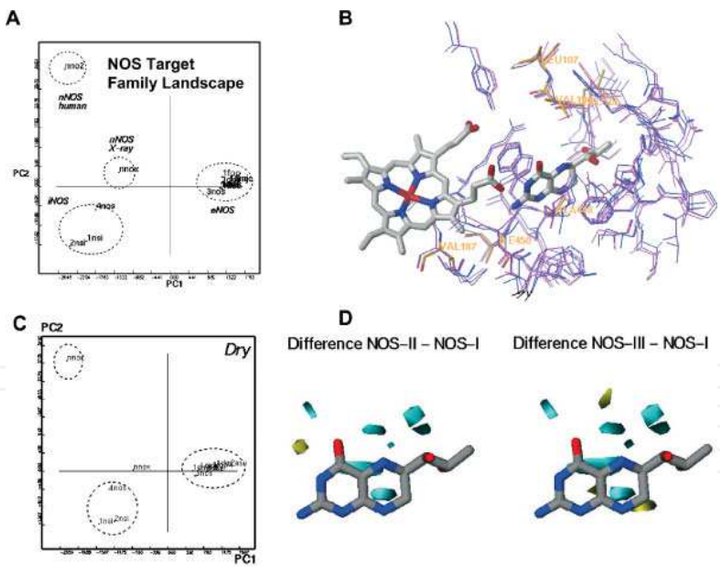

Fig. 4. A: Score plot from GRID/principal componentanalysis (PCA) based on13 conformations and 3NOS isoforms. B: SuperpositionofNOS-III (1nse, blue) toNOS-IX-ray (magenta) andhumanbrainNOS-I (homology, purple).C:Scoreplot fromGRID/CPCA for hydrophobic interactions (GRID dry probe). D:GRID/CPCA differential plots highlighting differences between NOS-I/NOS-II and NOS-I/NOS-III.Favorable interactions toachieveNOS-I isoformselectivities are shownincyancontours, unfavorable interactions are displayed in yellow with respect to H4Bipfromthe NOS-III1nse X-ray structure. Reproduced with permission from reference [Matter et al. 2004]

The mechanistic nature of three human NOS isoforms was expressed in the baculovirus expression system, and cell lysates as the enzyme source. iNOS potency and selectivity underestimates progressive inhibition of iNOS but not eNOS or nNOS; e.g. for 1400W the steady-state values of iNOS IC50 and selectivity have been estimated to be 0.1 μM, 250-fold (versus nNOS) and 5000-fold (versus eNOS) as reported by Young, et al. 2000. Highly selective compounds of over 50- or 100-fold selectivity, inhibit the NOS activity of a single isoform without affecting others. They have potential as selective therapeutic agents without side effects. Recently, 7-nitroindazole (7-NI) was reported as non selective nNOS inhibitor, of isolated NOS enzyme (Table 1). 7-NI showed inhibition of nNOS independent of increases in blood pressure but showed eNOS-dependent celltype specificity (neuronal verus endothelial), intracellular BH4 concentration, or depending on specific cellular transport or metabolism [Handy, et al. 1998]. All three NOS isoforms can be expressed in neurons and both eNOS and iNOS in endothelial cells. Cell-type specificity is clearly a very distinct phenomenon from isoform selectivity. Other pitfall is particular dose. For example, in humans, the non-selective NOS inhibitor l-NMMA causes a five-fold increase in vascular resistance with only a 10% change in blood pressure, because of reflex decreases in cardiac output 185±187 [Ross et al. 1998] Suppression of inhibitor-induced plasma nitrate (mediated predominantly by iNOS) and no effects on blood pressure has led to inhibitors as non selective, e.g. *S*-ethylisothiourea [Raman, et al. 1998]. Selectivity for iNOS versus eNOS distinct enzyme targets is another pitfall. Time-dependent NOS inhibition in assessing efficacy and selectivity of NOS inhibitors were first reviewed by Bryk and Wolff, 1999.

1.2.3 NOS inhibitor interactions with the NOS enzymes

Inhibitors of NOS have been described which interact with the NOS enzymes in a variety of ways: different sites, differing time- and substrate-dependence, and mechanism of inhibition.

L-Arginine site inhibitors identified so far as competitive with the substrate L-arginine binding at the arginine-binding site inhibitors (aminoguanidine, *S*-ethylisothiourea, thiocitrulline) [Raman, et al.1998].

Mechanism-based inhibitors of iNOS require active enzyme and NADPH substrate to permit inhibition to proceed through multiple enzyme covalent modification by a complex formation pathway: EI-EI* complex where E is iNOS, I is the inhibitor, EI is the initial non-covalent complex and EI* is a modified complex, either with a conformational change to tight binding or with covalent changes to the enzyme, inhibitor or both. The interactions of some of these pterin-site inhibitors with NOS reveal unexpected complexity. An example of a mechanism based iNOS inhibition was cited by aminoguanidine [197±199] and by the acetamidine inhibitors N-α-iminoethyl-l-ornithine (l-NIO) and *N*'-iminoethyl-lysine (l-NIL) [200±203], GW273629 (*S*-[2-[(1-iminoethyl)-amino]ethyl]-4,4-dioxo-l-cysteine) and GW274150 (*S*-[2-[(1-iminoethyl)amino]ethyl]-l-homocysteine) (see Table 1). **Heme-binding inhibitors** have been shown to bind with each NOS monomer, one to the haem iron and one to the arginine-binding region (Glu) in competition with CaM. These compounds affect the assembly of iNOS monomers into active dimer inhibiting the dimerization [Sennequier, et al. 1999]. A class of substituted

pyrimidine inidazoles have been identified which inhibit dimerization of iNOS during its synthesis and assembly.

1.2.4 Flavoprotein and CaM inhibitors

A range of flavoproteins (e.g. diphenylene iodonium) or CaM (e.g. trifluoperazine) has been shown to inhibit NOS. NOS inhibitors display selectivity of their isoforms as partially selective, highly selective.

Partially and highly isoform-selective NOS inhibitors

Identification of selective inhibitors of iNOS and nNOS "100-fold selectivity for iNOS versus eNOS are reported [Anon, 1999a, 1999b]. Partially-selective nNOS inhibitor amino acids for nNOS versus eNOS and iNOS were reported. For example, *S*-ethyl- and *S*-methyl-1-thiocitrulline, vinyl-l-NIO showed timedependent inhibition of nNOS with significant selectivities versus isolated eNOS and iNOS enzymes [Babu and Griffith, 1998]. Other partially-selective iNOS inhibitors such as acetamidine-containing analogues of arginine, l-NIO and l-NIL have been widely used to probe the effects of iNOS inhibition. For example, some 2-iminohomopiperidines and 2-iminopyrrolidines with high (100±900-fold) selectivity for iNOS versus eNOS, but similar potency was observed on iNOS and nNOS (1±13-fold selectivity), with dual action iNOS-nNOS inhibitors.

Highly-selective iNOS inhibitors

The `highly selective ' iNOS inhibitors versus eNOS are mostly bis-isothioureas. Of these, *S*,*S*-[1,3-phenylene bis-(1,2-ethanediyl)bis-thiourea (`PBITU') is an l-arginine-competitive, rapidly reversible inhibitor of human iNOS with a K_i of 47 nM, and a selectivity (in K_i terms) of 190-fold versus eNOS showing substrate-binding sites of full-length human iNOS and eNOS in solution or in cells and tissues. Inhibition of human iNOS by 1400W was competitive with l-arginine, NADPH-dependent either an irreversible, or reversible. Mechanism-based inhibitor action was reported as K_d value %7 nM and steady-state selectivity against eNOS and nNOS of 5000 and 250-fold respective effects on vascular leakage [Lazlo, et al.1997]. GW273629 and GW274150 are two novel NOS inhibitors for iNOS versus both eNOS and nNOS. Both are sulphur-substituted acetamidine amino acids acting in competition with l-arginine as NADPH-dependent, whereas the inhibition of human eNOS and nNOS is rapidly reversible. The heme-binding substituted pyrimidine imidazoles inhibit assembly of active dimeric iNOS during its synthesis. It will be interesting to see what the pharmacology and utility of such compounds will be, and whether other compound series are discovered with this NOS inhibition mechanism of action.

1.3 The pharmacological inhibition of inducible nitric-oxide synthase (iNOS) gene expression

Presently, inhibition of NOS gene expression approach is used in testing inhibitors of pharmacological value. In past, inhibition of NOS was ideal assay to measure less stable NO in tissues but less specificity of NOS was discouragement and spin trap agents have emerged as a new approach of detection and measurement of NO in both in vivo and in vitro assays and bioimaging. Some examples of NOS inhibitors are cited in following section.

1. AMP Kinase protein kinase induced inhibition of inducible nitric-oxide synthase (iNOS) Inducible NOS inhibition in endotoxic shock in chronic inflammatory states was observed in several cell types (myocytes, adipocytes, macrophages) and primarily resulted from post-transcriptional regulation of the iNOS protein. Best example is inhibition of inducible nitric oxide synthase by activators of AMP activated protein kinase to explain a new mechanism of insulin sensitizing drug action [Pilon, et al.2004].. Inflammatory cytokines and LPS trigger the iNOS transcription through a complex network of intracellular pathways including NF-κB, Janus kinase/signal transducers and activators of transcription, and mitogen-activated AMPK protein kinase by reducing the transcription of iNOS and mRNA expression [Blanchette et al. 2003]. AMPK switches off protein synthesis either through suppression of the mTOR-p70S6 kinase pathway or by direct activation of eukaryotic elongation factor 2 kinase, resulting in the phosphorylation and inactivation of eukaryotic elongation factor 2 [Horman et al. 2002]. AMPK reduces iNOS protein content by promoting its ubiquitination, required for targeting iNOS through the proteasome proteolysis pathway [Kolodziejski et al.2002].
2. Expression of exogenous Kalirin in pituitary cells dramatically reduces iNOS inhibition of ACTH secretion. Kalirin inhibits iNOS activity by affecting iNOS homodimerization, which is required for iNOS activity. Thus Kalirin may play a neuroprotective role during inflammation of the central nervous system by inhibiting iNOS activity [Ratovitski, et al. 1999].
3. N^5-(Iminoalkyl)- and N^5-(Iminoalkenyl)-ornithines (VNIO) and several L-VNIO analogs showed minor structural changes to produce inhibitors either iNOS-selective or nonselective [Bretscher et al. 2003]. Furthermore, derivatives having a methyl group added to the butenyl moiety of L-VNIO and L-VNIO derivatives display slow-on, slow-off kinetics rather than irreversible inactivation. These results elucidate isoform-selective inhibition by L-VNIO and may provide information useful in rational design of isoform-selective inhibitors. [Bretscher, et al. 2003]
4. Constitutive and inducible isoforms of NOS are inhibited by S-alkyl-L-thiocitrullines with n-alkyl groups of any one carbon. The NOS inhibition is reversible, stereoselective, and competitive with L-arginine[Narayanan, et al. 1995].
5. Autoinhibition of endothelial NOS was reported by presence of an electron transfer control element in the NOS. [Nishida, et al. 1999]. Investigators examined the role of the insert in its native protein context by deleting the insert from both wild-type eNOS and from chimeras obtained by swapping the reductase domains of the three NOS isoforms. The Ca^{2+} concentrations required to activate the enzymes decrease significantly when the insert is deleted, consistent with suppression of autoinhibition. Furthermore, removal of the insert greatly enhances the maximal activity of wild-type eNOS, the least active of the three isoforms. Despite the correlation between reductase and overall enzymatic activity for the wild-type and chimeric NOS proteins, the loop-free eNOS still requires CaM to synthesize zNO. However, the reductive activity of the CaM-free, loop-deleted eNOS is enhanced significantly over that of CaM-free wild-type eNOS and approaches the same level as that of CaMbound wild-type eNOS. Thus, the inhibitory effect of the loop on both the eNOS reductase and zNO-synthesizing activities may have an origin distinct from the loop's

inhibitory effects on the binding of CaM and the concomitant activation of the reductase and zNO-synthesizing activities.

6. A mechanism was reported as Ca^{2+} triggers cross-talk signal transduction between CaM kinase and NO and CaM-K IIa phosphorylating nNOS on Ser847, which in turn decreases the gaseous second messenger NO in neuronal cells by Calcium/Calmodulin-dependent Protein Kinase IIa in NG108-15 neuronal Cells. [Komeima, et al. 2000].
7. Nitric oxide (NO) is moderately produced under control of iNOS gene expression. In recent years, scientists solved the problem of visualizing very unstable NO by mapping iNOS inhibition using gene expression array, *in vivo* nitric oxide direct detection (by stabilizing NO with suitable spin-trapping reagents), bioluminesence and MRI techniques to estimate *in vivo* NO concentration [Hong et al. 2009]. New approaches are in the direction of multimodal bioimaging iNOS gene expression and NO bioimaging as biomarkers. Success depends on NOS gene sensitive MR relaxation signal in cells and specificity to inflammation [Nie et al.2008; Terashima et al. 2010].

2. NO inhibitors in imaging

Major nitric oxide imaging techniques utilize mapping NO in tissue using NO specific imaging contrast agents sensitive to fluorescence, magnetic resonance and electron spin resonance. Recently, focus is diverted towards imaging *in vivo* physical properties of tissue cells such as cell calcium signaling and NO-biomarker based proton magnetic resonance techniques to achieve nanomolar range of nitric oxide mapping without any toxic effect. Fluorescent nitric oxide cheletropic traps are currently available choices in nitric oxide imaging but all of these have pitfalls of causing neurotoxicity [Reif, et al.2009]. In following sections, we put evidence of the NO sensitive fluorescent probes as cell calcium signaling indicator in tissues and possibility of NO specific perfusion MRI tool to visualize physiological nanomolar dynamics of NO in living cells up to the detection limit of 0.1 nM. The cell signaling indicators such as intracellular calcium revealed that ~1 nM of NO was enough to detect apoptosis events such as caspase-3 activation [Green, 1998, Nagata, 1997, Kwon et al.2009]. Furthermore, the possibility of superparamagnetic iron oxide nanoparticle bound complexes serve as MRI imaging contrast agents based on dephasing contrast. The iron oxide chelates are still in active evaluation phase to test their toxicity. The nanomolar range of basal endothelial NO appears to be fundamental to vascular homeostasis, hypoxia, apoptosis and inflammation.

- different contrast mechanisms and contrast characteristics of known nitrosyl-iron complexes display possibility of potential multimodal MRI and EPR probes specific to NO with examples of dithiacarbamates and $Fe(MGD)_2$ complexs in different applications.
- fMRI detects the interaction of paramagnetic species with NO in blood but possibility is still controversial. We review different applications of NO bioimaging.

2.1 Dithiacarbamates, LPS and MGD complexes for bioimaging of NO

In following sections we highlight the existing mechanisms and description to NO sensitive signal generation. Existing mechanisms of NO sensitive signal generation are explored by

MRI and fluorescence arising out from paramagnetic metals, dithiacarbamates or lipopolysaccharides complexes. The mechanisms depend on three approaches:

- Use of paramagnetic metals (SPIO) in MRI and dithiacarbamates (DTC) or lipopolysaccharides (LPS) complexes sensitive to MRI and fluorescence effects;
- Use of cytochrome proteins sensitive to EPR effect;
- Use of NO synthase inhibitors to measure the reduced NO concentrations for fluorometry and blood oxygen sensitivity to reduced NO concentrations.

The following sections are focused on dithiacarbamates in fluorometry and less known imaging contrast agents in MRI to image nitric oxide in tissues.

The first evidence of dithiacarbamates (DTC) reported them as electron Fe(II)-chelate spin trap agents. Examples are N-methyl-D-glucamine dithiocarbamate (MGD), $(MGD)_2$-Fe(II)-NO and NO-Fe-DTC metal complexes as multimodal imaging agents. These were initially verified for EPR with possibility of visualizing the radical distribution by MR images [Kubrina, et al.1992]. The $(MGD)_2$-Fe(II)-NO complex enhanced the contrast in the vascular structures such as hepatic vein and inferior vena cava. The paramagnetic NO-Fe-DTC metal complex is also a potential MRI signal enhancer and acts as contrast agent. These contrast agents showed the magnetic relaxation changes of neighboring protons to visualize the NO generated in living animal tumors [Jordan et al. 2000]. Other contrast enhancement effect showed an impact of short NO exposure to hemoglobin during MRI signal recording as source of *in vitro* MRI and *in vivo* functional MRI (fMRI) [Di Salle, et al. 1997]. fMRI signal intensity of venous blood in T1-, T2-, and T2*-weighted images proportionately changed with NO real-time generation in brain. Later, different approaches of blood hemoglobin and NO interaction were attempted to monitor fMRI signal sensitive to NO: mainly metHb and NO-Hb enhanced the MRI signal intensity. These observations suggested a blood flow-independent effect and less utility [Di Salle, et al. 1997]. Still it is hope that NO sensitive fMRI techniques can detect slow epithelial intracellular processes such as metabolic integrity, vascular tonicity, stress, shear and inflammatory effects at early stages of the disease processs, allowing precise monitoring of onset in intact biological systems at cellular level. Other approaches are also emerging to use NO biosensors for multimodal imaging. Currently, use of fMRI as a non-invasive NO sensitive technique has emerged as potential and remarkable tool to detect apoptosis *in vivo*. The NO sensitive fMRI techniques can detect slow epithelial intracellular processes such as metabolic integrity, vascular tonicity, stress, shear and inflammatory effects at early stages of the process, allowing the onset in intact biological systems, providing a useful tool for monitoring at cellular level.

2.2 The source of intracellular NO and metabolic integrity- feasibility of MRI

The nitric oxide is released from the L-arginine in tissue along with molecular oxygen in the oxidative L-arginine degradation reaction of L-arginine pathway catalyzed by either of any three different NO synthase (NOS) isoenzymes. NO controls the intracellular redox state in tissue and protects the metabolic integrity in two ways [Kuppusamy, et al. 1994]. First, anions and cations in intracellular space or cellular redox state prevent apoptosis for example, NO in hepatocytes, neurons, glial cells and fibroblasts controls the release of mitochondrial apoptogenic factors and induces apoptosis by activation of caspases [Hortelano, et al.2005]. Second, peroxynitrites accumulate as product of nitric oxide and

superoxide anion. Peroxynitrites promote apoptosis through the indirect activation of caspases [Kuppusamy, et al. 1994, Hortelano, et al.2005]. However, all these approaches are still invasive to evaluate apoptosis.

Overproduction of nitric oxide and imaging the NO accumulation due to neurotoxicity was reported in neurological disorders or neurodegeneration. The reason of neurotoxicity was reported due to NO reactive oxidative properties in tissue [Caramia, et al. 1998]. This approach was reported not to solve the purpose of *in vivo* functional monitoring but NO properties indicated the state of tissue and follow-up of dynamic status of neurodegenerative factors in brain [Caramia, et al. 1998]. In other application of NO bioimaging to detect apoptosis, T2 weighted maps from control vs GSNO treated and z.VAD treated animals exhibited hyperintense areas perhaps due to toxicity of NO on the T2 maps while z-VAD treated animals showed small lesion areas due to reduced NO toxicity. The response of z-VAD injection was presumed as reduced toxicity due to caspases and NO-dependent apoptosis. These authors explained that GSNO increased T2 intensity 25% while z-VAD reduced this MRI signal [Komarov, et al. 1995]. These classic reports indicated that T2 hyperintensities on MRI positively offer the possibility of in vivo evaluation of cell death at different locations in whole tissues undergoing apoptosis. The apoptosis is also a major mechanism in brain neurodegeneration and post-myocardial infarction heart [Caramia, et al. 1998]. However, this approach seems as potential tool of functional imaging in near future to monitor the therapeutic intervention of new drugs to reduce neurodegeneration[Kuppusamy, et al. 1994, Hortelano, et al.2005, Foster, et al. 1998]. Currently, non-invasive NO sensitive techniques are big hope as potential and remarkable tools to detect apoptosis *in vivo*.

Initial studies on NO with iron-dithiocarbamate complexes had succeeded in direct detection of NO in mice by whole body electron paramagnetic resonance spectroscopy (EPR) at the L-band [Fujii, et al. 1997, Komarov, et al. 1995] with new possibilities by Magnetic Resonance Spectroscopy [Reif, et al. 2009, Li, et al. 2009]. Several authors demonstrated the feasibility of EPR imaging in visualizing free radical distributions *in vivo* at low resolution where the intrinsic line width of the radical is large, such as the spin-trapped NO [Yoshimura, et al. 1996, Kubrina, et al. 1992, Foster, et al. 1998]. This drawback of low resolution caught attention for feasible MRI contrast agents, such as stable (*N*-methyl-D-glucamine)$_2$-Fe(II)-NO complex to generate better resolution. The complex has a much longer *in vivo* half-life than most (stable) nitric oxide derived compounds. Recently N-methyl glucamine iron complexes have shown greater affinity with NO to make (MGD)$_2$-Fe(II)-NO complex useful for in vivo NO measurements by EPR [Caramia, et al. 1998]. In recent years, the art of MRI combined with NO spin trapping mechanism was evaluated as feasible method of mapping the distribution of NO spin-trap complex in animals with possibility in clinical use. In following section, our design of ultrafast MRI protocol is described using NO/NOS sensitive biosensor complexes for use at 21-Tesla MRI microimager.

2.3 Approach of stable NO sensitive lipopolysaccharides (LPS) as feasible imaging complexes

The LPS serves as encaged bag holding contrast agent. The LPS based NO imaging approach has following presumptions:

- spin-trapped NO is stable in intracellular tissue environment;
- NO-LPS contrast enhancement properties are MRI visible;
- NO-LPS complex is stable in tissues and organs; and
- simultaneous visualization and mapping of NO free radicals are possible by MRI.

The routine method of LPS injected animals after 6 hours of $(MGD)_2$-Fe(II) injection, usually serve as experimental model of subsequent MRI detection and visualization of NO generated in animals. It was confirmed by using a specific NOS inhibitor *N*-monomethyl L-arginine (L-NMMA) [Fujii, et al. 2007]. The observations indicated that the suppressed NO levels were proportional to NO sensitive LPS concentration independent of $(MGD)_2$-Fe(II)-NO contrast agent [Fujii, et al. 2007]. Next issue of feasibility and stability of $(MGD)_2$-Fe(II)-NO imaging contrast agent was major breakthrough reported in model systems to generate EPR and MRI signals. It is established that the NO complex $(MGD)_2$-Fe(II)-NO is very stable in model aqueous media. The NO complex $(MGD)_2$-Fe(II)-NO complex, if injected, is stable in tissues and organs as confirmed by L-band EPR measurements as reported elsewhere [Lai, et al. 1994, Mulsch, et al. 1999]. These authors confirmed the assignment as $(MGD)_2$-Fe(II)-NO from the hyperfine coupling J constant of this signal (see Figure 5). However, LPS complex accumulates in liver, brain, heart, kidney [Yoshimura, et al. 1996]. NOS inhibitor, *N*-monomethyl L-arginine (L-NMMA, 2 mM) confirmed that the NO complex is not bio-reduced or biodegraded *in vivo* based on the EPR spectrum of $(MGD)_2$-Fe(II)-NO complex. The stability of $(MGD)_2$-Fe(II)-NO complex was at least 12 hours. In other report, the reduction/ decomposition of the NO complex occurred in the presence of 1 mM ascorbic acid or glutathione inhibitor with a half-life of 40 and 48 min, respectively [Perrier, et al. 2009]. All these evidences indicate the NO complex as stable, non-biodegradable or decomposed form of $(MGD)_2$-Fe(II)-NO complex as strong proton relaxation enhancer with paramagnetic properties [Perrier, et al. 2009, Fujii, et al. 2007]. All these evidences also indicated the NO complex as stable, non-biodegradable or decomposed form of $(MGD)_2$-Fe(II)-NO complex as strong proton relaxation enhancer with paramagnetic properties.

Biosensor#		T1 (600/15) msec		r1 $L.mmol^{-1}.sec^{-1}$	r2 $L.mmol^{-1}.sec^{-1}$
DNIC (240 μmol/L)		931 ±3 7			
DNIC-cysteine				0.23 ± 0.06	0.33 ± 0.03
DNIC-GSH(230 μM)		850 ± 24		0.11 ± 0.02	0.19 ± 0.03
DNIC-BSA(160 μM)		247 ± 13		0.71 ± 0.09	1.37 ± 0.30
MNIC-MGD				0.97 ± 0.09	1.37 ± 0.03
MGD		55.5	52.4		
$(MGD)_2$-Fe(II)-NO	T1	13.3*	13.9**		
(100 nmol/g)	T2	8.3*	8.7**		
(MGD)2-Fe(II)		24.9	25		

The strong magnetic moment of the unpaired electron promotes both spin lattice and spin-spin relaxation of the surrounding water protons, resulting with decrease in their spin-lattice (T1) and spin-spin (T2) relaxation times or enhancement in signal intensity on T1 or T2 weighted MR images. Relaxation constants of $(MGD)_2$-Fe(II)-NO, $(MGD)_2$-Fe(II) at 500 MHz* and 300 MHz** is shown indicating that relaxivity is not magnetic field dependent over this range.

Table 2. Relaxation constants of biosensor complexes are shown for NO detection in aqueous solutions.

In other study, NO complex was prepared from NO gas and $(MGD)_2$-Fe(II) in glass capillaries. The strong magnetic moment of the unpaired electrons promote both spin lattice and spin-spin relaxation of the surrounding water protons and show a decrease in their spin-lattice (T1) and spin-spin (T2) relaxation constants or show enhanced signal intensity in T1 or T2 weighted MR images as shown in Table 2 and Figure 5 [Hortelano, et al. 2005]. Major points were:

- The relaxation constants of $(MGD)_2$-Fe(II)-NO in aqueous media were characteristic and complex concentration dependent;
- T1 and T2 relaxation constants of liver were measured 1.17(1/mM * sec) and 1.32 (1/mM * sec) respectively at 500 MHz at increasing concentration of NO;
- T1 relaxation constant of $(MGD)_2$-Fe(II), was reported 0.044 (1/mM * sec) at both 20 MHz and 85 MHz magnetic fields. The T1 relaxation constant was field independent;
- Distinct increase in relaxivity after complexing NO with $(MGD)_2$-Fe(II). These unique properties of complex suggested its feasibility to visualize the regional distribution in tissue *in vivo* where the NO was trapped.

In previous study, $(MGD)_2$-Fe(II)-NO and LPS complexes were used as in vivo MR contrast agents [Fujii, et al. 2007]. First, intraperitoneal injection of 2 ml of 9.1 mM $(MGD)_2$-Fe(II)-NO complex (150 nmol/g tissue) showed relative difference on T1-weighted MR images of rat liver site before and after injection of NO complex as shown in Figure 5.

- The images indicated the NO complex very effective ''intrinsic contrast agent,'' to enhance the contrast in several other organs.

The Second, LPS injected animals after 6 hours of $(MGD)_2$-Fe(II) injection, showed subsequent MRI detection and reproducible visualization of NO generated in liver of animals as shown in Figure 5 and Fig. 6a (indicated by the arrow) as plots against time with the intensity of the reference water sample. Figure 6b showed that the image intensity in the liver increased with the NO generation, without any intensity change in reference sample in the presence of the specific NOS inhibitor *N*-monomethyl L-arginine (L-NMMA).

Interestingly, other face of $(MGD)_2$-Fe(II)-NO complex is 'spin trap'. Spin traps are chemical compounds used to detect unstable free radicals such as hydroxyl (*OH) and superoxide (O_2^{*-}) in biological systems. Spin trapping compounds (spin traps) selectively react with NO and trap the nitric oxide. The spin-trap stock $(MGD)_2$-Fe(II) complex solution (mixture of deoxygenated saline MGD (100 mM) and $FeSO_4$ (20 mM) solutions in nitrogen) makes $(MGD)_2$-Fe(II)-NO complex by mixing $(MGD)_2$-Fe(II) with either pure NO gas or *S*-nitroso-*N*-acetyl DL-penicillamine (SNAP). The pure NO gas is prepared by passing NO gas through a KOH solution. Major concern was the coordination of NO to the Fe complex altered the solubility of N0-Fe(II)$(MGD)_2$ < 1 mM. The in vivo half life of N0-Fe(II)$(MGD)_2$ was 41 minutes and only 40% trapped NO was estimated by detection of Fe(II)$(MGD)_{2\ induced}$ inhibited NOS and decrease in NO formation and perfusion in the tissue [Fichtlscherer, et al. 2000].

$$2NO + \mathbf{Fe(III)}(MGD)_2 \xrightarrow{H_2O\ (*OH)} NO\text{-}\mathbf{Fe(II)}(MGD)_2 + NO_2^- \quad (1)$$

$$NO + \mathbf{Fe(III)}(MGD)_2 \xrightarrow{Reducing\ Equivalent} NO\text{-}\mathbf{Fe(II)}(MGD)_2\ (40\%)$$

MR contrast due to trapped NO can be expressed in Eq 2, 3:

$$1/T1[\text{NO-Fe(II)(MGD)}_2] = 1/T1_{(\text{observed})} - 1/T^* = r1_i[\text{NO-Fe(II)(MGD)}_2] \times \text{concentration} \quad (2)$$

$$1/T_{obs} = 1/T^* + r1_i[\text{NO-Fe(II)(MGD)}_2];\ i = 1, 2... \quad (3)$$

where $T1_{(observed)}$ is long longitudinal relaxation time constant and T1* is short longitudinal relaxation time constant in absence of $[\text{NO-Fe(II)(MGD)}_2]$, $r1_i$ is longitudinal relaxivity dpends on I = 1, 2, 3 the number of carbons in branch of MGD chain, $[\text{NO-Fe(II)(MGD)}_2]$, concentration and interaction with NO specific bioactive receptor, enzyme, antibody, hormone molecules in tissue.

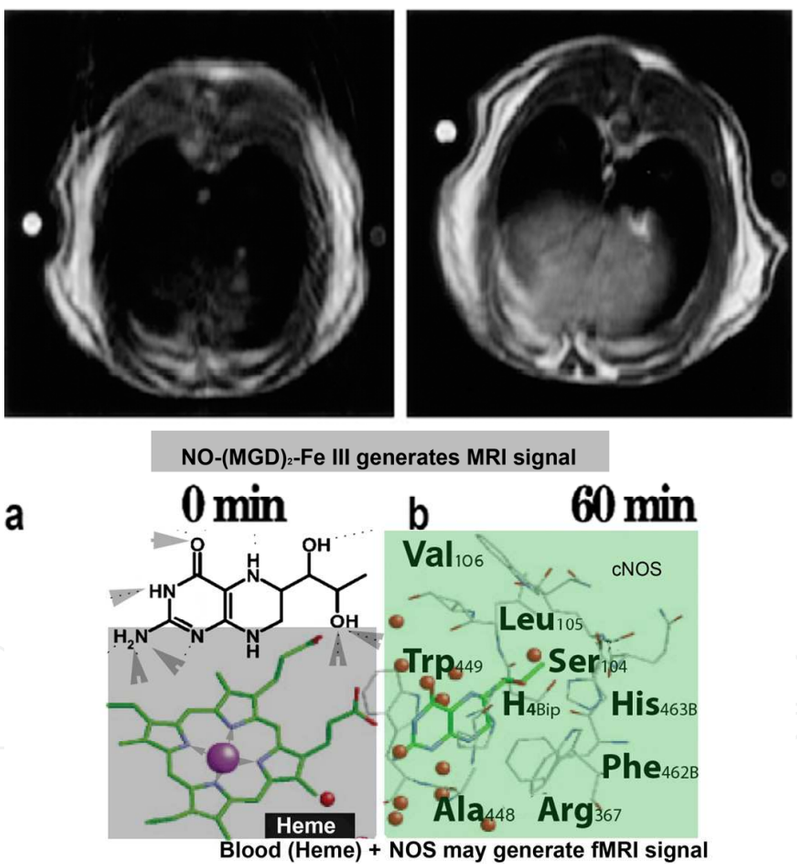

Fig. 5. Imaging of preformed $(MGD)_2$-Fe(II)-NO complex. Transverse T1-weighted MR images in the axial plane of the liver of Wistar rats. Two ml of 9.5 mM $(MGD)_2$-Fe(II)-NO complex was injected i.p. in the lower abdomen of 250 g rats (n = 3). **a:** Control, before injection; **b:** 60 min after injection of $(MGD)_2$-Fe(II)-NO complex. A sketch at bottom shows the interaction of No with heme as basis of MRI signal. Reproduced with permission for reference Fujii, et al. 2007.

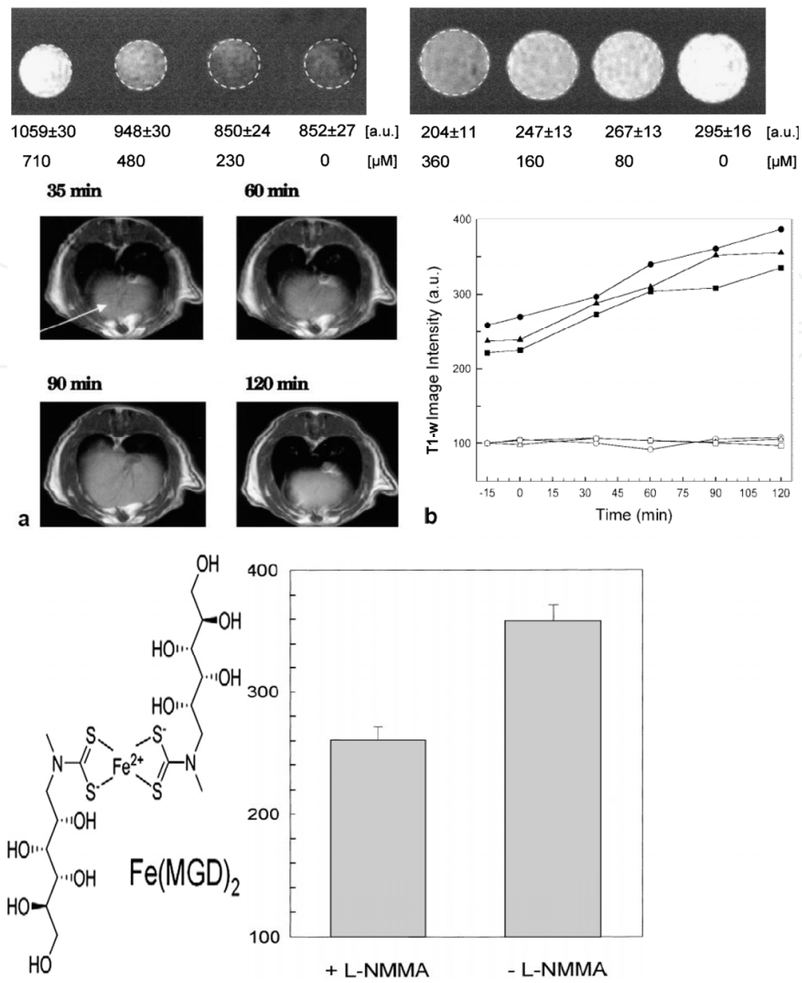

Fig. 6. Imaging of NO in six phantoms and LPS-treated rats. **a:** Transverse T1-weighted MR images focussed on a selected region of the liver in LPS-doped rats. The MR images were measured at the times indicated. Six hours after LPS injection, the NO spin-trap [3 ml of $(MGD)_2$-Fe(II), MGD: 100 mM, Fe: 20 mM] was administered i.p. **b:** Plot of MR image intensity with time. Signal intensities were averaged over the selected region indicated by the arrow in a (7*7 mm^2) for three different animals (filled symbols), normalized to intensity of a reference (water in a tube placed next to the animal, open symbols). At zero time, the spin-trap, (MGD)2-Fe(II), was added. **c:** Comparison of the signal intensity in a selected slice region of the liver in the presence and absence of the NOS inhibitor, L-NMMA. The image intensity in the liver was first normalized to the external standard noted above. The averaged intensity in the selected regions (7 x 7 mm^2) was averaged (n = 3). L-NMMA (50 mg/kg in saline) was injected i.p. 3 h after LPS injection (Reproduced from reference Fujii et al. 2007).

2.4 MRI measurement protocol design

We developed a MRI protocol to investigate the regional distribution of $(MGD)_2$-Fe(II)-NO in various organs. For whole animal imaging, protocols for relaxivity of $(MGD)_2$-Fe(II)-NO were designed on a Bruker 500 MHz, to achieve millimolar relaxivity. For the animal

experiments, anesthesia was administered as sodium pentobarbital (30 mg/kg, i.p.) and ketamine (20 mg/kg, intra-muscular injection) before injection of contrast agent in animals. For imaging, animals were anesthetized by intubating with 14 gauge, 2 inch intravenous catheter (Abbocath Lab, IL) on nose with 30% oxygen/70% nitrogen mixture containing 5% isoflurane/air mixture to continuous supply through nose during MRI session. Animals were kept in vertical direction to the side of MRI gantry and 30 mm diameter RF insert covering kidneys in the center of magnet. During six hours after administration of LPS to Wistar rats (150–200 g) they were injected intraparitoneally with 3 ml of $(MGD)_2$-Fe(II) [MGD:100 mM, Fe:20 mM] at different intervals. MR images of the anesthetized rats (n = 5) were obtained after 1 hr spin trap injection with a Bruker Biospin 500 MHz scanner (PARAVISION 3.2).

Different imaging techniques are available in our lab on 500 MHz and 900 MHz scanners. In vivo NO induction was carried out according to previously reported methods with slight modifications [Lai, et al. 1994, Yoshimura, et al. 1996, Green, et al. 1998].

- Axial T2-weighted spin echo sequence with fat suppression (TR 2000 ms, TE 100 ms, flip angle 30; EC 1/1 15.6 kHz) was used for more detailed T2-weighted information in detecting solid tissues.
- Axial T1-weighted images were acquired at TR/TE/flip angle = 750 ms/ 4.18 ms/25^o, FOV/matrix size/spatial resolution = 2.6 x 1.4 cm^2/ 256 x 256 ×75 µm, and the inversion time (TI approximately 250 ms) set to null the normal the background tissue.
- Gradient echo sequence in-phase and opposed-phase(TR 180 ms, TE 2.3 ms/4.5 ms, flip angle 30 were done as a dual echo sequence to show renal lesions hypointense and parenchyma isointense with hyperintense protein rich cyst. Opposed phased T1-weighted gradient echo sequences were sensitive to fat.
- Axial T1-weighted gradient echo sequence for dynamic perfusion/ diffusion weighted imaging (TR 130 ms, TE 1.0 ms, flip angle 30) was done after 30 ml intravenous gadolinium contrast injection for acquiring pre-contrast and post-contrast images in arterial phase to distinguish perfusion in the tissues. Parameters for T1-weighted spin-echo images were TR 1500 msec, TE 10 msec, 2 NEX, 1-mm slice thickness, 0.5-mm slice gap, field of view 12 x 3 x 12 cm^3, and matrix, 256 x 256.

The original bird-cage coil with 2.6 cm diameter Rf insert was used for MR imaging. We established in lab MR image analysis by shareware software NIH Image J, a PC version supplied by Scion Corporation. The analysis of averaged image intensities from selected regions of interest 15 x 3 x 15, and matrix , 256 x 256 served as best for measurement of signal enhancement. An external reference (saline solution in a sealed test tube) placed near the animal serves to normalize intensities from both control and test groups. Percentage enhancements can be calculated from the normalized data [35]. Functional dependence of the MR imaging signal intensity S on the intrinsic properties (proton spin density $N(H)$, T1, T2) has been derived based on the assumption of a monoexponential dependence on T1 and T2 with a spin-echo sequence: $S(TE,TR) = N(H)\exp(-TE/T2)\ [1 - \exp[-(TR/\ TE)/T1]]$. The term on the right reflects the T1 dependence, and the exponential expression on the left reflects the T2 effects. TE << T2 generates a T1-weighted. T1 image is obtained by means of least-squares fitting (Marquardt-Levenberg algorithm) of the mean intensity values versus

TR. T2 weighted image is obtained by TR >> T2. Mean intensity values are fitted versus the TE (Marquardt Levenberg algorithm).

T1 weitghted MR contrast due to trapped NO as NO-Fe(II)X spin trap in tissue can be expressed in Eq 4, 5:

$$1/T1[\text{NO-Fe(II)X}] = 1/T1_{(\text{observed})} - 1/T^* = r1_i[\text{NO-Fe(II)X}] \times \text{concentration} \quad (4)$$

$$1/T_{obs} = 1/T^* + r1_i[\text{NO-Fe(II)X}];\ i = 1, 2... \quad (5)$$

where $T1_{(observed)}$ is long longitudinal relaxation time constant and T1* is short longitudinal relaxation time constant in absence of [NO-Fe(II)X],

$r1_i$ is longitudinal relaxivity dpends on i= 1, 2, 3 the number of carbons in branch of X contrast agent, its concentration and interaction with NO specific bioactive receptor, enzyme, antibody, hormone molecules in tissue.

2.5 Approaches to NO evaluation by Magnetic Resonance Imaging (MRI) techniques

Two major developments reported in context with NO. First, a search of NO specific stable multimodal MR/EPR sensitive spin trap complex; second, calibrating imaging characteristics of spin trap complex on NMR/MRI/PEDRI techniques. NO is perfused in gaseous phase or remains in ionic phase by redox state in the tissues. Both forms of NO are captured or trapped by Fe(II)-$(DTC)_2$ complexes and show MRI signal change due to reactive nitrosylation (reaction of intracellular NO with Fe(II)$(DTC)_2$ to form NO-Fe(II)$(DTC)_2$ complex) shown in Eq 6. Second-order rate constant of the reaction of NO with Fe(II)$(ProDTC)_2$ was reported to be $(1.1 \pm 0.3)\times10^8$ M^{-1} s^{-1}[Caramia, et al. 1998].

$$Fe(II)(DTC)_2 \rightarrow Fe(II)(ProDTC)_2 + NO \rightarrow NO\text{-}Fe(II)(DTC)_2 \quad (6)$$

Recently, attempts have been made to overcome the limitations of EPR-based imaging with low resolution and large sample size by employing new approaches of nuclear magnetic resonance (NMR) and magnetic resonance imaging (MRI) techniques. Several paramagnetic metal complexes have been widely used as contrast agents in magnetic resonance imaging (MRI) due to their ability to enhance the NMR relaxation of neighboring protons [von Bohlen, et al. 2003]. Paramagnetic NO-Fe-DTC complex has been utilized to visualize NO generated in living rats with septic shock [Fichtlscherer, et al. 2000, Fujii, et al. 1999]. Paramagnetic nitrosyl iron complex showed contrast properties to enhance the signal intensity of SNP-perfused rat liver in MRI [Fichtlscherer, et al. 2000, Fujii, et al. 1999]. Thus, a paramagnetic nitrosyl iron complex may be potentially useful as a microscopic localizer MRI contrast agent specific for NO accumulation in living organisms. Other proton-electron-double-resonance-imaging (PEDRI) technique was based on the enhancement of proton NMR signal intensity in the presence of radicals through the Overhauser effect Mulsch et al. 1999,Foster, et al.1998]. Rat livers were exposed to SNP as an NO donor exhibited intense PEDRI images [Rast, et al. 2001, Jordan, et al.2004]. PEDRI imaging is a potential tool to study NO in large biological specimens. Still imaging application of MR and EPR spectroscopy using nitric oxide synthase inhibitors, oxygenation or perfusion are in infancy [von Bohlen, et al. 2003, Zhou, et al. 2009, Nagano, et al. 2002, Anbar, 2000]

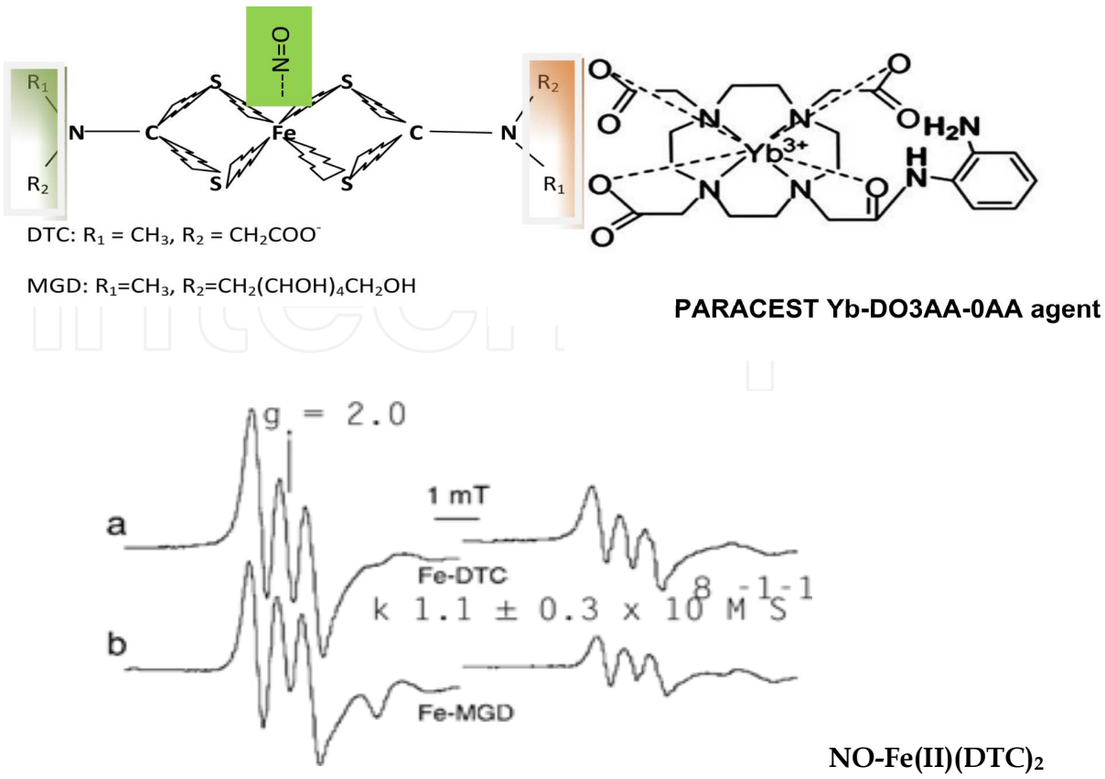

Fig. 7. NO sensitive biomarker imaging contrast agents. Example of NO-Fe(II)$(DTC)_2$ is cited to illustrate the signal change during changes in cerebral blood flow and possibility of functional MRI [Caramia, et al. 1998].

Two decades ago, NO activation-induced signal changes in functional MRI (fMRI) was observed [Di Salle, et al. 1997]. Hb–NO was found to produce marked stimulator dose and concentration-dependent NO sensitive fMRI signal intensity changes (increased after aqueous NO solution, nitrite, or dithionite and nitrite added to blood while it decreased on the addition of ascorbic acid) examined by T_1-, T_2-, and T_2^*-weighted MRI in venous erythrocytes with possibility of physiological MRI evaluation associated with NO change [Di Salle, et al. 1997]. Transient formation of two paramagnetic species (met Hb and NO-Hb) enhanced the signal intensity, while ascorbate reduced the signal intensity in fMRI experiment on healthy volunteers during standard tasks. Further, infusion of NO precursor, L-arginine increased the cerebral blood volume (measured by MRI) in nonischemic spontaneously hypertensive rats [Foster, et al. 1998]. In other study, administration of an NO donor, isosorbide dinitrate (ISDN) increased both tumor blood flow and partial oxygen pressure in mice implanted with liver tumor in the thigh [Jordan, et al. 2000]. These findings indicate blood flow-independent change in MRI signal produced by different additives or stimulators. These observations open a new perspective on the monitoring of NO and the in vivo speculation of NO effects to test new drugs by using magnetic resonance techniques. Fuji et al. 1999 first time reported *in vivo* MRI of NO using $Fe(MGD)_2$ as NO–$Fe(MGD)_2$ spin-trapping technique in a septic shock rat model [Fujii, et al. 1999]. (Fig. 6A). The reduced signal after administration of an iNOS inhibitor confirmed the MRI visibility of NO–

$Fe(MGD)_2$ complex especially in inflammation which has high levels of NO. Now many MRI visible nitrosyl-iron complexes are known for MRI mapping of NO using a conventional 1.5 T MR scanner. The principle is that after exposure to NO in tissues $Fe(MGD)_2$ imaging agents form nitrosyl-iron complexes, which shorten the T_1 and T_2 relaxation time in a concentration-dependent manner [Hong, et al. 2009]. Mainly, four major techniques are reported in quest of developing new NO sensitive MRI contrast agents. First, unpaired electrons of the nitrosyl–iron complexes can enter into dynamic nuclear polarization with water protons, a technique called proton-electron-double-resonance imaging (PEDRI). Second, superparamagnetic iron oxide (SPIO) or ferumoxides dephase T_2-weighted MRI signal dependent on SPIO: NO donor ratios indicating inverse relation of contrast enhancement by SPIO with increasing levels of NO in tissue. The MRI signal change was due to reduction of ferric to ferrous iron with result of decrease in paramagnetic relaxation of water protons [Kojima, et al.2001]. Third, technical development emerged as irreversible paramagnetic chemical exchange saturation transfer (PARACEST) based MRI contrast agents in imaging [Liu, et al. 2007, Zhang, et al. 2003, Wu, et al. 2008]. A PARACEST MRI agent, Yb(III)-(1,4,7,10-tetraazacyclododecane-1,4,7-triacetic acid)-orthoaminoanilide (Yb-DO_3A-OAA), was developed for NO detection (Fig. 6B) [9]. Fourth, NO and O_2 combine by irreversible covalent bond that causes a quick disappearance of the PARACEST effect captured in the MR images. PARACEST MRI is fast data acquisition (in few minutes) vs SPIO based imaging is slow (in few hours). PARACEST effect has poor sensitivity (only detects millimolar concentrations of NO).

2.6 Approach of real-time NO synthase inhibition as blood oxygenation dependent MRI signal

Nitric oxide synthase inhibition (NOSi) in humans by blood oxygenation level-dependent (BOLD) MRI as reduced response to NOSi was reported using BOLD MRI to compare changes in R_2* to direct measures of renal medullary oxygen levels and blood flow using N-nitro-L-arginine methyl ester invasive probes (OxyLite/OxyFlo) to examine for the first time the effect of NOSi on intrarenal oxygenation in humans [Li, et al. 2009, Di Salle, et al. 1997]. Authors showed that NOSi decreased medullary pO_2 and blood flow in a dose-dependent manner, and BOLD MRI showed an increase in medullary R_2* consistent with the invasive pO_2 measurements.

Other alternate approach of positron emission tomography (PET) was proposed in recent study using nitric oxide imaging probe prepared from [^{18}F] 6-(2-fluoropropyl)-4-methyl-pyridin-2-amine by substitution at position-6 of substituted 2-amino-4-methylpyridine with favorable properties as a PET tracer to image iNOS activation/expression with PET of animal lungs [Zhou, et al. 2009].

3. Major developments in NO bioimaging probes

3.1 Magnetic resonance relaxation enhancement mechanism

In 1999, the first in vivo MRI of NO was reported using the spintrapping technique in a septic shock rat model [Fujii, et al. 1999]. NO was trapped by $Fe(MGD)_2$ in vivo, which can be visualized by MRI. The NO–$Fe(MGD)_2$ complex displayed significantly enhanced

contrast in the vascular structure, such as the hepatic vein and inferior vena cava, which can be reduced after administration of an iNOS inhibitor.Initially, NO mapping was reported by whole body EPR imaging at poor resolution [Claudette, et al. 2005,Yoshimura, et al. 1996]. Recently, MRI strategies combined with in vivo spin-trapping map ''NO distributions'' within tissues and organs showed much higher spatial resolution using $(MGD)_2$-Fe(II)-NO as a NMR contrast agent in vivo [Fichtlscherer, et al. 2000]. The MR images also provided follow-up of NO generation kinetics at different sites within the organ at much higher spatial resolution than with EPR [Claudette, et al. 2005,Yoshimura, et al. 1996]. NO makes stable complex such as $(MGD)_2$-Fe(II)-NO. In vivo, hemoglobin is normally the natural NO spin-trap such that NO tends to bind with hemoglobin or oxidize the hemoglobin, followed by conversion to nitrosyl-hemoglobin or methemoglobin, both of these complexes are paramagnetic. Authors believe that during brain stimulation, NO is generated in some regions and it is quite possible that (paramagnetic) nitrosyl-hemoglobin and methemoglobin are formed in these active regions in brain. The MRI signal intensity enhancement in these regions results from changes in blood flow rich with these complexes. However, for blood flow–independent effects in MRI, the paramagnetic relaxation from spin-trapped NO might provide a new fMRI contribution in future. To our knowledge, there have been no reports successfully imaging or detecting free radicals such as NO in vivo by NMR or fMRI. Further, both short lifetime and rapid diffusion of NO in time preclude any effective relaxation enhancement mechanisms. NMR spin trapping serves to overcome these problems such as NO short lifetime and its fast diffusion in tissues to some extent. In other classic study on rats, spin relaxation constants of dinitrosyl-iron bound albumin or GSH and mononitrosyl-iron dithiocarbamate MGD complexes showed concentration dependence by MRI technique [Fujii, et al.1999].

3.2 Emission enhancement mechanism

Present state of art in NO detection was developed over last 2 decades using fluorescein cheletropic compounds visualized by emission enhancement and photoinduced electron transfer mechanisms. Fluorescence properties of fluorescein derivatives are controlled by the photoinduced electron transfer (PET) process from the benzoic acid moiety to the fluorophore, the xanthene ring. PET is a widely accepted mechanism for fluorescence quenching in which electron transfer from the PET donor to the excited fluorophore diminishes the fluorescence of the fluorophore. A brief survey of these compounds and their fluorescence mechanisms will catch the attention of readers with the newer developments of NO detection in tissues. EPR (also known as electron spin resonance or ESR) explores the magnetic moment associated with the unpaired electron(s) in free radicals and paramagnetic metal ions [Mader, 1998, Swartz, 2007]. It has been applied for the detection of free radicals and paramagnetic metal ions in various biological conditions [Berliner, et al. 2004]. When an unpaired electron in a paramagnetic molecule is subjected to an external magnetic field, the energy level of the electron splits into two quantum states with different energy levels. Typically, the magnetic field is scanned with a fixed microwave frequency of approximately 9.5 GHz (usually called the X-band). Specimens less than about 100 µL are measurable in an Xband spectrometer. However, larger biological samples (e.g., tissues, organs, and live animals) cannot be measured with a conventional X-band spectrometer due to the high dielectric loss of water at such frequencies and the small size of the EPR cavity resonator.

EPR spectroscopy at lower frequencies, the L-band (0.4–1.6 GHz) or S-band(1.6–4 GHz), can be used for in vivo EPR imaging. EPR imaging is generally considered to be the most effective technique for noninvasive observation of the spatial distribution of free radicals [Kleschyov, et al. 2007]. Direct EPR detection of endogenous free radicals in biological samples requires that the radical of interest is present at a concentration higher than the practical detection limit (0.1–0.01 μM) and has a relatively long lifetime. Although such requirement can be met at cryogenic temperature, in vivo detection is almost impossible since most radicals do not have a sufficiently long lifetime. Therefore, spin-trapping techniques have been developed in which the spin traps can react with unstable free radicals to form a relatively stable adduct [Berliner, et al. 2004, Davie, et al. 2004]. The formation of the long lived adduct results in accumulation of steady-state free radicals which can be detected readily by EPR spectroscopy.

In principle, the fluorescence properties of fluorescein derivatives are controlled by the photoinduced electron transfer (PET) process from the benzoic acid moiety to the fluorophore, the xanthene ring. PET is a widely accepted alternate mechanism for fluorescence quenching in which electron transfer from the PET donor to the excited fluorophore diminishes the fluorescence of the fluorophore. The fluorescein structure has two parts confirmed by X-ray analysis, i.e., the benzoic acid moiety as the PET donor and the xanthene ring shown as the fluorophore in previous study [Liu, et al. 2007]. The study showed that only small alterations in absorbance were observed among fluorescein and its derivatives. The dihedral angle (ϕ) between the benzoic acid moiety and the xanthene ring was almost 90^{o}. It also suggested that there is little ground-state interaction measured by HOMO energy levels between these two parts.

The relationship of HOMO energy levels and (ϕ) angle of fluorescent compounds predict the fluorescence mechanism of benzoic acid moiety in the compounds. If the HOMO energy level of the benzoic acid moiety is high enough for electron transfer to the excited xanthene ring, the ϕ value will be small. In other words, fluorescein derivatives with a high ϕ value must have benzoic moieties with low HOMO energy levels. The HOMO energy levels of 3-aminobenzoic acid, 3-benzamidobenzoic acid, 3,4-diaminobenzenecarboxylic acid (DAB-COOH), and benzotriazole-5-carboxylic acid (BT-COOH), which are the benzoic moieties of aminofluorescein, benzamidofluorescein, DAF-2, and DAF-2T, respectively were estimated by semi-empirical (PM3) calculations. DAB-COOH and aminobenzoic acid, which are the benzoic acid moieties of weakly fluorescent fluorescein derivatives, have higher HOMO levels than BT-COOH and amidobenzoic acid. These results were consistent with the PET mechanism.

Further, to confirm this mechanism 9-[2-(3-carboxy)-naphthyl]-6-hydroxy-3H-xanthen-3-one (NX) and 9-[2-(3-carboxy)anthryl]-6-hydroxy-3H-xanthen-3-one (AX) were synthesized [Nagano, et al. 2002]. It is well-known that expanding the size of aromatic conjugates makes their HOMO levels higher, similar with by introducing electron-donating substituents. Thus, naphthoic acid and anthracene-2-carboxylic acid would have higher HOMO levels than benzoic acid, and therefore, the fluorescence properties of NX and AX would differ from those of fluorescein.. The absorbance maximum (Ex_{max}) and emission maximum (Em_{max}) of NX and AX were closer and not much altered among these fluorescein derivatives. However, the ϕ values were greatly altered; NX is highly fluorescent, whereas

AX is almost nonfluorescent [Nagano, et al. 2002]. Thus, a small change in the size of conjugated aromatics, namely, from naphthalene to anthracene, causes a great alteration of the fluorescence properties. Authors compared the HOMO levels of the benzoic acid moieties with xanthine ring and naphthoic acid. Napthoic acid moiety is present in highly fluorescent fluorescein and NX. The HOMO levels of benzoic acid moiety were lower than that of the xanthene ring, while the HOMO level of anthracenecarboxylic acid moiety in fluorescent AX, was higher than that of the xanthene. These results were consistent with the idea that a PET process controls the fluorescence properties of fluorescein derivatives and that these properties can be predicted from the HOMO level of the benzoic acid moiety, with a threshold at around -8.9 eV. This in turn provides a basis for developing novel fluorescence probes with fluorescein-derived structure. Still much remains to justify the fluorescent probes in NO bioimaging.

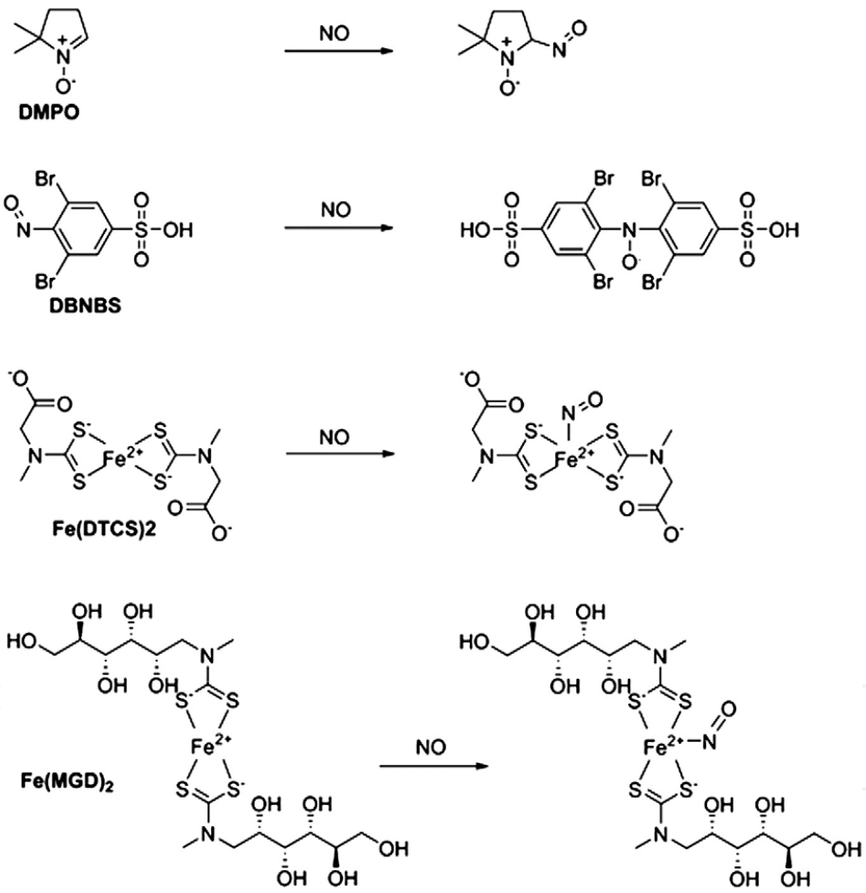

Fig. 8. Representative spin-trapping agents for EPR imaging of NO.

$Fe(MGD)_2$ or $Fe(DETC)_2$ have also been tested for EPR imaging to map the spatial distribution of NO generation in the ischemic myocardium [Kuppusamy, et al. 1996]. Subsequently, $Fe(MGD)_2$ was used in both EPR and MR imaging in rats with sepsis shock [Fujii, et al.1999]. It was reported that $Fe(MGD)_2$ can reduce nitrite to NO at physiological pH, which may cause some detection Inaccuracy as shown in Figure 8, although the rate

constant is quite slow (1–5 M^{-2} s^{-1}) [Tsuchiya, et al. 2000]. $Fe(DETC)_2$ has been used for imaging vascular NO production in rabbits [Kleschyov, et al. 2000], animal brain injury [Ziaja, et al. 2007], vascular disease [Khoo, et al. 2004], and even in plants [Xu, et al. 2004, Vanin, et al. 2007]. Heme proteins, such as myoglobin, cytochrome c, and catalase, have been used as NO-trapping agents in various biological specimens[Kleschyov, et al. 2000]. Although the EPR signals of heme–NO species can be observed in tissues exposed to elevated levels of NO, it is almost impossible to discriminate between the individual nitrosylated heme proteins due to overlapping of the signal. Generally, the dominant heme–NO EPR signal belongs to the major heme protein expressed in the tissue (e.g., myoglobin in the heart [Konorev, et al. 1996]). The most frequently used heme protein in EPR research is hemoglobin (Hb) [Kosaka, et al. 1994], which can interact with NO to generate several paramagnetic Hb–NO derivatives detectable by EPR spectroscopy [Picknova, et al. 2005]. Different preparations of deoxy-Hb have been used for NO trapping in isolated cells and organelles [Kozlov, et al. 1996].

3.3 NO imaging and fluorescent dyes

Several fluorescence indicators for direct detection of NO have been generated, which might be useful for in vitro or in vivo NO-imaging. These substances interact with NO to form a fluorescent complex. Several fluorescent dyes have been developed, which can be used for NO bioimaging. However, several of these promising fluorescent dyes have been found not to be very specific such as 2′,7′-dichlorofluorescein (DCF) or to be cytotoxic such as 2,3-diaminonaphthalene (DAN). Of specific mention, iron (II) N-(dithiocarboxyl) sarcosine($Fe(DTCS)_2$; Fig. 5) trapping agents within 1 h after injection of the spin trap generated stable signal which indicated that the formation of the steady-state free radical had reached equilibrium. The same trapping agent was also tested for NO imaging in lipopolysaccharide-treated mice [Quaresima, et al. 1996]. Subsequently, EPR measurements and EPR-CT (CT denotes computed tomography) imaging with $Fe(DTCS)_2$ were carried out in live mice [Yokoyama, et al. 1997]. The use of $Fe(DTCS)_2$ resulted in a clear EPR-CT image showing high intensity areas in the ventral regions, while other NO-bound iron complexes such as Nmethyl-D-glucamine dithiocarbamate ($Fe(MGD)_2$; Fig. 5) or N,Ndiethyl-dithiocarbamate ($Fe(DETC)_2$) gave much lower signal-to-noise ratios. Several compounds such as 5,5-dimethyl-1-pyrroline N-oxide (DMPO; Fig. 5), α-phenyl-N-tert-butylnitrone(PBN), or 3,5-dibromo-4-nitrosobenzene sulfonate (DBNBS), NO cheletopic traps (NOCTs), aci anions of nitroalkanes, iron (II)–dithiocarbamate(DTC) complex and(DAFs) are fluorescein derivatives. DAFs themselves scarcely fluoresce while DAF-Ts are strong fluorescent compounds. However, the mechanisms accounting for the diminution of fluorescence in DAFs and fluorescence enhancement in DAF-Ts remain unclear.Other fluorescent $Fe(DTCS)_2$ and Cobalt based dyes have been tested in some cell culture systems, but these substances have not been tested in in vivo or in vitro acute brain slice preparations or tissues [von Bohlen, et al. 2003, Zhou, et al. 2009]. Until now, several other fluorescent dyes have been promising candidates for the evaluation of the temporal and spatial aspects of NO generation and distribution even under microscopic observation, including diaminofluoresceins (DAFC), diaminorhodamines (DAR), diaminoanthraquinone (DAQ), fluorescent resonance energy transfer (FRET) and the "fluorescent nitric oxide cheletropic traps" as shown in Table 3 [von Bohlen, et al. 2003, Zhou, et al. 2009].

In following section, we will summarize the progress to date on multimodality imaging of NO and NOS expression and address future research directions and obstacles for NO/NOS imaging using biosensors as outlined in Figure 9. For interested readers, basic methods of NO detection and imaging are given in Appendix in then end of this chapter.

- **Fluorescence imaging of NO**:
  2,7-dichlorofluorescin was introduced for NO detection. When it is oxidized by NO, a fluorescent compound (dichlorofluorescein) is formed. Besides a relatively poor detection sensitivity (~ 10 μM of NO), 2,7-dichlorofluorescein also has very low specificity for NO. Later several iron (II) complexes, fluorescently labeled cytochrome c (a hemoprotein that binds NO selectively), cobalt complexes and fluorescent NO cheletropic traps (FNOCTs) were introduced. The iron(II) complex of quinoline pendant cyclam has fluorescence emission at 460 nm, which can be quenched effectively by NO from NO releasing agents. 2,2,6,6-tetramethylpiperidine-N-oxyl (TEMPO) labeled with acridine and Fe(II)-(N-(dithiocarboxy) sarcosine)$_2$ complex (Fe(DTCS)$_2$) (Fig.5), was developed. The addition of an NO-releasing reagent causes a decrease in the fluorescence signal due to the irreversible binding of NO to the Fe(II).
- DAFCs are the most successful and extensively investigated agents for NO imaging. In vivo imaging of NO in whole living vertebrate with the DAF compounds was reported, where diaminofluorophore 4-amino-5-methylamino-2′-7′-difluorofluorescein diacetate (DAF-FM-DA) was used to detect NO production sites in the zebrafish Danio rerio. The specificity of the fluorescent signal was confirmed by a decrease in animals exposed to a NO scavenger or a NOS inhibitor, as well as an increase in the presence of a NO donor. Local changes in NO production in response to stressful conditions could also be imaged by this agent, suggesting that DAF-FM-DA can be used to monitor changes in NO production which may have future applications in drug screening and molecular pharmacology. Best example of NO imaging in vivo with the DAF compound in zebrafish is quite transparent. The major limitation of the DAF-2 compound is that it is not specific to NO because it can also react with dehydroascorbic acid (DHA) and ascorbic acid (AA) to generate new compounds that have fluorescence emission profiles similar to that of DAF-2T.
- Similar to DAF and DAR, rhodamine fluorophore was developed and it was termed “the DAR”. To image NO in living cells, DARs should be membrane permeable. Therefore, an ethyl group was introduced into the carboxyl group of DAR-1 (4,5-diamino-N,N,N′,N′-tetra ethyl rhodamine), anticipating that the ethyl ester would be hydrolyzed by cytosolic esterases after permeation through the cell membrane [Kojima et al. 2001].
- New class of DAQ compounds of DAFC family called diaminocyanines (DACs) were prepared with a tricarbocyanine as the NIR fluorophore and o-phenylenediamine as the NO sensitive fluorescence modulator. It was reported that these compounds can react faster with NO than the DAFs and the reaction efficiency was at least 50 times higher than that of DAF-2. Although it was demonstrated that NO can be imaged in isolated rat kidneys, in vivo imaging of NO using these compounds has not been reported.
- A new class of difluoroboradiaza-s-indacene-based agents have been widely used in the detection of NO in cells or tissues [Huang, et al. 2002a]. One of these compounds, 1,3,5,7-tetramethyl-8-(4′-aminophenyl-N-(2″-amino)-phenzyl)-difluoroboradiaza-s-indacene (TMAPABODIPY), was shown to have high photostability, high sensitivity (detection limit is 5 nMof NO), and no pH dependency over a wide pH range (see

Figure 9). Subsequently, a similar compound, 1,3,5,7-tetramethyl-2,6-dicarbethoxy-8-(3′,4′diaminophenyldifluoroboradiaza-s-indacene (TMDCDABODIPY), was applied for real-time imaging of NO in cells [Huang, et al. 2002b].

	MGD	DAF	DAR	DAQ
Emission (color)	~520 nm (green)	~515 nm(green)	>580 nm(red)	460 nm(blue)
Excitation	~460 nm	~495 nm	~550 nm	~520 nm
Reacts with ROS	Generates	No	--	No
Tested in neurotoxic tissues	No	Yes	No	Yes
Neurotoxic	--	No	--	No

Table 3. Properties of fluorescent NO-indicators

- In copper-based fluorescent compounds copper (II) is coordinated with certain fluorophores, the base-catalyzed reaction with NO leads to the reduction of the metal center and the intramolecular nitrosylation of a secondary amine. Based on this mechanism, a series of fluophore coordinated copper (II) complexes were designed for NO imaging [Lim, 2007]. Reduction of the Cu (II) core by NO to Cu(I) with nitrosation of the fluorescent ligand is accompanied by bright fluorescence emission. Any nitrogen/oxygen reactive species or ascorbic acid do not cause any significant fluorescence alteration in Cu(II)-based agents. Cu(II) complexes are quite successful in NO imaging in cell culture but they have not been tested in vivo likely due to the suboptimal emission wavelength, the potential toxicity, and the poor in vivo stability of the Cu(II) complex. Recently, several benzimidazole derivatives have been tested in vivo for NO imaging [Quyang, et al. 2008]. The fluorescent 5′-chloro-2-(2′-hydroxyphenyl)-1H-naphtho[2,3-d]imidazol and 4-methoxy-2-(1H-naphtho [2,3-d]imidazol-2-yl)phenol can coordinate with Cu(II) to form a nonfluorescent coordination compound, which can detect NO production in inflammation with a turn-on fluorescence. NO production was imaged successfully in both activated murine macrophages and an acute severe hepatic injury (ASHI) mouse model. Although these agents represent the first successful attempt of in vivo fluorescence imaging of NO, the actual imaging was performed ex vivo on frozen tissue slices due to the suboptimal fluorescence emission wavelength as shown in Figure 10. Much further optimization of these Cu(II)-based agents will be needed in the future, in particular fluorescence emission in the NIR range and reduction of the toxicity.
- Imaging NO/NOS with FRET: FRET agents react with NO covalently a irreversible sensors for NO. Further, some of the organic dyes can accumulate in subcellular membranes and emit fluorescence signals in an NO-independent manner which can cause significant background signal and interfere with the detection of NO. To overcome these limitations, a NO-selective sensor with the heme domain of soluble guanylate cyclase (sGC) was developed [Barker, et al. 1999]. The heme domain of the sGC was labeled with a fluorescent dye and domain changes in the fluorescence intensity of the dye based on the sGC heme domain's characteristic binding of NO. It was found that these sensors have fast, linear, and reversible responses to NO unaffected by other radical species. However, the detection limit is only about 10 μM of NO which makes less useful.

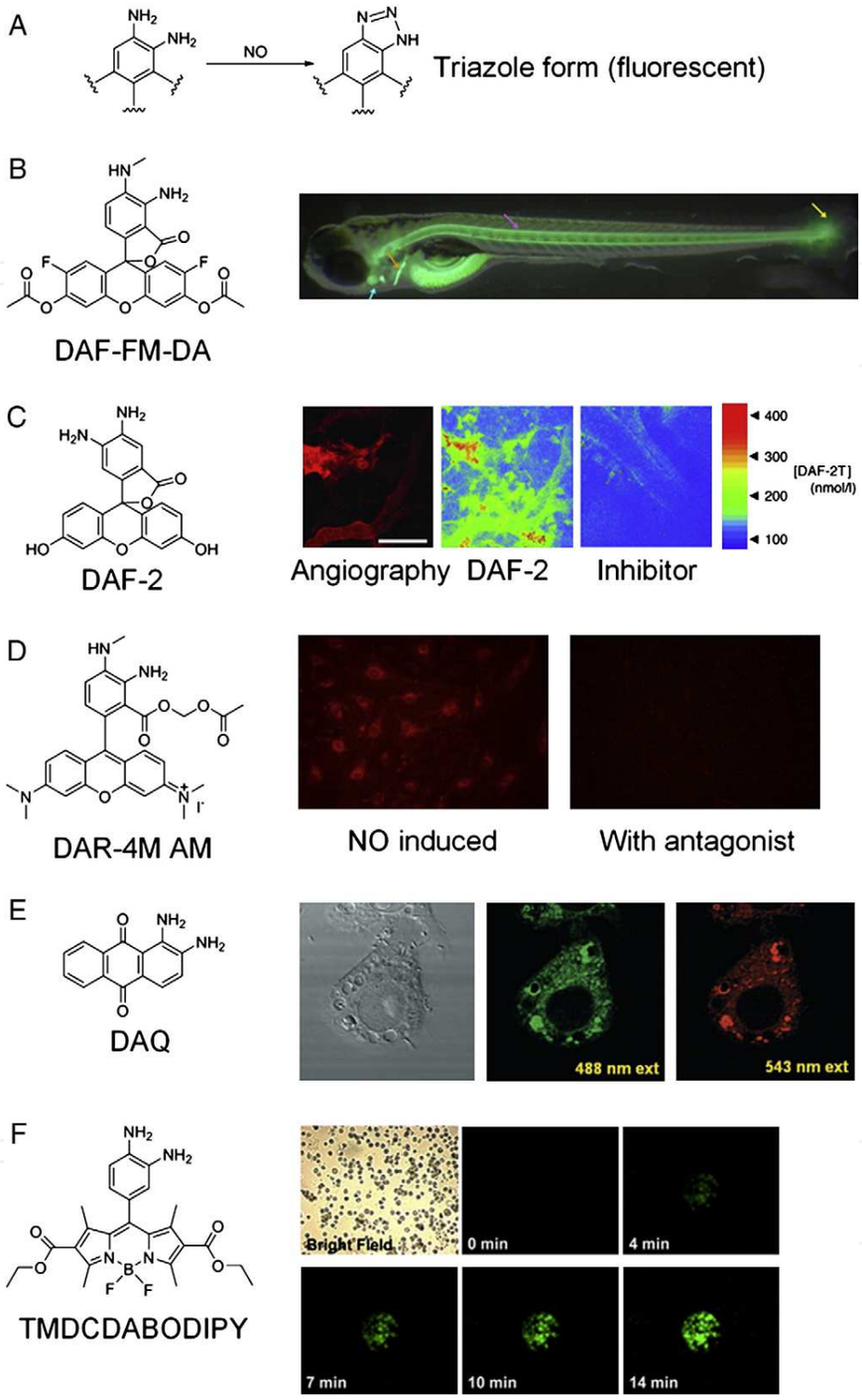

Fig. 9. Imaging NO with diamino-aromatic fluorescent compounds. (A) The general reaction that leads to NO detection by fluorescence with this class of agents.
(B) Fluorescence image of live zebrafish larvae loaded with DAF-FM-DA. Blue arrow, heart; orange arrow, the cleithrum; purple arrow, the notochord; yellow arrow, the caudal fin.
(C) Distribution of NO in B16F10 tumors grown in the cranial window in mouse. Left: microangiography using tetramethylrhodamine-dextran; middle: representative

microfluorography captured 1 h after the loading of DAF-2 in tumors; right: The animals were treated with NOS inhibitor. Color bar shows calibration of the fluorescence intensity with known concentrations of DAF- 2T. (D) Left: fluorescent image of endothelial cells with DAR-4M AM at 10 min after the stimulation. Right: an antagonist of the stimuli strongly abolished the fluorescence intensity. (E) Confocal laser fluorescence microscopy image of cells loaded with DAQ and stimulated to produce NO. Left: bright-field; middle: 488 nm excitation; right: 543 nm excitation. (F) Bright-field and fluorescence images of activated PC12 cells loaded with TMDCDABODIPY in the presence of arginine. Adapted from [Huang, et al. 2007a, 2007b].

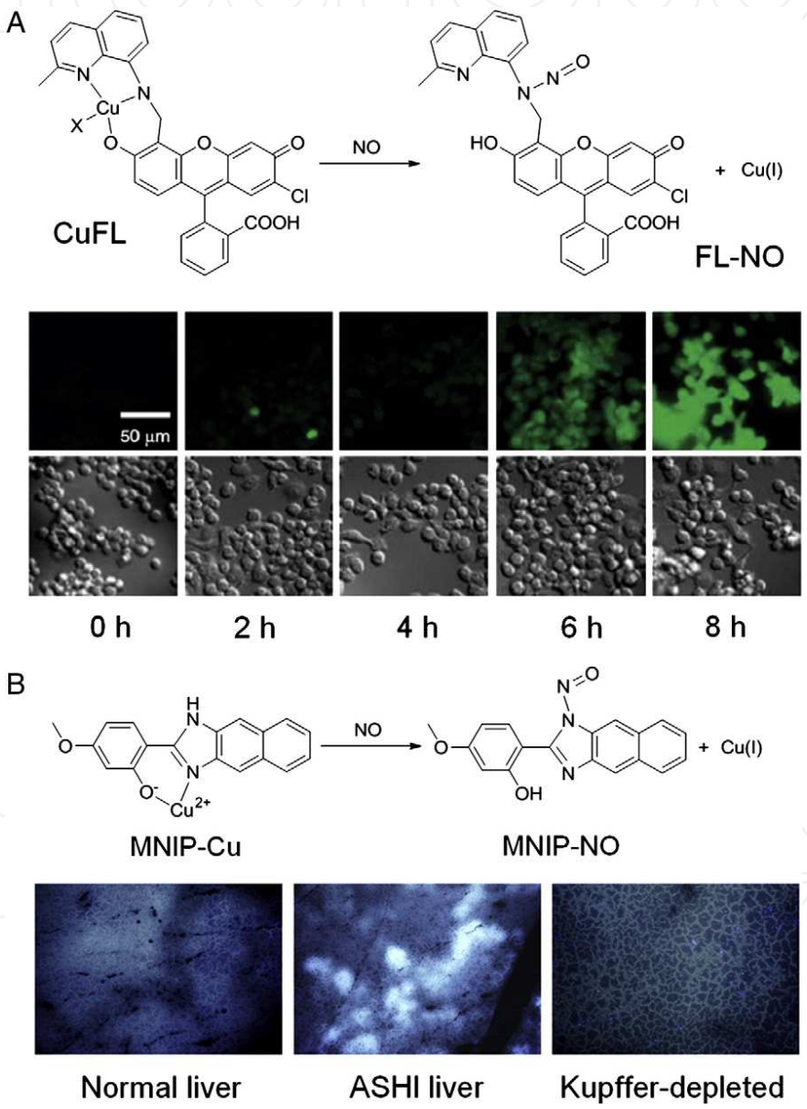

Fig. 10. Copper-based fluorescence imaging of NO. (A) CuFL detection of NO produced by iNOS in macrophage cells after different time of incubation. Top: fluorescence images; Bottom, bright-field images. (B) Fluorescence images of excised liver slices harvested from live animals after intravenous injection MNIP-Cu. Left: normal mouse liver; center: ASHI liver; right: Kupffer cell-depleted ASHI liver. Adapted from reference [Quyang, et al. 2008].

Subsequently, a genetically encoded fluorescent indicator for NO was developed based on FRET, which can reversibly detects NO with high sensitivity (detection limit of 0.1 nM) and visualizes the nanomolar dynamics of NO in single living cells on NO induction [Jares-Erijman, et al. 2003]. However, this approach requires genetic encoding and it generates the biologically active molecule cyclic guanosine monophosphate (cGMP), which can induce other cellular responses. The cGMP molecules can bind to both the NO-associated and the No free probe, resulting in an increase in fluorescence. Therefore, the signal generated is a reflection of the intracellular concentration of cGMP rather than that of NO per se. Recently, the use of confocal based spectral imaging with NO-sensitive FRET reporters enabled NO imaging in the vasculature of intact, isolated perfused mouse lung[St Croix, et al. 2008]. Using calibration spectra, it is possible to unambiguously separate the cross-talk between overlapping donor and acceptor emissions. Overall, FRET is a very powerful technique in cell-based experiments but with only very limited potential applications in animal studies as shown in Figure 11.

3.4 NO bioimaging by bioluminescence and chemiluminescence imaging

The major application of chemiluminescence in NO imaging/ detection lies in gas phase or liquid phase measurements[Taha, et al. 2003]. The major chemiluminescence activators for NO imaging include ozone, luminol, and lucigenin. Gas phase chemiluminescence detection of NO is generally based on the reaction of NO with ozone to produce excited-state nitrogen dioxide. When it returns to the normal state, light is emitted at about 600 nm wavelength. Such gas phase detection has been widely used for measuring NO in exhaled breath to detect inflammatory diseases of the lung. Gas phase chemiluminescence detection has very high specificity, as well as extreme sensitivity, which can reach parts per billion (ppb). However, drawbacks include inconvenient instrumentation, high cost, and timeconsuming detection procedure. To overcome these problems, an optimized chemiluminescence detection system for NO was developed. For liquid phase chemiluminescence imaging of NO, currently the luminol/H_2O_2 detection system is the most useful [Robinson, et al. 1999]. Alkaline luminol can react with NO to generate luminescence. The presence of H_2O_2 as an activator can enhance the sensitivity by about 20-fold. Two approaches have been used for luminol/H_2O_2-based imaging of NO. In the first approach, the sample is directly added to the luminol/H_2O_2 mixture. This strategy can detect very low levels of NO, which is quite useful for visualizing the production of NO from cells or organs, but it lacks NO specificity since luminol can react with many free radical species. In the second strategy, a selective dialysis membrane is placed between the sample and the luminol/H_2O_2 mixture. This procedure can offer better specificity yet it suffers from poor sensitivity, slow response time, and undesirable NO detection limit (μM level). Besides ozone and luminol, lucigenin is can also be used for NO detection. Lucigenin has been widely used as a chemiluminescent substrate to monitor vascular superoxide formation. In particular, lucigenin at a concentration of 5 μM could be used as an indirect probe to estimate basal vascular NO release. Generally, chemiluminescence is a very sensitive method for NO imaging/detection. However, the disadvantages such as low specificity and time-consuming procedure make chemiluminescence not very useful as an independent technique for NO imaging/detection.

Several other imaging techniques have been investigated for NO detection. As an important component of molecular imaging, ultrasound is not inherently suitable for direct NO imaging, although it can be used for evaluating the endothelial function or vasodilation

caused by NO [Heiss, et al. 2008]. It is worth noting that ultrasound at different frequencies can stimulate NO production in different contexts such as in endothelial cells, osteoblasts, and vascular dilation. A few other techniques such as time-resolved photoion and photoelectron imaging, Hb spectral alteration imaging, laser induced fluorescence detection (LIF), and calcium amplification imaging have also been studied for NO detection. In particular, LIF imaging was able to detect the NO release in a single cell, which makes it a very powerful tool for studying the kinetics of NO release by neuronal cells during neurotransmission. PET imaging of anesthetized dogs with inhaled radiolabeled ^{13}NO has been performed to study the in vivo kinetics of NO [McCarthy, et al. 1996]. In future, molecular imaging may provide more accurate information on NO in intact living systems. EPR-CT [Yokoyama, et al. 1997], EPR-MRI [Berliner, et al. 2004], and EPR-chemiluminescence imaging [Nagano, 2002] have all been attempted and much further research/optimization will be needed before any potential clinical investigation can be in place.

3.5 Multimodal bioimaging of NOS gene expression

Initially NOS was considered a sole enzyme to produce NO. Nitric oxide synthase (NOS) is also under extensive investigation [Crowell et al. 2003]. NO is biosynthesized as three distinct mammalian NOS isoforms shown in section 1. Neuronal NOS (nNOS or NOS I) and endothelial NOS (eNOS or NOS III) are constitutively expressed in neuronal and endothelial cells, respectively and both are referred to as cNOS. Inducible NOS (iNOS or NOS II) is expressed in cells involved in inflammation, such as macrophages and microglias when stimulated by cytokines and/or endotoxins. Although cNOS and iNOS do not have a significant difference in activity (both function through NO), cNOS expression can be stimulated by Ca^{2+} whereas iNOS activity is Ca^{2+}-independent. Generally, the NO levels produced by cNOS in stimulated endothelial and neuronal cells are much lower (in nanomolar [nM] range) than those generated by iNOS in macrophages (micromolar [μM] range). Aside from NOS synthesis, recent studies have pointed out that nitrite reduction can also serve as a possible source of biologically relevant NO [Gladwin, et al. 2005]. Excessive production of NO is believed to be responsible for various pathophysiologies, while very low levels of NO are needed to maintain normal physiological conditions. Since the production of NO is closely associated with the expression of NOS, blocking NOS expression is a more convenient approach to inhibit the function of NO than intervention through NO itself.

Molecular imaging refers to the characterization of NO/NOS and measurement of biological processes at the molecular level [Massoud, et al. 2003]. It takes advantage of traditional diagnostic imaging techniques and introduces molecular probes to measure the expression of indicative molecular markers at different stages of diseases. Molecular imaging modalities include molecular magnetic resonance imaging (MRI), magnetic resonance spectroscopy (MRS), optical imaging, targeted ultrasound, single photon emission computed tomography (SPECT), and positron emission tomography (PET). Many hybrid systems that combine two or more of these modalities are already commercially available and certain others are under active development. Molecular imaging can give whole body readout in an intact system at the cost of less workload, inexpansive drug development trial, and provide more statistically relevant results since longitudinal studies can be performed

in the same subjects [Cai, et al. 2008a, 2008b]. In the clinical setting, molecular imaging can significantly aid in early lesion detection, patient stratification, and treatment monitoring, which can allow for much earlier diagnosis, earlier treatment, better prognosis, and individualized patient management. To date, the multimodal imaging modalities for visualization of NO include optical imaging (fluorescence and chemiluminescence), electron paramagnetic resonance (EPR) imaging, and MRI. Meanwhile, NOS has been mainly investigated using optical and PET imaging. In following section, we describe recently developed multimodal techniques in their infancy.

3.5.1 Optical imaging of NOS expression

Imaging enzyme expression and function is quite challenging. Compared to the vast number of literature reports on NO imaging, much less effort has been directed toward NOS imaging. Briefly, the major modalities for NOS imaging include optical imaging, PET, and some other techniques such as electron microscopy. Historically, the study of NOS physiology was constrained by the lack of suitable probes to detect NOS in living cells or animals. In one pioneering study, a fluorescent iNOS inhibitor, pyrimidine imidazole FITC (PIF), was developed and investigated for microscopy of iNOS in living cells [Panda, et al.2005]. It is an isoform-selective molecule with high affinity to iNOS and the binding is essentially irreversible, which allowed for iNOS imaging in many cell types as well as freshly obtained human lung epithelium. This study indicated that fluorescent probes (e.g., PIF) can be valuable for studying iNOS cell biology and understanding the pathophysiology of diseases that involve dysfunctional iNOS expression. In another report, immunofluorescence staining was performed to evaluate nNOS expression on left inferior alveolar nerve (IAN) injury in ferrets [Davies, et al. 2004]. A possible translocation of nNOS protein from the cell body to the site of nerve injury was proposed. Lastly, some ruthenium(II) and rhenium(I)-diimine wires were reported to be capable of binding to iNOS in vitro to generate NIR fluorescence (710 nm emission), which may potentially be useful as a fluorescent imaging probe for iNOS [Dunn, et al. 2005]. The inflammatory modulating effects of iNOS on laser therapy were studied using bioluminescence imaging (BLI) [Moriyama, et al. 2005]. In this study, the efficiency of different wavelengths laser therapy at different wavelengths in modulating iNOS expression was determined using transgenic animals with a luciferase gene driven by the iNOS gene. On induction of inflammation followed by laser treatment, imaging of iNOS expression was performed at various times by measuring the bioluminescence signal. When compared with the nonirradiated animals, a significant increase in the bioluminescence signal was observed after laser irradiation which demonstrated that iNOS expression can be detected by noninvasive BLI. Comparing the two strategies for NOS imaging with optical techniques, many fluorescently labeled NOS inhibitors have charges which makes them not cell membrane permeable. NOS-controlled luciferase expression appears to be a preferable choice, yet much further optimization will be needed in future studies. Generally speaking, the limited penetration of light in tissue renders optical imaging only suitable for a limited number of scenarios (e.g., superficial regions-of-interest and endoscopy-accessible tissues). Another drawback of optical imaging is that it cannot give accurate quantitative analysis of the imaging result. Combination of quantum dot optical and radionuclide-based imaging techniques (e.g., PET) may significantly help in this aspect [Cai, et al.2007a, 2007b].

3.5.2 PET imaging of NOS expression

Small animal PET scanners have very good spatial resolution (1 mm) and they are also becoming increasingly widely available. PET does not have a tissue penetration issue, it is highly quantitative, and it can be used for both diagnosis and treatment monitoring. To date, PET imaging of NOS expression has been focused on the clarification of nNOS function in neurological diseases [Pomper, et al. 2000, Zhang, et al. 1997]. PET imaging of nNOS was initially investigated with a ^{11}C-labeled nNOS inhibitor, S-methyl-L-thiocitrulline (MTICU) (FIG 11, 12) [Zhang, et al. 1997]. Biodistribution of ^{11}C-MTICU gave a brain-to-blood ratio of 1:2 at 30 min postinjection. Uptake in the cerebellum (high nNOS expression) was 20% higher than that of the cortex or the brain stem (low nNOS expression). Blockage using 1 mg/kg of MTICU was able to reduce the uptake in the cerebellum and the cortex, but not in the brain stem. Study demonstrated the potential of ^{11}CMTICU as a potentially useful tracer in determining nNOS levels in vivo. In another report, two nNOS-selective PET tracers, AR-R 17443 [N-(4-(2-(phenylmethyl) (methyl)-amino)ethyl)phenyl)-2-thiophenecarboximidamide)] and AR-R 18512 [(N(2-methyl-1,2,3,4-tetrahydroisoquinoline-7-yl)-2 thiophenecarboximidamide)] were synthesized and evaluated in rodents and primates [Pomper et al. 2000]. Another strategy has been employed for iNOS imaging using antisense oligonucleotide with hybridization properties for iNOS mRNA using RT-PCR. The oligonucleotide was then labeled with ^{18}F (FIG 12) [de Varies, et al. 2004]. Cellular uptake or efflux showed no selectivity for iNOS expressing cells. Thus PET imaging of NOS expression has not been very successful which is likely due to several reasons. First, the expression of NOS is in the cytoplasm. Although the radiolabeled NOS inhibitors usually have high affinity for NOS, they may not permeate through cell membrane efficiently which dramatically affects the tracer uptake. Second, the specificity of these NOS inhibitors may not be high enough for imaging applications; many of them can undergo nonspecific adsorption to other proteins such as albumin. Third, the stability of those tracers in vivo is a major concern. Uptake in the tumor or other targeted organs may not truly reflect the distribution of the intact tracer. Lastly, these NOS inhibitors are small molecules. Although replacing the $^{12}CH_3$ with $^{11}CH_3$ will not change the chemical structure, in many cases this cannot be achieved. Recently, a novel NOS inhibitor design strategy, termed the "anchored plasticity approach," may give rise to novel NOS inhibitors for PET imaging applications in the future [Garcin et al. 2008].

3.5.3 Imaging NOS expression with other techniques

Besides optical and PET imaging, other techniques have been explored for NOS-related research, mainly electron microscopy and immunohistochemistry [Heinrich, et al. 2005, Lajoix, et al. 2006]. Electron microscopy was applied to visualize the subcellular localization of NOS in different cell organelles using gold particles conjugated with anti-NOS antibodies, which gave exquisite distribution information of NOS in cells. Immunohistochemistry also uses anti-NOS antibodies, easier to perform than electron microscopy yet the resolution is not as high. Both approaches are invasive and not suitable for in vivo imaging; however, the experimental findings are typically quite reliable and thus they can serve as ex vivo validation for in vivo imaging studies.

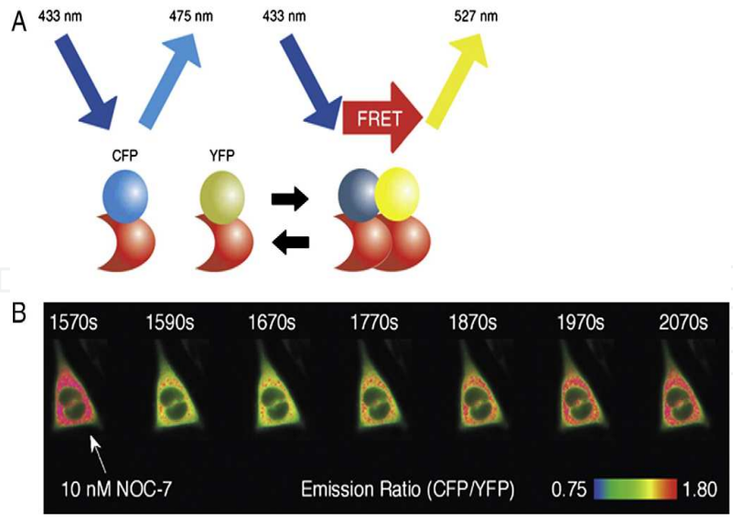

Fig. 11. (on left) Imaging NO with FRET. (A) Basic principles of FRET between CFP and YFP. CFP: cyan fluorescent protein; YFP: yellow fluorescent protein. (B) Pseudocolor images of the CFP/YFP emission ratio of the cell before (1570 s) and after addition of NOC-7, an NO-donating reagent that releases 2 mol of NO per mole. Adapted from reference [Hong et al. 2009]

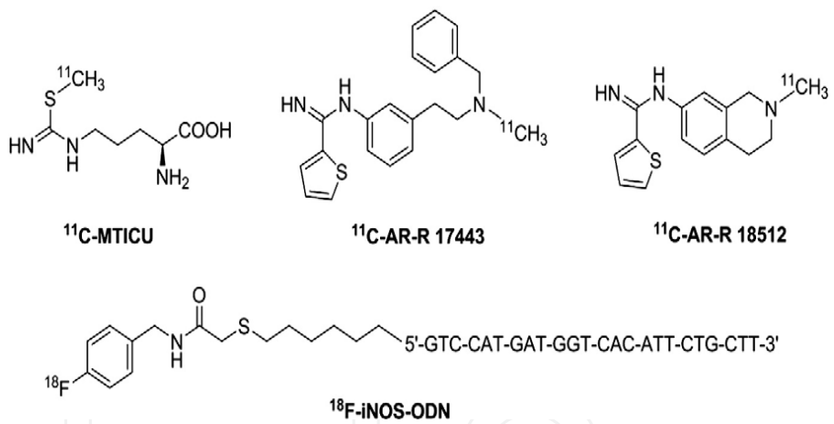

Fig. 12. (on right) Several NOS inhibiters and an antisense oligonucleotide for iNOS mRNA have been radiolabeled for PET imaging of NOS expression.Adapted from reference [Hong, et al. 2009]

4. Biological applications of NO imaging

Still development and applications of fluorescent agents in cell imaging and NO sensitive MRI contrast agents for in vivo physiological fMRI are in infancy. MRI imaging of NO based on nitrite concentration can detect physiological changes such as cerebral blood volume change in nonischemic spontaneously hypertensive rats [Caramia et al. 1998], increase in tumor blood flow and partial oxygen pressure after NO donor administration [Jordan et al. 2000], NO production alteration in humans after a 30-min exposure to a 1.5 T magnetic field [Sirmatel, et al. 2007]. Interestingly, high magnetic strength can cause NO concentration fluctuations during a MRI scanning of NO-related diseases.

The major advantages of MRI include high resolution, good soft tissue contrast, wide availability, sufficiently large field-of-view, and the ability to provide both functional and anatomical information. Nitric oxide bioimaging has emerged as technique to visualize the intracellular metabolism based on redox reactions, mitochondrial oxidation and nitric oxide synthase enzyme NOSi [Anbar, 2000, Zhao, et al. 2009]. Recently, nitric oxide was invented as active mechanism to play role in vascular physiology in lungs, kidney, heart, brain, sex organs. Endothelial cell, smooth muscle cells, oxygenation and perfusion, hypoxia, ischemia are the possible targets of nitric oxide biotransformation. These physiological changes are likely to be visualized by nitric oxide bioimaging in real time manner and reviewed in the following sections.

4.1 Cardiovascular and endothelial cell injury

DAF-FM is useful tool to visualize the temporal and spatial distribution of intracellular NO. Endogenous ATP plays a central role in HTS-induced NOS in endothelial cell injury. Endothelial cNOS, a calmodulin-dependent enzyme is critical for vascular homeostasis and makes detectable basal level of NO production at low extracellular Ca^{2+}. cNOS expression can be stimulated by Ca^{2+} while iNOS activity is Ca^{2+}-independent. Actin microfilaments in primary artery endothelial cells (PAEC) regulates L-arginine transport and this regulation can affect NO production by PAEC, DAR-4M may be useful for bioimaging of samples that have strong autofluorescence [Lai, et al. 1994, Kojima, et al. 2001]

4.2 Apoptosis in cells

Apoptosis plays a key role in many pathological circumstances, such as neurodegenerative diseases. In these processes, the involvement of nitric oxide (NO) has been well established, and the ability of NO to exert cellular damage due to its reactive oxidative properties is perhaps the primary neurotoxic mechanism. Emerging evidences indicate that apoptosis contributes to neuronal death to explain neurodegeneration [Fujii et al. 1997]. The major biochemical change in activation of the cystein protease (caspase-3) was reported to execute apoptosis in the central nervous system disorders such as stroke, spinal cord trauma, head injury and Alzheimer's disease [Green,1998, Nagata,1997]. Although numerous techniques have been described to evaluate apoptosis, these approaches involve invasive techniques and cannot provide detailed information about apoptosis *in vivo* [Anbar, 2000].

4.3 Renal and cardiovascular imaging

A new approach of irreversible responsive PARAmagnetic Chemical Exchange Saturation Transfer (PARACEST) for MRI contrast agents constituted a new type of agent for molecular imaging. A novel PARACEST MRI contrast agent, Yb(III)-(1,4,7,10-tetraazacyclododecane-1,4,7-triacetic acid)-orthoaminoanilide (Yb-DO3A-oAA), was developed to image nitric oxide (NO). The agent exhibited two CEST effects at -11 ppm and +8 ppm chemical shifts, which were assigned to chemical exchange from amide and amine functional groups, respectively. This responsive PARACEST MRI contrast agent indicated the change in the presence of NO and $O_{(2)}$, which caused an irreversible disappearance of both PARACEST effects from MR images. This report highlighted the advantages of irreversible MRI contrast agents and demonstrated that large changes in PARACEST can be used to in vivo

biomedical applications in molecular imaging [Liu, et al. 2007]. In other study, the clinical detection of evolving acute tubular necrosis (ATN) and differentiating it from other causes of renal failure was performed. Herein, sodium magnetic resonance imaging (^{23}Na MRI) was applied to study the early alteration in renal sodium distribution in rat kidneys 6 h after the induction of ATN combined with inhibition of nitric oxide and prostaglandin synthesis. Hence, ^{23}Na MRI non-invasively quantified changes in the corticomedullary sodium gradient in the ATN kidney during morphologic tubular injury [Maril, et al. 2006]. Other newer application of ^{19}F NMR spin-trapping technique for in vivo *NO detection was employed to elucidate the significance of *NO availability in animal models of hypertension. In vivo *NO-induced conversion of the hydroxylamine from fluorinated nitrosyl nitroxide (HNN) to the hydroxylamine of the iminonitroxide (HIN) was evidenced in hypertensive ISIAH and OXYS rat strains [Bobko, et al. 2005]. The NMR detected positive levels of nitrite/nitrate for *in vivo* evaluation of *NO production and provided the basis for in vivo *NO imaging [Kojima, et al. 2001, Kojima, et al. 2001].

The cardiovascular ischemia in tissues generates the nitric oxide (NO). It is an enzyme-independent mechanism of NO generation and more pathogenesis. So, the NO formation in mice after cardiopulmonary arrest could be imaged. Real-time measurement of NO generation was performed by detection of naturally generated NO-heme complexes in tissues using L-band electron paramagnetic resonance (EPR) spectroscopy. Measurements of NO generation were imaged on the intact animal at the levels of the head, thorax, and abdomen within 3 hours [Ueno, et al. 2002]. Very recently, nitric oxide was recognized as biomarker of vascular dysfunction in renal, clitoris and penile sex organs to detect the physiology [Ockalli, et al. 1999, Kakiailatu, 2000, Burnett, 2002, Barouch, et al. 2002, Hillebrandt, et al. 2009, Ciplak, et al. 2009, Gragasin, et al. 2004, Richards, et al. 2003]. The NO complexes were found to have maximum levels in lung, heart, and liver by three-dimensional spatial mapping of the NO complex in the intact animal subjected to cardiopulmonary arrest. The images also confirmed the maximum NO formation in the lungs, heart, and liver [Kuppusamy, et al. 2001].

4.4 Calcium-imaging and NO-imaging

The combined real-time bioimaging of calcium and nitric oxide with continuous electrophysiological intracellular recording has gained enormous interest. For intracellular monitoring by calcium imaging in cells, Fura-2 is a calcium-sensitive fluorescent probe. Using Fura-2, intracellular free calcium ion concentration ($[Ca^{2+}]_i$) of single neurons was measured [Richards, et al. 2003]. Calcium-imaging with Fura-2 was used to monitor and modulate the intracellular Ca^{2+} evoked by NMDA and AMPA in cultured hippocampal pyramidal cells [Keelan, et al. 1999] Calcium and NO play role in excitotoxic mitochondrial depolarization in the hippocampus [Berkels, et al. 2000]. The combination of NO bioimaging with calcium imaging may distinguish the temporal rise in NO and calcium to suggest that NO is being produced as a consequence of Ca^{2+} enhancement and Ca^{2+} induced NO Synthase activity). Recently, imaging intracellular calcium imaging was achieved together with NO imaging by using two monochromators DAF-2 and Fura-2 AM as excitation light source. The DAF-2 excited at 485 nm and Fura-2 AM excited at 340 nm [Berkels, et al. 2000]. The emission maximum of fura-2 is about 510 nm different while the emission maximum of DAF-2 is about 515 nm. By using dichroic or multichroic mirrors calcium and NO levels can

be measured simultaneously [Pittner, et al. 2003]. Other example of monochromator complex is DAQ and DAR-4M AM. These are calcium sensitive non-neurotoxic dyes with unique fluorescent patterns of DAQ (excitation ~520 nm; emission ≥580 nm) and DAR-4M AM (excitation ~ 550 nm; emission ≥ 580 nm). These can also combine with the calcium-sensitive dye Fura-2 as potential tools in fluorescence microscopy.

4.5 Kupffer cell NO bioimaging

A new mechanism was reported in nonparenchymal cells based on Bcl-2/adenovirus EIB 19-kDa interacting protein 3 (BNIP3), a cell death-related member of the Bcl-2 family, was upregulated in vitro and in vivo by nitric oxide (NO) downregulation of BNIP3 gene expression as one mechanism of hepatocyte cell death and liver damage. Authors proposed that inflammatory stresses can lead to the modulation of BNIP3 [Metukuri, et al. 2009].

4.6 Combining electrophysiology and NO-imaging

The calcium-imaging with electrophysiological recording was excitement in the hippocampus imaging art because of calcium accumulation in hippocampus pyramidal cells during synaptic activation [Regehr, et al. 1989]. Now a day, calcium-imaging combined with electrophysiological stimulation and recording has emerged as present state of art of calcium-signaling and intracellular free calcium ion concentration $[Ca^{2+}]_i$ of single neurone. Moreover, little is understood how neuronal signals stimulate NO production. Potential applications of fluorescent NO indicators in bioimaging are to monitor NO in response to pharmacological manipulation using NO-donors, NOS substrate, and NOS or NOS isoform inhibitors as enhancers of NO production in vivo and in vitro [Moore, et al. 1997, Southan, et al. 1996]. Other emerging techniques of bioimaging by NO inhibitor are targeting the differential cofactor requirements of the various isoforms; pharmacological agents targeting the differential substrate requirements of cell expression of various isoforms of the NOS [Salerno, et al. 2002]. However, this approach suffers due to lack a marked isoform selectivity or direct affecting the arginine transport into cells, like N^G-methyl-L-arginine (L-NMA). Other example of NOS inhibitors such as 7-nitroindazole (7-NI), might have unexpected side-effects in neuronal tissues, since 7-NI interferes with monoamine oxidase [Castagnoli, et al. 1999, Desvignes, et al. 1999]. However, selective NOS-inhibitors together with fluorescent NO-imaging appear as useful tools for the investigation of the biological functions of the different NOS-isoforms in neuronal tissues [Chen, et al. 2001, Brown, et al. 1999]. The combined NO-imaging with in vitro electrophysiology methods visualize the NO generation and NO distribution with localization of NO induced by neurotransmitter stimulations, e.g., NO formation after neuronal stimulation with NMDA, in normal synaptic transmission, in paired-pulse facilitation, in long-term depression or LTP. Thus, in a single preparation, the spatial distribution of NO after induction of hippocampal LTP has been evaluated [Schuppe, et al. 2002]. Main unsolved issues of precise time-point of NO release and selective NOS isoform-inhibitors in neuronal activity still remain to investigate before the combined fluorescent NO-imaging and electrophysiology method becomes an acceptable bioimaging tool. In near future, the researchers will thrive to combine electrophysiology with simultaneous calcium-imaging and NO-imaging to get better answers of the role and interaction of calcium and NO in physiological and pathological

neuronal processes with continuous monitoring the calcium and NO by dichroic or multichroic mirrors in synaptic plasticity.

4.7 Alveolar cells

Human alveolar macrophages and alveolar epithelium is the site of nitric oxide synthase-2 (NOS-2) messenger ribonucleic acid (mRNA) and protein expression in alveolar wall in lung of patients with pulmonary malignancies. In the process of NO production, pro-inflammatory cytokines interleukin (IL)-1β, tumour necrosis factor (TNF)-α, interferon (IFN)-γ or lipopolysaccharide (LPS) play significant role to induce the effect of human surfactant protein-A (SP-A) on IFN-γ-mediated NOS-2 mRNA expression [Pechkovsky, et al. 2002].

4.8 Endothelial cells

Kojima et al. 2001, reported NO bioimaging in cultured bovine aortic endothelial cells. The cultured bovine aortic endothelial cells were incubated with DAF-FM DA for 1 h for dye loading. After stimulation with bradykinin, the fluorescence intensity in the cells increased and that in the cytosol increased more than that in the nucleus. NO is produced in the cytosol, where NOS exists [von Bohlan, et al. 2002]. This observation implies that little of the produced NO diffuses into the nucleus or if it does diffuse into the nucleus little of it is oxidized there. The augmentation of the fluorescence intensity was suppressed by an NOS inhibitor. In conclusion, DAF-FM is a useful tool for visualizing the temporal and spatial distribution of intracellular NO. Kimura et al.2001, examined the effects of acute glucose overload on the cellular productivity of NO in bovine aortic endothelial cells (BAEC) using DAF-2. ATP induced an increase in NO production, assessed by DAF-2, mainly due to Ca^{2+} entry as shown in Figure 13. In contrast, the ATP-induced increase in DAF-2 fluorescence was impaired by glucose overload. The results indicate that glucose overload impairs NO production via the O_2^--mediated attenuation of Ca^{2+} entry. In addition, Kimura et al. 2000, examined in detail the mechanism by which mechanical stress induces NOS in endothelium. Hypotonic stress (HTS) induced ATP release, which evoked Ca^{2+} transients in BAEC. HTS also induced NOS, assessed by DAF-2 fluorescence. The results obtained indicate that endogenous ATP plays a central role in HTS-induced NOS in BAEC. Broillet et al. 2001, reported that Ca^{2+}, Mg^{2+}, or incident light promoted the reaction of DAF-2 and NO. However, Nagano et al. 2002, probed that the enhancement of fluorescence intensity was caused not by increasing the reaction rate between DAF-2 and NO but by promotion of NO-releasing rate of NO donors. Endothelial NOS, a Ca^{2+}/calmodulin-dependent enzyme, is critical for vascular homeostasis [Suzuki, et al. 2002]. To determine the signaling pathway for endogenous eNOS, Lin et al. 2000, directly measured NO production in bovine pulmonary artery endothelial cells (PAEC). Endothelial cells grown in a monolayer produce very low levels of NO which are below the detection range of traditional assays. Therefore, they employed DAF-2 DA to measure NO production in real-time. PAEC had detectable basal NO production which increased slightly after thapsigargin treatment in the presence of low extracellular Ca^{2+}. In contrast, a large increase in NO production was detected in the presence of 4 mM extracellular Ca^{2+}, suggesting that capacitative Ca^{2+} entry regulates wild-type eNOS activity. Zharikov et al. 2001, investigated possible involvement of the actin cytoskeleton in the regulation of the L-arginine/NO pathway in pulmonary artery

endothelial cells (PAEC). DAF-2 DA was used for detection of NO in PAEC. They conclude that the state of actin microfilaments in PAEC regulates L-arginine transport and that this regulation can affect NO production by PAEC. Berkels et al. 2000, presented a new method to measure intracellular Ca^{2+} and NO simultaneously in endothelial cells. The method makes it possible to follow intracellular Ca^{2+} and NO distributions online and is sensitive enough to monitor changes of NO formed by the constitutive endothelial NOS. Franz et al. 2000, reported DAR-4M AM applied to imaging of NO in bovine aortic endothelial cells using aminotroponiminates[Franz et al. 2000]. DARs are more photostable than DAFs. The fluorescence in cells was observed after stimulation with bradykinin (see Figure 14), which raises the intracellular Ca^{2+} level and thereby activates NOS, and this increase was suppressed by addition of an NOS inhibitor. DAR-4M should be useful for bioimaging of samples that have strong autofluorescence in the case of 490 nm excitation in which the intracellular pH may fall below 6. Hiratsuka et al. 2009, reported in vivo visualization of nitric oxide and intracellular inflammatory interactions among platelets, leukocytes, and endothelium following hemorrhagic shock and reperfusion.

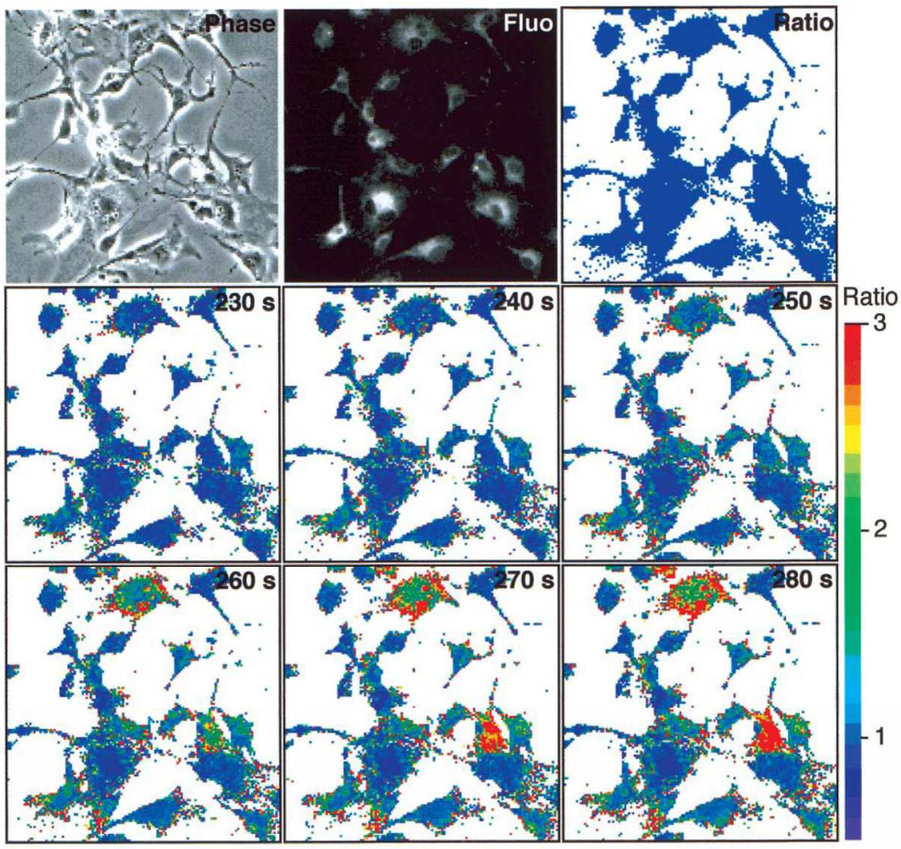

Fig. 13. Bright-field and fluorescence images of cultured bovine aortic endothelial cells loaded with DAR-4M AM. The upper images are the bright-field, the fluorescence, and the fluorescence ratio images at the start of measurement, respectively. The middle and the lower images are fluorescence ratio images at the indicated times after the start of measurement. The fluorescence ratio images indicate the ratio of the intensity to the initial intensity at the start. Adopted from reference Kimura, et al. 2001

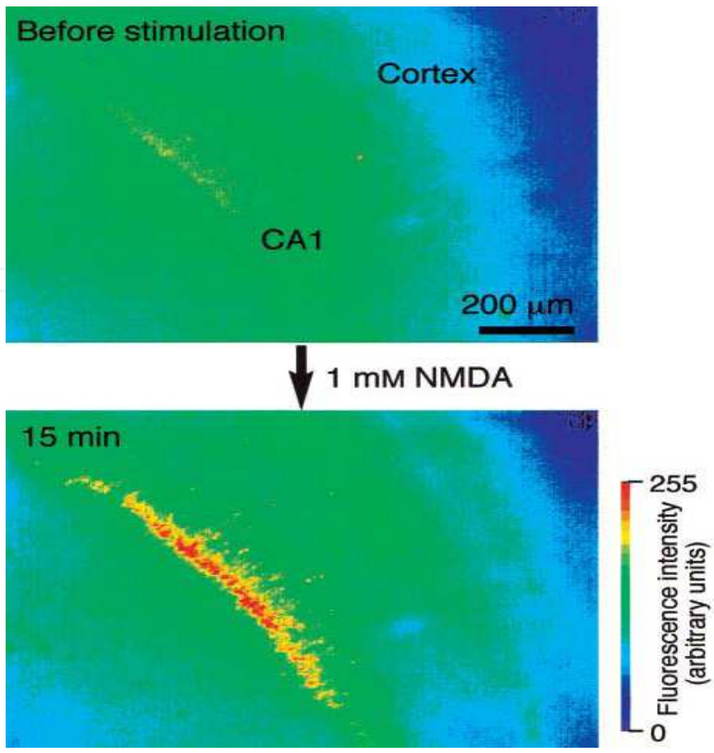

Fig. 14. Fluorescence images of a rat brain slice loaded with DAF-2 DA. The fluorescence intensity is shown in pseudocolor. (Reproduced from reference Nagano, et al. 2002)

4.9 Smooth muscle cells

DAF-2 DA was applied to the imaging of NO in cultured rat aortic smooth muscle cells by using a fluorescence microscope equipped with fluorescence filters for fluorescein chromophores. Confocal laser scanning microscopy indicated that fluorescence was emitted from the whole cell body, including the nucleus. This implies that DAF-2 regenerated intracellularly by esterase is distributed throughout the whole cell. There was no indication of any cell damage caused by loading the dye. The results show that the fluorescence intensity in endotoxin- and cytokine-activated cells increased owing to DAF-2 T production from DAF-2 by reaction with NO. The fluorescence did not increase in inactivated cells, which did not produce NO. The probe is very useful for bioimaging of NO in cultured rat aortic smooth muscle cells. Itoh et al. detected DAF-FM T using reversed-phase high-performance liquid chromatography with a fluorescence detector [Itoh et al. 2000]. This sensitive method enabled them to detect the spontaneous and substance P-induced NO release from isolated porcine coronary arteries, both of which were dependent entirely on the NOS activity in vascular endothelial cells. Furthermore, they obtained fluorescence images of cultured smooth muscle cells of the rat urinary bladder after loading with DAF-FM DA. In the cells pretreated with cytokines, the fluorescence intensity increased with time after DAF-FM loading. In recent studies on imaging of nitric oxide in nitrergic neuromuscular neurotransmission suggested the new insight of molecular mechanisms in animal organs [Thatte, et al. 2009, Perrier, et al. 2009, Di Cesare Mannelli, et al. 2009].

4.10 Brain and neuronal behavior

Reif et al. 2009, reported the influence of functional variant of neuronal nitric oxide synthase on impulsive behaviors in humans. The biological functions of NO in the neuronal system remain controversial. Using DAF-2 DA for direct detection of NO, Nagano et al. 2002, examined both acute rat brain slices and organotypic culture of brain slices to ascertain NO production sites. The fluorescence intensity sensitive to Ca^{++} in the CA1 region of the hippocampus was augmented, especially after stimulation with NMDA, in acute brain slices. This NO production in the CA1 region was also confirmed in cultured hippocampus. Glutamate and NO were important mediators, since antagonists of both N-methyl-D-aspartate (NMDA) and NOS inhibitors were effective in attenuating neurotoxicity. This is the first direct evidence of NO production in the CA1 region as shown in Figure 4. There were also fluorescence cells in the cerebral cortex after stimulation with NMDA. Imaging techniques using DAF-2 DA should be very useful for the clarification of neuronal NO functions. Calcium sensitive fluorescent probe can monitor intracellular calcium by FURA-2. Combined calcium and NO together can be imaged by excitation light source (DAF-2) excited at 485 nm, and Fura-2 AM excited at 340 nm using dichroic or multichroic mirrors.DAQ, DAR-4M AM are other choices. NOS-II may be involved in Alzheimer's disease as b-amyloid induces NOS-II expression in astrocytes Astrocytes which which can be potentiated by cytokines [Vodovotz et al. 1996].

DAF-FM DA was also applied to imaging of NO generated in rat hippocampus slices by exposure to an aglycemic medium [Reif et al. 2009]. NO production was observed mainly in the CA1 area and was dependent on the concentration of O_2. During exposure to an anoxic-aglycemic medium, NO was hardly produced while marked elevation of intracellular Ca^{2+} was observed. Production of NO increased sharply as soon as the perfusate was changed to the normal medium. These results suggest that NOS is activated after reperfusion rather than during ischemia. ROS and NO are important participants in signal transduction that could provide the cellular basis for activity-dependent regulation of neuronal excitability [Yermolaieva, et al. 2000]. In young rat cortical brain slices and undifferentiated PC 12 cells, paired application of depolarization/agonist stimulation and oxidation induces long-lasting potency of subsequent Ca^{2+} signaling that is reversed by hypoxia. This potency critically depends on NO production and involves cellular ROS utilization. Using the fluorescent dye DAF-2, NO production was measured in PC 12 cells during depolarization or histamine application [Yermolaieva, et al. 2000]. Application of 100 μM histamine induced a significant increase in NO production. The crucial role for NO in oxidative potentiation of Ca^{2+} signaling triggered by pairing of electrical/agonist stimulation and oxidation demonstrated here provides an insight into the cellular mechanisms involved in neuronal developmental plasticity. NO could influence its effectors by stimulating the cGMP-dependent signaling pathway and/or by acting as a weak radical. Perrier et al. 2009, reported the effect of uncoupling endothelial nitric oxide synthase on calcium homeostasis in aged porcine endothelial cells in heart. In other report, Sergeant et al. 2009, reported the spontaneous Ca^{2+} waves in rabbit corpus cavernosum were modulated by nitric oxide. Role of cGMP was crucial in regulation of calcium dependent neuroactive energy changes.

4.11 Ion channels

Most voltage-gated Na^+ channels are almost completely inactivated at depolarized membrane potentials, but in some cells a residual Na^+ current is seen that is resistant to

inactivation. The biological signaling mechanisms that regulate the persistence of Na^+ channels are not well understood. Ahern et al. 2000, showed that in nerve terminals and ventricular myocytes, NO reduces the inactivation of Na^+ current. This effect was independent of cGMP and blocked by *N*-ethylmaleimide. Thus, ROS act directly on the channel or a closely associated protein. Application of ionomycin to raise the intracellular Ca^{2+} concentration in myocytes activated NOS. The NO produced in response to ionomycin was detected with DAF-2 DA. They concluded that NO is a potential endogenous regulator of persistent Na^+ current under physiological and pathophysiological conditions. Choi et al. 2000, reported that the NMDA receptor (NMDAR)-associated ion channel is modulated not only by exogenous NO, but also by endogenous NO. They examined inhibition of NMDAR responses by endogenous NO to determine the underlying molecular mechanism. For this purpose, HEK 293 cells transfected with nNOS were transiently transfected with wild-type NR1/NR2A or mutant NR1/NR2A (C399A) receptors. NMDA responses were monitored by digital Ca^{2+} imaging with fura-2. Production of endogenous NO by these HEK-nNOS cells was measured with DAF-2. It was concluded that endogenous *S*-nitrosylation may regulate ion channel activity.

4.12 Fertilization and developmental biology

Kuo et al. 2000, demonstrated that NO is necessary and sufficient for egg activation at fertilization. The early steps that lead to the rise in Ca^{2+} and egg activation at fertilization are unknown but are of great interest, particularly with the advent of in vitro fertilization techniques for treating male infertility and whole-animal cloning by nuclear transfer. They showed that active NOS is present at high concentration in sperm after activation by the acrosome reaction. An increase in nitrosation within eggs is evident seconds after insemination and precedes the Ca^{2+} pulse of fertilization. They used DAF-2 DA for detection of NO. It was concluded that NOS- and NO-related bioactivity satisfy the primary criteria of an egg activator, i.e. they are present in an appropriate place, active at an appropriate time, and necessary and sufficient for successful fertilization.

4.13 Inflammation

NO plays important roles in inflammatory processes. Lopez-Figueroa et al. 2000, examined whether changes in NOS mRNA expression lead to similar temporal and anatomical changes in NO production in an experimental model of CNS inflammation. iNOS mRNA expression was analyzed 2, 4, 6, and 24 h after intracerebroventricular (icv) injection of interleukin-1β or the vehicle. Increased expression of iNOS mRNA was observed surrounding the microinjection site and meninges. Using DAF-2 DA for the direct detection of NO production, they observed a significant increase in NO production after 4 and 6 h. They conclude that increase in iNOS mRNA following icv administration of IL-1β leads to increases in NO production. They proposed that the DAF-2 DA method can be used as a potential marker in the diagnosis of CNS inflammation. MRI of NO is very useful because NO is available at high concentrations in millimolar levels in immune-related diseases (e.g., inflammation).Terashima et al. 2010, reported in vivo detection of iNOS expression in murine carotid lesions by biuoluminescence may provide a valuable approach for monitoring vascular gene expression and inflammation in small animal models. The phasic

nature of inflammation is also associated with a decrease in NOS activity. NOS inhibitors are effective at alleviating pain and have disease modifying effects. Induction of NOS-II is seen in models of septic shock. NOS-II inhibitors (dexamethasone) prevent hypotension and decrease in PO_2.

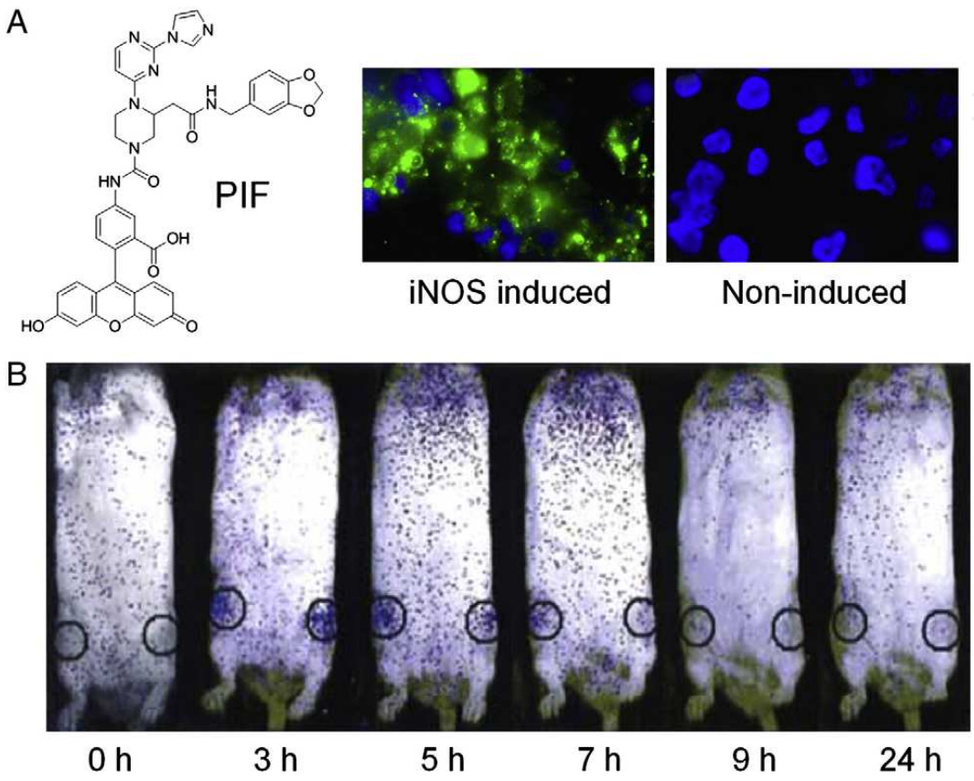

Fig. 15. Optical imaging of iNOS expression. (A) Fluorescence imaging of iNOS in living cells. Left: cells were induced for iNOS expression; Right: cells were not induced for iNOS expression. (B) Bioluminescence signal from the knee joints (circle) indicates iNOS expression following inflammation induction. Adapted from reference [Panda, et al. 2000].

4.14 Adrenal zona glomerulosa

Adrenal zona glomerulosa (ZG) cells do not contain NOS. Hanke et al. 2000, conferred endothelial NOS activity upon adrenal ZG cells through transduction with a recombinant adenovirus encoding the endothelial NOS gene (AdeNOS) to determine the effect of endogenous NO on aldosterone synthesis. AdeNOS-transduced cells exhibited DAF-2 DA fluorescence, which was blocked by pretreatment with an NOS inhibitor. In conclusion, adenovirus-mediated gene transfer of eNOS in ZG cells results in the expression of active endothelial NOS enzyme, and this endogenous NO production by ZG cells decreases aldosterone synthesis.

4.15 Bone marrow stromal cells

Gorbunov et al. 2000, reported that using the reverse transcription-polymerase chain reaction and immunofluorescence analysis of murine bone marrow stromal cells after γ-

irradiation doses of 2-50 Gy stimulated the expression of iNOS. The activation of iNOS was accompanied by an increase in the fluorescence of DAF-2 and accumulation of 3-nitrotyrosine within cellular proteins in a dose-dependent manner.

4.16 Mitochondria

NO has been implicated in the modulation of mitochondrial respiration, membrane potential, and subsequently apoptosis. Although the presence of mitochondrial NOS was reported while there is no direct evidence in vivo of the presence of NO within mitochondria. Using DAF-2 DA, Lopez-Figueroa et al. observed NO production in PC 12 and COS-1 cells by conventional and confocal fluorescence microscopy [Lopez-Figueroa, et al. 2000]. The subcellular distribution of NO production is consistent with the presence of a mitochondrial NOS.

4.17 Retina

In the retina, NO functions in network coupling, light adaptation, neurotransmitter receptor function, and synaptic release. Neuronal NOS is present in the retina of every vertebrate species so far investigated. However, although nNOS can be found in every retinal cell type, little is known about the production of NO in specific cells or about the diffusion of NO within the retina. Blute et al. 2000, used DAF-2 to image real-time NO production in turtle retina in response to stimulation with NMDA. In response to NMDA, NO was produced in somata in the ganglion cell and inner nuclear layers, in synaptic boutons and processes in the inner plexiform layer, in processes in the outer plexiform layer, and in photoreceptor inner segments. They concluded that NO may function at specific synapses, modulate gene expression, or coordinate events throughout the cell. Matsuo et al. 2000, reported that basal NO production is enhanced by hydraulic pressure in cultured human trabecular cell. He measured the intracellular NO level in real-time using DAF-2.

4.18 Drosophila

Wingrove and O'Farrell 1999, reported that *Drosophila* utilizes components of the NO/cGMP signaling pathway to respond to hypoxia. Hypoxic exposure rapidly induced exploratory behavior in larvae and arrested the cell cycle. These behavioral and cellular responses were diminished by an inhibitor of NOS and by a polymorphism of cGMP-dependent protein kinase. Regions of the larvae that specialize in responding to hypoxia should express significant levels of the activities involved. They used DAF-2 DA to define possible foci of function. DAF-2 DA stained the pouch of tissue surrounding the anterior spiracles as well as neuronal-like processes within the pouch. This staining near the openings of the tracheal system is interesting because the location is consistent with a possible role in governing the opening of the spiracles to increase access to oxygen. DAF-2 DA is useful for clarification of response mechanisms to hypoxia.

4.19 Plants

Leaves and callus of *Kalanchoe daigremontiana* and *Taxus brevifolia* were used to investigate NO-induced apoptosis in plant cells [Huang, et al. 2000]. NO production was visualized in cells and tissues with DAF-2 DA. The NO burst preceded a significant increase in nuclear

DNA fragmentation and cell death. L-NMMA significantly decreased NO production and apoptosis in both species. Pedroso et al. 2000a, 2000b concluded that NO is involved in DNA damage leading to cell death and proposed a potential role of NO as a signal molecule in these plants. Foissner et al.2000, used DAF-2 DA, in conjunction with confocal laser scanning microscopy, for in vivo real-time imaging of an elicitor-induced NO burst in tobacco. A growing body of evidence suggests that NO, an important signaling and defense molecule in mammals, plays a key role in activating disease resistance in plants, acting as a signaling molecule and possibly also as a direct antimicrobial agent. The results revealed additional similarities between plant and animal host responses to infection.

5. NO/NOS bioimaging: Future prospects

The existing techniques based on quenching spin trap or paramagnetic heavy metals pose a concern of contrast agent toxicity with limitations of event capturing to generate NO image of isolated cells by EPR or in vivo body image by MGD enhanced MRI. However, unique role of short lived NO molecule in the cell is peculiar to give insight of rapid ionic regulatory mechanisms such as calcium, sodium dependent signaling events including dietary effects, antimicrobial therapy on inflammation, angiogenesis and hypoxia reported in last three years [Manuel, et al. 2002, Palombo, et al. 2009]. To date, the main imaging modalities for visualization of NO include fluorescence and bio/chemiluminescence optical imaging, electron paramagnetic resonance (EPR) imaging, and MRI. cNOS has been mainly investigated using optical and PET imaging. Paper has presented a progress to date on multimodality imaging of NO and addressed the future research directions and obstacles of NO imaging. Other major developments are expected in design of robust imaging hardware with improved image generating capability and highly sensitive to the rapid changes of NO/NOS molecular EPR signal and MRI frequency with time. In this direction, active research efforts suggest the development and availability of less toxic ion sensitive contrast agents attached with EPR and MRI visible molecules as labels sensitive to fluorometric and magnetic resonance techniques respectively. It is attributed that cytochromes are best candidates as fluorochromic agents while lipopolysaccharides and carbamates with paramagnetic agents are potential as MRI contrast agents. More likely, fast imaging techniques such as parallel phase array, SENSE, FISP MRI imaging, xenon based PARACEST techniques may be available to capture rapid NO changes or distribution associated with metabolic short lived events such as oxygen sensitivity, sodium sensitivity in the intact tissue. In future, advances in ionic ratiomatric techniques will be available to capture the short living NO molecular distribution in cells as real-time events associated with motion. Still major issues to resolve are:

- lack of NO sensitive EPR or MRI contrast agent to generate quicker and enough MRI or EPR signal visible as image;
- the EPR and MRI signals are not true representative of NO concentrations;
- the images generated from MRI visible paramagnetic ions or EPR visible spin trap agents may represent several physical and molecular events sensitive to attached NO quenching carbamates or polysaccharides for MRI and cytochrome proteins for EPR.

The biggest disadvantage of MRI is its low molecular sensitivity. The need for a high dose of imaging agents (typically more than 100 mM injection) undoubtedly raises major concerns

about the potential toxicity caused by such studies. Lastly, relatively long data acquisition time is typically needed to generate a detectable MR signal in MR imaging. Since the lifetime of NO and/or related species is usually short, the accuracy of MRI measurement of NO concentration is questionable. After these issues are resolved, it will need sequence of investigations to calibrate linearity of NO concentration and image signal intensity, image reproducibility, image component analysis, signal measurement accuracy and precision of NO sensitive imaging techniques as shown in Table 4.

Target	Modality	Resolution	Sensitivity	Penetration	Clinical potential
NO	Optical	++++	++++	+	Low
NO	EPR	++	++++	+++	Medium
NO	MRI	+++	+	++++	Medium
NO	PET	++	++++	+++	Medium
cNOS	Optical	++++	+++	++	Low
cNOS	PET	+++	++++	++++	Medium-High

Table 4. Comparison of molecular imaging of NO and cNOS expression

5.1 Real-time NO imaging

Nitric oxide (NO) is a small uncharged free radical abundant in nanomolar quantities that is involved in diverse physiological and pathophysiological mechanisms.

- When generated in vascular endothelial cells, NO plays a key role in vascular tone regulation and EPR/optical/MRI visible signals visualize the vascular physiology (induced fitting of L-arginine specific NOS active site) as prosposed by author to inhibit NOS and low NO production shown in Figure 5.

In this direction, short lived NO specific amplifier-coupled fluorescent indicator was reported to visualize physiological nanomolar dynamics of NO in living cells (detection limit of 0.1 nM)[Ueno, et al. 2002, Burnett, et al. 2002]. An amplifier-coupled fluorescent indicator visualizes NO in single living cells. Its domain structures are sGCα, sGCβ, CGY, sGCα-CGY, and sGCβ-CGY. This genetically encoded high-sensitive indicator revealed that ≈1 nM of NO was enough to relax blood vessels [Ueno, et al. 2002, Burnett, et al. 2002, Barouch, et al. 2002, Hillebrand et al. 2009, Ciplak, et al. 2009, Gragasin, et al. 2004]. The nanomolar range of basal endothelial NO thus revealed appeared to be fundamental to vascular homeostasis. A fuorescent probe, 1,3,5,7-tetramethyl-2,6-dicarbethoxy-8-(3,4-diaminophenyl)-diXuoroboradiaza-*s*-indacence (TMDCDABODIPY), produced real-time image NO of PC12 cells, Sf9 cells and human vascular endothelial cells in the presence of L-arginine with inverted fuorescence microscope [Manuel, et al. 2002]. NO production in the cells was successfully captured and imaged with improved temporal and spatial resolution. The bioimaging applications of TMDCDABODIPY as a fuorescent imaging probe for NO in living cells was compared with the other fuorescent imaging probes for NO. The TMDCDABODIPY had the advantages of shorter reaction time, higher photostability and minimal background. The study has indicated that TMDCDABODIPY-based fuorescence microscopy may be a promising approach for NO-related pathological and physiological

studies [Hiratsuka, et al. 2009]. A recent review highlighted the possibilities if nitric oxide bioimaging becomes reality as clinical imaging tool [Hong, et al. 2009]. Current state-of-the-art multimodality imaging may detect NO and NOS enzyme expression [Matter et al. 2004, Zhang, et al. 2011]. Optical (fluorescence, chemiluminescence, and bioluminescence), electron paramagnetic resonance (EPR), magnetic resonance (MR), and positron emission tomography (PET) noninvasive imaging techniques may reveal the biodistribution of NO or

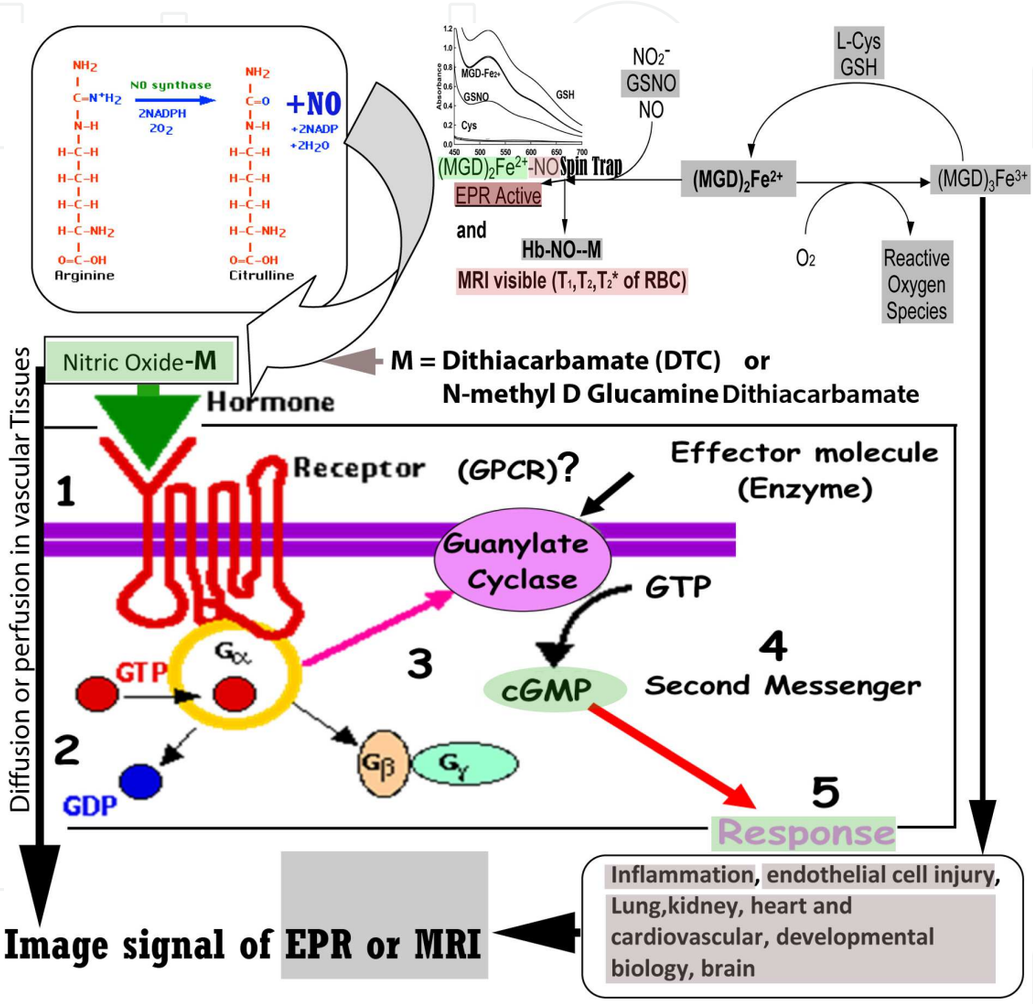

Fig. 15. (on top) Formation and release of NO in tissues is shown. No is trapped by $Fe^{2+}(MGD)_2$ to make MRI/EPR visible trap NO-(MGD)2-Fe^{3+}. (in middle row)The figure represents how different levels of Nitric oxide (1) activate cytosolic guanylate cyclase (2) and thus elevate intracellular levels of cyclic GMP (3 and 4) as secondary messenger. The cyclic GMP stimulates response (5) in different tissues and nitric oxide can be detected as biomarker of tissue pathology.(at bottom) The relation of released NO across the membrane is shown with different biological and physiological changes to generate EPR and MRI signal visible by imaging techniques. Notice the NO regulation by enzyme guanylate cyclase over intracellular responses (cell injury, inflammation etc.) sensitive to spin trap MRI/EPR image signals. A proposal of multimodal nitric oxide imaging is shown for development of multimodal spin trap applicable in imaging.

NOS in living subjects with high fidelity which will greatly facilitate scientists and clinicians in the development of new drugs and patient management[Oliveira, et al. 2010, Payne, et al. 2010]. Lastly, novel NO/NOS imaging agents with optimal in vivo stability and suitable pharmacokinetics such as pteridines, imidazoles, quinolines for clinical translation will benefit in patient management [Payne, et al. 2010, Bonnefous, et al. 2009].

Imaging of NOS expression mainly relies on labeling high affinity, preferably also high specificity, NOS inhibitors with optimal membrane permeability and pharmacokinetics. Of all the fluorescence imaging agents for NO, the DAFC compounds are the most widely used. The requirement of oxygen restricts their applicability in cancer-related NO imaging to a certain extent, although some have been tested for NO imaging during tumor angiogenesis [Kashiwagi, et al. 2005]. Copper-based fluorescent compounds do not require oxygen for NO imaging, yet the stability and toxicity of those compounds are questionable. FRET-based NO imaging is a clever approach, yet it is too technically challenging to be widely available and useful. With spin-trapping technology, EPR imaging of NO can be quite accurate, yet it is not applicable for clinical studies due to many reasons. MRI can have high resolution and large field-of-view for potential clinical imaging studies, yet it is usually quite slow in data acquisition and the intrinsic low sensitivity makes molecular MRI unlikely to succeed in the clinic. NOS imaging is also important in elucidating NO-related physiological and pathological processes. NOS imaging has not been well studied to date. To the best of our knowledge, no clinical studies of NO or NOS imaging have been reported. Whether NO/NOS imaging can help and improve patient management remains to be demonstrated in the future. The deregulation of iNOS in melanoma has been correlated directly with poor survival [Madunapantula, et al. 2008] and NOS expression in patients with neurological disorder has been studied [Broholm, et al. 2004]. Given the fact that NO and NOS plays diverse roles in many diseases such as inflammation, neurodegeneration, cancer, and vascular malfunctions, further understanding of the disease mechanisms and clarification of the temporal/ spatial NO/NOS expression are certainly very important in patient management. Whether imaging NO or NOS is more relevant depends primarily on the disease. eNOS and nNOS typically only produces low levels of NO; therefore, imaging NO is expected to be more difficult than imaging the NOSs themselves. On the other hand, iNOS can produce high concentrations of NO in immunological processes and/or cancer; hence imaging NO may be more desirable in these scenarios. Granted that NO imaging is more relevant since it directly affects the physiological and pathological processes, imaging of NO may not always be feasible and imaging NOS expression (as an alternative) can provide valuable insights. The notion that nitrite reduction can also serve as a possible source of biologically relevant NO tilted the balance toward NO imaging [Bryan, 2006]. Nitrite reduction to NO can occur via several routes involving enzymes, proteins, vitamins, or even simple protons [Galdwin, 2004, Lundberg, et al. 2005]. Nitrite is now under active investigations in physiology, pathophysiology, and therapeutics. The ideas that nitrite can be a "storage" form of NO and the possible importance of dietary nitrite are two vibrant research areas today. Similar to the important role of L-arginine for optimal NOS activity, nitrite may emerge as an essential nutrient. This pathway may serve as a backup system for NO generation in conditions such as hypoxia, in which the NOS/L-arginine system is compromised. We envision that imaging NO and NOS in the same system will undoubtedly give a more thorough picture in understanding the functions of NO and NOS. For potential clinical translation of NO/NOS imaging probes, PET tracers have the best chances of

success. Each imaging modality has its advantages and disadvantages in terms of sensitivity, spatial resolution, temporal resolution, probe availability, and cost [Massoud, et al. 2003]. With the development of hybrid imaging systems such as PET/CT, SPECT/CT, and PET/MRI Catana et al. 2006; Sharma, 2002, 2008, 2011;Townsend, et al. 2002], a multimodality approach may offer synergistic advantages over any single modality alone in the future.

6. Conclusion

Nitric oxide (NO) *in vivo* image visualizes the distribution of NO using the ''spin-trapping'' technique. Available NO visualizing chemical probes combined with the spin traps and fluorescent dyes are promising. Physiological mechanisms of NO production by NOS and role of NOS gene expression altered by NOS inhibitors is illustrated. **Scope:** Different multimodal contrast mechanisms are introduced using nitrosyl-iron complexes as MRI-PET signal intensity enhancers and fluorescent or bioluminescent NO visualizing cheletropic trap agents. NO synthase enzyme is the source of NO formation in presence of competitive inhibitor N-monomethyl-L-arginine in the tissues.

- **General Significance:** NO makes stable paramagnetic with N-methyl-D-glucamine dithiocarbamate (MGD), as $(MGD)_2$-Fe(II)-NO metal complex *in vivo* by spin trapping and may serve as effective EPR and/or MRI contrast agent than other less stable nitrogen containing radicals, such as bound nitric oxides. MRI spin-trapping induces the magnetic resonance relaxation changes of neighboring protons and visualizes spatial distributions of NO free radicals in pathologic organs and tissues but not confirmed. Other paramagnetic NO-Fe-dithiacarbamate metal complexes serve as contrast agents in EPR bioimaging. Recently, real time physiological in vivo monitoring using tissue physical properties such as fluorescence and magnetic resonance in tissues is revisted to visualize nanomolar range of nitric oxide mapping.
- **Major conclusions**: 1. More applications of NO bioimaging and fluorescent probes are emerging in imaging apoptosis, vascular imaging, smooth muscle cells, neurodegeneration, calcium channel imaging and endothelial stress. 2. The status of NO production by NOS in cells gives insight of inflammation, fertilization, mitochondrial oxidation injury, bone structure and adrenal gland and retina. 3. The real time NO imaging application is emerging in animals and plants.
- **Major highlights:**
  - Nitric oxide bioimaging is emerging as rapid noninvasive multimodal molecular imaging techniques by fluorescent, MRI, PET, optical bioimaging for wider applications;
  - Significant progress is made to explain the mechanism of multimodal NO spin trap contrast agent enhanced MRI and fluorescent bioimaging;
  - Both MRI and fluorescent contrast agents may serve as potential MRI/fluorescent multimodal spin traps as well as contrast agents in clinical or bioimaging;
  - NO sensitive MRI of vital soft tissues is major achievement to visualize very short lived NO in real time manner.
  - Development of NOS inhibitors or NO production suppressors and in vivo NO/NOS evaluation is a booming industry in diagnostics of stroke, sepsis, neurodegeneration, inflammation and new drug discovery.

Spin trap contrast agents may enable the simultaneous EPR-MRI and fluorescent imaging of NO distribution in the organs and tissues in muscle vascular system, retina, adrenal gland, brain, bone marrow to monitor intracellular metabolic events such as apoptosis, inflammation, nerve activation and calcium ions etc. To our knowledge, there are no reports of successfully imaging or detecting free radicals such as NO in vivo clinical imaging. Due to short lifetime and rapid diffusion of NO in tissue, it is a challenge to devise any effective relaxation enhancement mechanism(s) for noninvasive clinical imaging. NMR spin trapping may serve to overcome these problems of NO short lifetime and diffusion to some extent.

7. Appendix 1: Protocols on NOS and NO* radical detection

Source: Cai H., Dikalov S, Griendling K.K., Harrison, D.G.(2007) Detection of reactive oxygen species and nitric oxide in vascular cells and tissues. Chapter 20 In: Methods in Molecular Medicine, Vascular Biology Protocols. Editor: Sreejayan N. and Ron J., Humana Press Inc. Totowa, NJ. Pp 293-311.

Electronic configuration in NO* with 11 valence electrons:
$(K^2K^2)(2s\sigma^b)^2(2s\sigma^*)^2(2p\pi^b)^4(2p\sigma^b)^2(2p\pi^*)^1$

Detection of Nitric Oxide Radical

It has been challenging to detect nitric oxide radical (NO•) directly from biological samples. NO• "production" is measured by NO• synthase activity using the L-arginine conversion assay or NO• metabolites nitrite and nitrate using the Griess reagent. New methods are NO•-selective electrode and ESR represent specific and quantitative assays for detection of functional NO•.

Materials needed:

1. NO•-Specific Microelectrode
   Nafion and o-PD coated carbon electrode can directly detect NO• in the low micromolar range.
2. ESR with NO•-Specific Spin Traps
   Dithiocarbamate (DTC), N-methylglucamine dithiocarbamate (MGD) detect extracellular NO*, and diethyldithiocarbamate (DETC) trap and detect the NO* in cellular lipid membrane.
   iron-MGD and iron-DETC.
3. ESR measurement:
   - Endothelial or vascular smooth muscle cells.
   - Modified Krebs/HEPES buffer (see Subheading 2.1.1.2.).
   - Cyclic hydroxylamine CPH or 1-hydroxy-3-methoxycarbonyl-2,2,5,5-tetramethylpyrrolidine
   - (CMH) stock solution (10 mM) (Alexis Biochemicals, San Diego, CA,
   - USA) in modified Kreb's/HEPES buffer containing metal chelator, 25–50mM
   - deferoximine, and 3」 5mM DETC. This stock solution should be de-oxygenated by
   - nitrogen gas continuously to maintain low background oxidation of the spin traps.
   - Lysis buffer containing protease inhibitors: 50mM Tris–HCl buffer, pH 7.4,
   - containing 0.1mM ethylenediamine tetraacetic acid (EDTA), 0.1mM ethylene

- glycol tetraacetic acid (EGTA), 1mM phenylmethyl sulfonyl fluoride, 2mM bestatin, 1mM pepstatin, and 2mM leupeptin.
- NADPH (0.2 mM).
- Xanthine (0.1 mM).

Detection of Nitric Oxide Radical

NO•-Specific Microelectrode

- Carbon fiber electrodes (100µm length and 30µm outer diameter; Word Precision
- Instruments, Sarasota, FL, USA).
- o-PD solution (in 0.1M PBS with 100µM ascorbic acid).
- Nafion (5% in aliphatic alcohols; Sigma-Aldrich).
- Modified Kreb's/HEPES buffer.
- Axopatch 200B amplifier (Axon Instruments, Union City, CA, USA).
- Silver/silver chloride reference electrode.

Iron-DETC for Trapping of NO•

- Culture endothelial cells.
- Saline (0.9% NaCl).
- $Fe^{2+}(DETC)_2$: $FeSO4 \cdot 7H2O$, 4.45 mg/10 ml for 1.6 mmol/l stock and DETC, 7.21 mg/10 ml for 3.2 mmol/l stock.
- PBS.
- Modified Kreb's/HEPES buffer.
- Ferrous sulfate (4 mM).
- N-methyl-d-glucamine dithiocarbamate MGD (20 mM).

Methods:

Detection of Nitric Oxide Radical

NO•-Specific Microelectrode

- Coat bare carbon fiber electrodes (100µm length and 30µm outer diameter; Word
- Precision Instruments) with nafion and o-PD. Coat with freshly made o-PD solution at constant potential (+0.9V vs. Ag/AgCl reference electrode) for 45 min. Dip in nafion solution for 3 s and dry for 5 min at 85°C. The nafion-coating cycle should be repeated 10–15 times.
- Culture endothelial cells on 35-mm dishes or prepare fresh tissue samples in freshly made modified Kreb's/HEPES buffer.
- Place the electrode tip at the surface of an individual cell, endocardium, or lumen of blood vessels, and then withdraw precisely 5µm.
- Record NO•-dependent oxidation currents (voltage clamp mode, hold at 0.65 V, approximately the voltage for peak NO• oxidation) immediately after addition of agonists using an Axopatch 200B amplifier (Axon Instruments). A silver/silver chloride reference electrode is used. Use pCLAMP 7.0 program (Axon Instruments) for delivery of voltage protocols and data acquisition and analysis.
- Calculate NO• concentrations from a standard curve obtained using dilutions of de-oxygenated, saturated NO* gas solutions.

Iron-DETC Protocol for Intracellular Trapping of NO•

- Culture endothelial cells on 100-mm Petri dishes or prepare vascular segments (6–12, 2-mm vessel segments).
- Bubble freshly prepared saline (0.9% NaCl) with nitrogen gas to remove oxygen.
- Aspirate media and rinse cells with warm PBS once, add 1.5 ml modified Kreb's/HEPES buffer with or without desired agonists, then mix Fe^{2+}(DETC)2, and immediately add to culture dish (500µl of each solution, final volume 2.0 ml).
- Incubate in cell culture incubator for desired period for cumulative trapping of NO•.
- Aspirate buffer, gently collect cells into a 1-ml insulin syringe, snap freeze in liquid nitrogen, then transfer sample column into a finger dewer, and capture Fe2+(DETC)2–NO• signal using ESR at the following settings:
- Bruker EMX: Field sweep, 160 G; microwave frequency, 9.39 GHz; microwave power, 10MW; modulation amplitude, 3 G; conversion time, 2621 ms; time constant, 328 ms; modulation amplitude, 3 G; receiver gain, 1×10^4; and four scans.
- Miniscope 200: Biofield, 3267; field sweep, 100 G; microwave frequency, 9.78 GHz; microwave power, 40 mW; modulation amplitude, 10 G; 4096 points resolution; and receiver gain, 900.

Iron-MGD Protocol for Extracellular Trapping of NO•

- Culture endothelial cells on 100-mm Petri dishes or prepare vascular segments (6–12, 2-mm vessel segments).
- Bubble freshly prepared saline (0.9% NaCl) with nitrogen gas to remove oxygen, and then make stock solutions of $FeSO4\cdot7H_2O$, 4 mM, and MGD, 20 mM.
- Prepare stock solutions of Fe^{2+}MGD by mixing FeSO4 and MGD at the ratio of 1:5 or 1:10 (final Fe concentration: 0.5 mM).
- Aspirate media and rinse cells with warm PBS once, add 1.5 ml modified Kreb's/HEPES buffer with or without desired agonists, then mix $Fe^{2+}(MGD)_2$, and immediately add to culture dish.
- Incubate in cell culture incubator for desired period for cumulative trapping of NO•.
- Collect 1 ml of post-incubation supernatant into a 1-ml insulin syringe and snap freeze in liquid nitrogen, then transfer sample column into a finger dewer, and capture Fe^{2+}MGD–NO• signal using ESR settings as described above for $Fe^{2+}(DETC)_2$.

8. Acknowledgements

Author acknowledge the manuscript preparation, corrections, expert suggestions by Dr Soonjo Kwon, Utah State University, Logan, UT and Professor Ching J Chen at Florida State University, Tallahassee for extending expert modifications and comments in this manuscript. Prof Avdhesh Sharma, JNV University, corrected manuscript.

9. References

Ahern, G.P., Hsu, S.F., Klyachko,V.A., Jackson, M.B. (2000) Induction of persistent sodium current by exogenous and endogenous nitric oxide. J Biol Chem, Vol 275, No 37, pp 28810-5.

Alderton, W.K., Cooper, C.E., Knowles, R.G.(2001) Nitric oxide synthases: structure, function and inhibition. Biochem J, Vol 357, 593-615.

Anbar, M.(2000) Detection of cancerous lesions by measuring nitric oxide concentrations in tissue. US Patent 6,035,225. In: Omnicorder Technologies, Stoneybrook, N.Y: U.S.A.

Anon (1999a) Nitric oxide synthase inhibitors with cardiovascular therapeutic potential. Expert Opin.Ther. Pat. Vol 95, pp 537-547

Anon (1999b) The inhibition of isoforms of nitric oxide synthase : non-cardiovascular aspects. Expert Opin. Ther. Pat. Vol 95, pp 549-556

Babu, B. R. and Griffith, O. W. (1998) N5-(1-imino-3-butenyl)-L-ornithine. A neuronal isoform selective mechanism-based inactivator of nitric oxide synthase. J. Biol. Chem. Vol 273, pp 8882-8889.

Barker, S. L., Zhao, Y., Marletta, M. A., Kopelman, R. (1999) Cellular applications of a sensitive and selective fiber-optic nitric oxide biosensor based on a dye-labeled heme domain of soluble guanylate cyclase. Anal. Chem. Vol 71, pp 2071–2075.

Barouch, L.A., Harrison, R.W., Skaf, M.W. , Rosas, G.O., Cappola, T.P., Kobeissi, Z.A., Hobai, I.A., et al. (2002) Nitric oxide regulates the heart by spatial confinement of nitric oxide synthase isoforms Nature Vol 416, pp 337-339.

Berkels, R., Dachs, R., Roesen, R., Klaus, W. (2000) Simultaneous measurement of intracellular Ca(2+) and nitric oxide: a new method. Cell Calcium, Vol 27, No 5, pp. 281-286.Berliner, L.J., Fujii, H. (2004) In vivo spin trapping of nitric oxide. Antioxid Redox Signal. Vol 6, No 3, pp 649-56.

Berliner, L. J.; Fujii, H.(2004) In vivo spin trapping of nitric oxide. Antioxid. Redox Signal. Vol 6, pp 649– 656.

Blanchette, J., Jaramillo, M., Olivier, M. (2003) Signalling events involved in interferon-gamma-inducible macrophage nitric oxide generation.Immunology Vol 108, pp 513–522.

Bobko, A.A., Sergeeva, S.V., Bagryanskaya, E.G., Markel, A.L., Khramtsov, V.V., Reznikov, V.A., Kolosova, N.G. (2005) 19F NMR measurements of NO production in hypertensive ISIAH and OXYS rats. Biochem Biophys Res Commun. Vol 330, No 2, pp 367-70.

Bretscher L.E., Li, H., Poulos, T.L., Griffth, O.W. (2003) Structural Characterization and Kinetics of Nitric-oxide Synthase Inhibition by Novel *N*5-(Iminoalkyl)- and *N*5-(Iminoalkenyl)-ornithines. J. Biol. Chem. Vol. 278, No. 47, Issue of November 21, pp. 46789–46797.

Broholm, H., Andersen, B.,Wanscher, B., Frederiksen, J. L., Rubin, I., Pakkenberg,B., Larsson, H. B., Lauritzen, M. (2004) Nitric oxide synthase expression and enzymatic activity in multiple sclerosis. Acta Neurol Scand. Vol 109, pp 261–269.

Broillet, M., Randin, O., Chatton,J. (2001) Photoactivation and calcium sensitivity of the fluorescent NO indicator 4,5-diaminofluorescein (DAF-2): implications for cellular NO imaging. FEBS Lett, Vol 491, No 3, pp 227-32.

Brown, L.A., Key, B.J., Lovick,T.A. (1999) Bio-imaging of nitric oxide-producing neurones in slices of rat brain using 4,5-diaminofluorescein. J Neurosci Methods, Vol 92, No 1-2, pp 101-10.

Bryan, N. S.(2008) Nitrite in nitric oxide biology: cause or consequence? A systems based review. Free Radic. Biol. Med. Vol 41, pp 691–701.

Bryk, R. and Wolff, D. J. (1999) Pharmacological modulation of nitric oxide synthesis by mechanism-based inactivators and related inhibitors. Pharmacol. Ther. Vol *84*, pp 157-178

Bryk, R., Wolff, D.J.(1998) Mechanism of inducible nitric oxide synthase inactivation by aminoguanidine and L-N6-(1-iminoethyl)lysine. Biochemistry.Vol 37, No 14, pp 4844-52.

Burnett, A.L. (2002) Nitric Oxide Regulation of Penile Erection: Biology and Therapeutic Implications. Journal of Andrology,Vol 23, No 5, pp 2002:20-26.

Butle, T.A., Lee, M.R., Eldred, W.D. (2000) Direct imaging of NMDA-stimulated nitric oxide production in the retina. Vis Neurosci, Vol 17, No 4, pp 557-66.

Cai, W., Niu, G., Chen, X.(2008b) Imaging of integrins as biomarkers for tumor angiogenesis. Curr. Pharm. Des. Vol 14, pp 2943–2973.

Cai,W., Chen, K., Li, Z. B., Gambhir, S. S., Chen, X. (2007) Dual-function probe for PET and near-infrared fluorescence imaging of tumor vasculature. J. Nucl. Med. Vol 48, pp 1862–1870.

Cai,W., Chen, X.(2008a) Multimodality molecular imaging of tumor angiogenesis. J. Nucl. Med. Vol 49 (Suppl. 2), pp 113S–128S; 2008.

Cai,W., Hsu, A. R., Li, Z. B., Chen, X. (2007a) Are quantum dots ready for in vivo imaging in human subjects? Nanoscale Res. Lett. Vol 2, pp 265–281.

Caramia, F., Yoshida, T., Hamberg, L.M., Huang, Z., Hunter, G., Wanke, I., Zaharchuk, G., Moskowitz, M.A., Rosen, B.R.(1998) Measurement of changes in cerebral blood volume in spontaneously hypertensive rats following L-arginine infusion using dynamic susceptibility contrast MRI. Magn Reson Med, Vol 39, No 1, pp 160-3.

Castagnoli, K., Palmer, S., Castagnoli, Jr.,N.(1999) Neuroprotection by (R)-deprenyl and 7-nitroindazole in the MPTP C57BL/6 mouse model of neurotoxicity. Neurobiology (Bp), Vol 7, No 2, pp 135-49.

Catana, C.,Wu, Y., Judenhofer,M. S., Qi, J., Pichler, B. J., Cherry, S. R. (2006) Simultaneous acquisition of multislice PET and MR images: initial results with a MR compatible PET scanner. J. Nucl. Med. Vol 47, pp 1968–1976.

Chen, X., Sheng, C., Zheng, X. (2001) Direct nitric oxide imaging in cultured hippocampal neurons with diaminoanthraquinone and confocal microscopy. Cell Biol Int, Vol 25, No 7, pp 593-8.

Choi, Y.B., Tenneti, L., Le, D.A., Ortiz, J., Bai, G., Chen, H.S.V., Lipton, S.A. (2000) Molecular basis of NMDA receptor-coupled ion channel modulation by S-nitrosylation. Nat Neurosci, 2000; 3(1): 15-21

Ciplak, M., Pasche, A., Heim, A., Haeberli, C., Waeber, B., Liaudet, L., Feihl, F., Engelberger, R.(2009) The vasodilatory response of skin microcirculation to local heating is subject to desensitization.Microcirculation. Vol 16, No 3, pp 265-75

Claudette, M., Croix, S., Molly, S., Watkins, S.C., Pitt, B.R.(2005) Fluorescence Resonance Energy Transfer–Based Assays for the Real-Time Detection of Nitric Oxide Signaling. Methods in Enzymology, Vol 396, pp 317-326.

Crowell, J. A., Steele, V. E., Sigman, C. C., Fay, J. R.(2003) Is inducible nitric oxide synthase a target for chemoprevention? Mol. Cancer Ther. Vol 2, pp 815–823.

Davies, M. J.; Hawkins, C. L.(2004) EPR spin trapping of protein radicals. Free Radic. Biol. Med. Vol. 36, pp 1072–1086.

Davies, S. L., Loescher, A. R., Clayton, N. M., Bountra, C., Robinson, P. P.,Boissonade, F. M. (2004) nNOS expression following inferior alveolar nerve injury in the ferret. Brain Res. Vol. 1027, pp 11–17.

Day, R.W., White, K.S., Hedlund, G.L. (2005) Nitric oxide increases the signal intensity of the T1-weighted magnetic resonance image of blood. J Cardiovasc Magn Reson. Vol 7, No 4, pp 667-9.

de Vries, E. F., Vroegh, J., Dijkstra, G., Moshage, H., Elsinga, P. H., Jansen, P. L., Vaalburg, W. (2004) Synthesis and evaluation of a fluorine-18 labeled antisense oligonucleotide as a potential PET tracer for iNOS mRNA expression. Nucl. Med. Biol. Vol 31, pp 605–612.

Desvignes, C., Bert, L., Vinet, L., Denoroy, L., Renaud, B., Lambas-Senas, L. (1999) Evidence that the neuronal nitric oxide synthase inhibitor 7-nitroindazole inhibits monoamine oxidase in the rat: in vivo effects on extracellular striatal dopamine and 3,4-dihydroxyphenylacetic acid. Neurosci Lett, Vol 264, No 1-3, pp 5-8.

Di Cesare, M. L., Nistri, S., Mazzetti, L., Bani, D., Feil, R., Failli, P. (2009) Altered nitric oxide calcium responsiveness of aortic smooth muscle cells in spontaneously hypertensive rats depends on low expression of cyclic guanosine monophosphate-dependent protein kinase type I.J Hypertens. Vol 26, No 6, pp 1258-1267.

Di Salle, F., Barone, P., Hacker, H., Smaltino, F., Marco, I. (1997)Nitric oxide-haemoglobin interaction: a new biochemical hypothesis for signal changes in fMRI. Neuroreport, Vol 8, No 2, pp 461-4.

Dunn, A. R., Belliston-Bittner, W., Winkler, J. R., Getzoff, E. D., Stuehr, D. J., Gray, H. B. (2005) Luminescent ruthenium(II)- and rhenium(I)-diimine wires bind nitric oxide synthase. J. Am. Chem. Soc. Vol 127, pp 5169–5173.

Engelsman, A.F., Krom, B.P., Busscher, H.J., van Dam, G.M., Ploeg, R.J., van der Mei, H.C.(2009) Antimicrobial effects of an NO-releasing poly(ethylene vinylacetate) coating on soft-tissue implants in vitro and in a murine model. Acta Biomater. Vol 5, No 6, pp 1905-1910.

Fichtlscherer, B., Mülsch, A. (2000) MR imaging of nitrosyl-iron complexes: experimental study in rats.Radiology. Vol 216, No 1, pp 225-31.

Flögel, U., Jacoby, C., Gödecke, A., Schrader, J. (2007) In vivo 2D mapping of impaired murine cardiac energetics in NO-induced heart failure. Magn Reson Med. Vol 57, No 1, pp 50-8.

Foissner, I., Wendehenne D, Langebartels C, Durner J. (2000) In vivo imaging of an elicitor-induced nitric oxide burst in tobacco. Plant J, Vol 23, No 6, pp 817-24.

Foster, M.A., Seimenis, I., Lurie, D.J.(1998) The application of PEDRI to the study of free radicals in vivo. Phys Med Biol, Vol 43, No 7, pp 1893-7.

Franz, K.J., Singh, N., Spinler, B., Lippard, S.J.(2000) Aminotroponiminates as ligands for potential metal-based nitric oxide sensors. Inorg Chem, Vol 39, No 18, pp 4081-92.

Freeman, B. A., Lancaster Jr., J. R., Feelisch, M., Lundberg, J. O. (2005) The emerging biology of the nitrite anion. Nat. Chem. Biol. Vol 1,pp 308–314.

Fujii, H., Itoh, K., Pandian, R.P., Sakata, M., Kuppusamy, P., Hirata, H. (2007) Measuring brain tissue oxygenation under oxidative stress by ESR/MR dual imaging system. Magn Reson Med Sci. Vol 6, No 2, pp 83-9.

Fujii, H., Koscielniak, J., Berliner,L.J.(1997) Determination and characterization of nitric oxide generation in mice by in vivo L-Band EPR spectroscopy. Magn Reson Med, Vol 38, No 4, pp 565-8.

Fujii, H., Wan, X. Zhong, J., Berliner, L. J., Yoshikawa, K. (1999) In vivo imaging of spintrapped nitric oxide in rats with septic shock: MRI spin trapping. Magn. Reson. Med. Vol 42, pp 235–239.

Garcin, E. D., Arvai, A. S., Rosenfeld, R. J., Kroeger, M. D., Crane, B. R., Andersson, G., Andrews, G., Hamley, P. J., Mallinder, P. R.et al. (2008) Anchored plasticity opens doors for selective inhibitor design in nitric oxide synthase. Nat. Chem. Biol. Vol 4,700–707.

Gladwin, M. T. (2004) Haldane, hot dogs, halitosis, and hypoxic vasodilation: the emerging biology of the nitrite anion. J. Clin. Invest. Vol 113, pp 19–21.

Gladwin, M. T., Schechter, A. N., Kim-Shapiro, D. B., Patel, R. P., Hogg, N., Shiva, S., Cannon III, R. O., Kelm, M., Wink, D. A., Espey, M. G., Oldfield, E. H., Pluta, R. M.,

Gorbunov, N.V., Pogue-Geile, K.L., Epperly, M.W., Bigbee, W.L., Draviam, R., Day, B.W., Wald, N., Watkins, S.C., Greenberger, J.S.(2000) Activation of the nitric oxide synthase 2 pathway in the response of bone marrow stromal cells to high doses of ionizing radiation. Radiat Res, Vol 154, No 1, pp 73-86.

Gragasin, F.S., Michelakis, E.D., Hogan, A., Moudgil, R., Hashimoto, K., Wu, X., Bonnet, S., Haromy, A., Archer, S.L. (2004) The neurovascular mechanism of clitoral erection: nitric oxide and cGMP-stimulated activation of BKCa channels. FASEB J. 2004;18:1382-1391.

Green, D.R.(1998) Apoptotic pathways: the roads to ruin. Cell, Vol 94, No 6, pp. 695-8.

Haga, K.K., Gregory, L.J., Hicks, C.A., Ward, M.A., Beech, J.S., Bath, P.W., Williams, S.C., O'Neill, M.J. (2003) The neuronal nitric oxide synthase inhibitor, TRIM, as a neuroprotective agent: effects in models of cerebral ischaemia using histological and magnetic resonance imaging techniques. Brain Res. Vol 993, No 1-2, pp 42-53.

Handy, R. L. and Moore, P. K. (1998) A comparison of the effects of L-NAME, 7-NI and L-NIL on carrageenan-induced hindpaw oedema and NOS activity. Br. J.Pharmacol. Vol 123, pp 1119-1126

Heinrich, U. R., Selivanova, O., Feltens, R., Brieger, J., Mann,W. (2005) Endothelial nitric oxide synthase upregulation in the guinea pig organ of Corti after acute noise trauma. Brain Res. Vol 1047, pp 85–96.

Heiss, C., Sievers, R. E., Amabile, N., Momma, T. Y., Chen, Q., Natarajan, S., Yeghiazarians, Y., Springer, M. L. (2008) In vivo measurement of flow-mediated vasodilation in living rats using high-resolution ultrasound. Am. J. Physiol, Heart Circ. Physiol. Vol 294, pp H1086–H1093; 2008.

Hillebrand, U., Lang, D., Telgmann, R.G., Hagedorn, C., Reuter, S., Kliche, K., Stock, C.M., Oberleithner, H., Pavenstädt, H., Büssemaker, E., Hausberg, M. (2009) Nebivolol

decreases endothelial cell stiffness via the estrogen receptor beta: a nano-imaging study.J Hypertens. Vol 27, No 3, pp 517-26.

Hiratsuka, M., Katayama, T., Uematsu, K., Kiyomura, M., Ito, M. (2009) In vivo visualization of nitric oxide and interactions among platelets, leukocytes, and endothelium following hemorrhagic shock and reperfusion. Inflamm Res. Vol 58, No 8, pp 463-471.

Hong, H., Sun, J., Cai, W. (2009) Multimodality imaging of nitric oxide and nitric oxide synthases. Free Radic Biol Med. Vol 47, No 6, pp 684-698.

Horman, S., Browne, G., Krause, U., Patel, J., Vertommen, D., Bertrand, L., Lavoinne, A., Hue, L., Proud, C. & Rider, M. (2002) Activation of AMP-activated protein kinase leads to the phosphorylation of elongation factor 2 and an inhibition of protein synthesis. Curr. Biol. 12, pp 1419–1423.

Hortelano, S., Zeini, M., Traves, P.G., Bosca, L. (2005) Nitric Oxide and Cell Signaling: In Vivo Evaluation of NO-Dependent Apoptosis by MRI and Not NMR Techniques. Method in Enzymol Vol 396, pp 579-584.

Hsiao, J.K., Chu, H.H., Wang, Y.H., Lai, C.W., Chou, P.T., Hsieh, S.T., Wang, J.L., Liu, H.M. (2008) Macrophage physiological function after superparamagnetic iron oxide labeling. NMR Biomed. Vol 21, No 8, pp 820-9

Huang, K. J., Zhang, M., Xie, W. Z., Zhang, H. S., Feng, Y. Q., Wang, H. (2007) Sensitive determination of nitric oxide in some rat tissues using polymer monolith microextraction coupled to high-performance liquid chromatography with fluorescence detection. Anal. Bioanal. Chem. Vol 388, pp 939–946.

Huang, KJ.,Wang, H., Ma, M., Zhang, X., Zhang, H.S. (2007b) Real-time imaging of nitric oxide production in living cells with 1,3,5,7-tetramethyl-2,6-dicarbethoxy-8-(3',4'-diaminophenyl)-difluoroborad iaza-s-indacence by invert fluorescence microscope. Nitric Oxide, Vol 16, No 1, pp 36-43.

Itoh, K., Watanabe, M., Yoshikawa, K., Kanaho, Y., Berliner, L.J., Fujii, H. (2004) Magnetic resonance and biochemical studies during pentylenetetrazole-kindling development: the relationship between nitric oxide, neuronal nitric oxide synthase and seizures. Neuroscience. Vol 129, No 3, pp 757-66.

Itoh, Y., Ma, F.H., Hoshi, H., Oka, M., Noda, K., Ukai, Y., Kojima, H., Nagano, T., Toda, N. (2000) Determination and bioimaging method for nitric oxide in biological specimens by diaminofluorescein fluorometry. Anal Biochem, Vol 287, No 2, pp 203-9.

Janssen-Heininger, Y.M., Mossman, B.T., Heintz, N.H., Forman, H.J., Kalyanaraman, B., Finkel, T., Stamler, J.S., Rhee, S.G., van der Vliet, A.(2008) Redox-based regulation of signal transduction: principles, pitfalls, and promises. Free Radic Biol Med. Vol. 45, No 1, pp 1-17.

Jares-Erijman, E. A.; Jovin, T. M. FRET imaging. Nat. Biotechnol. 21:1387–1395.

Jordan, B.F., Misson, P.D., Demeure, R., Baudelet, C., Beghein, N., Gallez, B. (2000) Changes in tumor oxygenation/perfusion induced by the no donor, isosorbide dinitrate, in comparison with carbogen: monitoring by EPR and MRI. Int J Radiat Oncol Biol Phys, Vol 48, No 2, pp 565-70.

Jordan, B.F., Sonveaux, P., Feron, O., Gregoire, V., Beghein, N., Dessy, C., Gallez, B., (2004) Nitric oxide as radiosensitizer:Evidence for an intrinsic role in addition to its effect on oxygen delivery and consumption. Int J Cancer.Vol 109, No 5, pp 768-773.

Kakiailatu, F.A.(2000) The role of nitric oxide in the mechanism of penile erectionClinical Hemorheology and Microcirculation. Vol 23, No 2-4, pp 283-286.

Kashiwagi, S., Izumi, Y., Gohongi, T., Demou, Z. N., Xu, L., Huang, P. L., Buerk, D. G., Munn, L. L., Jain, R. K., Fukumura, D. (2005) NO mediates mural cell recruitment and vessel morphogenesis in murine melanomas and tissue-engineered blood vessels. J. Clin. Invest. Vol 115, pp 1816–1827.

Keelan, J., Vergun, O., Duchen, M.R. (1999) Excitotoxic mitochondrial depolarisation requires both calcium and nitric oxide in rat hippocampal neurons. J Physiol, Vol 520 Pt 3, pp 797-813.

Khoo, J. P., Alp, N. J., Bendall, J. K., Kawashima, S., Yokoyama, M., Zhang, Y. H., Casadei, B., Channon, K. M. (2004) EPR quantification of vascular nitric oxide production in genetically modified mouse models. Nitric Oxide. Vol.10, pp 156–161.

Kimura, C., Koyama, T., Oike, M., Ito, Y. (2000) Hypotonic stress-induced NO production in endothelium depends on endogenous ATP. Biochem Biophys Res Commun, Vol 274, No 3, pp 736-40.

Kimura, C., Oike, M., Koyama, T., Ito, Y. (2001) Impairment of endothelial nitric oxide production by acute glucose overload. Am J Physiol Endocrinol Metab,Vol 280, No 1, pp 171-8.

Kleschyov, A. L., Mollnau, H., Oelze, M., Meinertz, T., Huang, Y., Harrison, D. G., Munzel, T. (2000) Spin trapping of vascular nitric oxide using colloid Fe(II)-diethyldithiocarbamate. Biochem. Biophys. Res. Commun. Vol. 275, pp 672–677.

Kleschyov, A. L., Muller, B., Keravis, T., Stoeckel, M. E., Stoclet, J. C. (2000) Adventitia derived nitric oxide in rat aortas exposed to endotoxin: cell origin and functional consequences. Am. J. Physiol, Heart Circ. Physiol. Vol 279, pp H2743–H2751.

Kleschyov, A. L.,Wenzel, P., Munzel, T. (2007) Electron paramagnetic resonance (EPR) spin trapping of biological nitric oxide. J. Chromatogr., B Analyt. Technol. Biomed. Life Sci. Vol 851, pp 12–20.

Kojima, H., Hirata, M., Kudo, Y., Kikuchi, K., Nagano, T. (2001a) Visualization of oxygen-concentration-dependent production of nitric oxide in rat hippocampal slices during aglycemia. J Neurochem, Vol 76, No 5, pp 1404-10.

Kojima, H., Hirotani, M., Nakatsubo, N., Kikuchi, K., Urano, Y., Higuchi, T., Hirata, Y., Nagano, T. (2001b) Bioimaging of nitric oxide with fluorescent indicators based on the rhodamine chromophore.Anal Chem. Vol 73, No 9, pp 1967-73.

Kolodziejski, P. J., Musial, A., Koo, J. S. & Eissa, N. T. (2002) Ubiquitination of inducible nitric oxide synthase is required for its degradation.Proc. Natl. Acad. Sci. U. S. A. 99, 12315–12320

Komarov, A.M. Lai, C.S.(1995) Detection of nitric oxide production in mice by spin-trapping electron paramagnetic resonance spectroscopy. Biochim Biophys Acta, Vol 1272, No 1, pp 29-36.

Komeima, K., Hayashi, Y., Naito, Y., Watanabe, Y. (2000) Inhibition of neuronal nitric-oxide synthase by calcium/calmodulin dependent protein kinase II through Ser847

phosphorylation in NG108-15 neuronal cells.J. Biol. Chem. Vol.275, No.36, pp 28139-28143

Konorev, E. A.,Joseph, J.,Kalyanaraman, B. (1996) S-Nitrosoglutathione induces formation of nitrosylmyoglobin in isolated hearts during cardioplegic ischemia—an electron spin resonance study. FEBS Lett. Vol 378:111–114.

Kosaka, H., Sawai, Y., Sakaguchi, H., Kumura, E., Harada, N.,Watanabe, M., Shiga, T. (1994) ESR spectral transition by arteriovenous cycle in nitric oxide hemoglobin of cytokine-treated rats. Am. J. Physiol. Vol 266, pp C1400–C1405.

Kozlov, A. V., Bini, A., Iannone, A., Zini, I., Tomasi, A. (1996) Electron paramagnetic resonance characterization of rat neuronal nitric oxide production ex vivo. Methods Enzymol. Vol 268, pp 229–236.

Kubrina, L.N., Caldwell, W.S., Mordvintcev, P.I., Malenkova, I.V., Vanin, A.F. (1992) EPR evidence for nitric oxide production from guanidino nitrogens of L-arginine in animal tissues in vivo. Biochim Biophys Acta, Vol 1099, No 3, pp 233-7.

Kuppusamy, P., Chzhan, M., Vij, K., Shteynbuk, M., lefer, D.J., Giannella, E., Zweier, J.L. (1994) Three-dimensional spectral-spatial EPR imaging of free radicals in the heart: a technique for imaging tissue metabolism and oxygenation. Proc Natl Acad Sci U S A, Vol 91, No 8, pp 3388-92.

Kuppusamy, P., Shankar, R.A., Roubaud, V.M., Zweier, J.L. (2001) Whole body detection and imaging of nitric oxide generation in mice following cardiopulmonary arrest: detection of intrinsic nitrosoheme complexes.Magn Reson Med. Vol 45, No 4, pp 700-7.

Kuppusamy, P.,Wang, P., Samouilov, A., Zweier, J. L. (1996) Spatial mapping of nitric oxide generation in the ischemic heart using electron paramagnetic resonance imaging. Magn. Reson. Med.Vol 36, pp 212–218.

Labet, V., Grand, A., Morell, C., Cadet, J., Eriksson, L.A. (2009) Mechanism of nitric oxide induced deamination of cytosine. Phys. Chem. Chem. Phys., Vol. 11, pp 2379 – 2386.

Lai, C.S., Komarov, A.M.(1994) Spin trapping of nitric oxide produced in vivo in septic-shock mice. FEBS Lett, Vol 345, No 2-3, pp 120-4.

Lajoix, A. D., Badiou, S., Peraldi-Roux, S., Chardes, T., Dietz, S., Aknin, C.,Tribillac, F., Petit, P., Gross, R. (2006) Protein inhibitor of neuronal nitric oxide synthase (PIN) is a new regulator of glucose-induced insulin secretion. Diabetes Vol 55, pp 3279–3288;

Laszlo, F. and Whittle, B. J. (1997) Actions of isoform-selective and non-selective nitric oxide synthase inhibitors on endotoxin-induced vascular leakage in rat colon. Eur. J. Pharmacol. *334*, pp 99-102.

Li, L., Storey, P., Kim, D., Li, W., Prasad, P. (2003) Kidneys in hypertensive rats show reduced response to nitric oxide synthase inhibition as evaluated by BOLD MRI. J Magn Reson Imaging. Vol 17, No 6, pp 671-5.

Li, L.P., Ji, L., Santos, E.A., Dunkle, E., Pierchala, L., Prasad, P.(2009) Effect of nitric oxide synthase inhibition on intrarenal oxygenation as evaluated by blood oxygenation level-dependent magnetic resonance imaging. Invest Radiol. 2009 Vol.44, No 2, pp 67-73.

Lim, M. H.(2007) Preparation of a copper-based fluorescent probe for nitric oxide and its use in mammalian cultured cells. Nat. Protoc. Vol. 2, pp 408–415.

Lin, S., Fagan, K.A., Li, K.X., Shaul, P.W., Cooper, D.M.F., Rodman, D.M. (2000) Sustained endothelial nitric-oxide synthase activation requires capacitative Ca2+ entry. J Biol Chem, Vol 275, No 24, pp 17979-85.

Liu, G., Li, Y., Pagel, M.D. (2007) Design and characterization of a new irreversible responsive PARACEST MRI contrast agent that detects nitric oxide. Magn Reson Med. Vol 58, No 6, pp 1249-56.

Lopez-Figueroa, M.O., Caamano, C., Morano, M.I., Ronn, L.C., Akil, H., Watson, S.J. (2000) Direct evidence of nitric oxide presence within mitochondria. Biochem Biophys Res Commun, Vol 272, No 1, pp 129-33.Hanke, C.J., O'Brien, T., Pritchard, K.A., Campbell, W.B. (2000) Inhibition of adrenal cell aldosterone synthesis by endogenous nitric oxide release. Hypertension, Vol 35, No 1 Pt 2, pp 324-8.

López-Figueroa, M.O., Caamaño, C.A., Inés Morano, M.A., Stanley, H., Watson, J. (2002) Fluorescent imaging of mitochondrial nitric oxide in living cells. Methods in Enzymology, Vol 352, pp 296-303Maril, N., Margalit, R., Rosen, S., Heyman, H., Degani, H. (2006) Detection of evolving acute tubular necrosis with renal 23Na MRI: studies in rats. Kidney Int, Vol 69, No 4, pp 765-8.

Lopez-Figueroa, M.O., Day, H.W., Lee, S., Rivier, C., Akil, H., Watson, S.J. (2000) Temporal and anatomical distribution of nitric oxide synthase mRNA expression and nitric oxide production during central nervous system inflammation. Brain Res, Vol 852, No 1, pp 239-46.

Lundberg, J. O., Weitzberg, E. (2005) NO generation from nitrite and its role in vascular control. Arterioscler. Thromb. Vasc. Biol. Vol 25, pp 915–922.

Mader, K. (1998) Pharmaceutical applications of in vivo EPR. Phys. Med. Biol. Vol. 43, pp 1931–1935.

Madhunapantula, S. V., Desai, D., Sharma, A., Huh, S. J., Amin, S., Robertson, G. P.(2008) PBISe, a novel selenium-containing drug for the treatment of malignant melanoma. Mol. Cancer Ther. Vol 7, pp 1297–1308; 2008.

Massoud, T. F., Gambhir, S. S. (2003) Molecular imaging in living subjects: seeing fundamental biological processes in a new light. Genes Dev. Vol.17, pp 545–580.

Matsuo, T.(2000) Basal nitric oxide production is enhanced by hydraulic pressure in cultured human trabecular cells. Br J Ophthalmol, Vol 84, No 6, pp 631-5.

Matter, H., Kotsonis, P.(2004) Biology and chemistry of the inhibition of nitric oxide synthases by pteridine-derivatives as therapeutic agents. Med Res Rev Vol 24, pp 662-684.

McCarthy, T. J., Dence, C. S., Holmberg, S.W., Markham, J., Schuster, D. P.,Welch, M. J. (1996) Inhaled [13N]nitric oxide: a positron emission tomography (PET) study.Nucl. Med. Biol. Vol 23, pp 773–777.

Metukuri, M.R., Beer-Stolz, D., Namas, R.A., Dhupar, R., Torres, A., Loughran, P.A., et al.(2009) Expression and subcellular localization of BNIP3 in hypoxic hepatocytes and liver stress. Am J Physiol Gastrointest Liver Physiol. Vol 296, No 3, pp G499-509.

Moore, P.K., Handy, D.W. (1997) Selective inhibitors of neuronal nitric oxide synthase--is no NOS really good NOS for the nervous system? Trends Pharmacol Sci, Vol 18, No 6, pp 204-11.

Moriyama, Y., Moriyama, E. H., Blackmore, K., Akens,M. K., Lilge, L.(2005) In vivo study of the inflammatorymodulating effects of low-level laser therapy on iNOS expression using bioluminescence imaging. Photochem. Photobiol. Vol 81, pp 1351–1355.

Mulsch, A.,Lurie, D.J., Seimenis, I., Fichhtischerer, B., Foster, M.A. (1999) Detection of nitrosyl-iron complexes by proton-electron-double-resonance imaging. Free Radic Biol Med, Vol 27, No 5-6, pp 636-46.

Nagano, T., Yoshimura, T. (2002) Bioimaging of nitric oxide. Chem Rev. Vol 102, pp 1235-1269.

Nagata, S.(1997) Apoptosis by death factor. Cell, Vol 88, No 3, pp 355-65.

Narayanan, K., Spack, L., McMillan, K., Kilbourn, R.G. (1995)S.Alkyl-L-thiocitrullines. Potent stereoselective inhibitors of nitric oxide synthase with strong pressor activity in vivo. J. Biol. Chem. Vol.270, No.19, pp 11103-11110.

Nie F, Mai XL, Chen J, Gu N, Shi HJ, Cao AH, Ge YQ, Zhang Y, Teng GJ. [In vitro MR imaging of Fe2O3-arginine labeled heNOS gene modified endothelial progenitor cells]. Zhonghua Xin Xue Guan Bing Za Zhi. 2008 Aug;36(8):695-701.

Nishida, C., R., Ortiz de Montellano. (1999) Autoinhibition of endothelial nitric oxide synthase. J. Biol. Chem. Vol. 274, No. 21, pp 14692-14698]

Ny, L., Li, H., Mukherjee, S., Persson, K., Holmqvist, B., Zhao, D., Shtutin, V., Huang, H., Weiss, L.M., Machado, F.S., Factor, S.M., Chan, J., Tanowitz, H.B., Jelicks, L.A. (2008) A magnetic resonance imaging study of intestinal dilation in Trypanosoma cruzi-infected mice deficient in nitric oxide synthase. Am J Trop Med Hyg. Vol 79, No 5, pp 760-7.

Ockaili, R., Emani, V.R., Okubo, S., Brown, M., Krottapalli, K., Kukreja, R.C. (1999) Opening of mitochondrial K_{ATP} channel induces early and delayed cardioprotective effect: role of nitric oxide. Am J Physiol Heart Circ Physiol Vol 277, pp 2425-2434.

Ouyang, J., Hong, H., Shen, C., Zhao, Y., Ouyang, C., Dong, L., Zhu, J., Guo, Z., Zeng, K., Chen, J., Zhang, C., Zhang, J. (2008) A novel fluorescent probe for the detection of nitric oxide in vitro and in vivo. Free Radic. Biol. Med. Vol. 45, pp 1426–1436.

Palombo, F., Cremers, S.G., Weinberg, P.D., Kazarian, S.G. (2009) Application of Fourier transform infrared spectroscopic imaging to the study of effects of age and dietary L-arginine on aortic lesion composition in cholesterol-fed rabbits.J R Soc Interface. Vol 6, No 37, pp 669-680.

Panda, K., Chawla-Sarkar, M., Santos, C., Koeck, T., Erzurum, S. C., Parkinson, J. F., Pomper, M. G.,Musachio, J. L., Scheffel, U., Macdonald, J. E., McCarthy, D. J., Reif, D. W., Villemagne, V. L., Yokoi, F., Dannals, R. F., Wong, D. F. (2000) Radiolabeled neuronal nitric oxide synthase inhibitors: synthesis, in vivo evaluation, and primate PET studies. J. Nucl. Med. Vol 41, pp 1417–1425.

Pechkovsky, D.V., Zissel, G., Stamme, C., Goldmann, T., Ari Jaffe, H., Einhaus, M., Taube, C., Magnussen, H., Schlaak, M., MullerQuernheim, J. (2002) Human alveolar epithelial cells induce nitric oxide synthase-2 expression in alveolar macrophages. Wur Respir J. Vol 16, pp 672-683.

Pedroso, M.C., Magalhaes, J.R., Durzan, D. (2000a) A nitric oxide burst precedes apoptosis in angiosperm and gymnosperm callus cells and foliar tissues. J Exp Bot, Vol 51, No 347, pp 1027-36.

Pedroso, M.C., Magalhaes, J.R., Durzan, D. (2000b) Nitric oxide induces cell death in Taxus cells. Plant Sci, Vol 157, No 2, pp 173-180.

Perrier, E., Fournet-Bourguignon, M.P., Royere, E., Molez, S., Reure, H., Lesage, L., Gosgnach W., Frapart, Y., Boucher, J.L., Villeneuve, N., Vilaine, J.P. (2009) Effect of uncoupling endothelial nitric oxide synthase on calcium homeostasis in aged porcine endothelial cells. Cardiovasc Res. Vol 82, No 1, pp 133-42.

Piknova, B.; Gladwin, M. T.; Schechter, A. N.; Hogg, N.(2005) Electron paramagnetic resonance analysis of nitrosylhemoglobin in humans during NO inhalation.J. Biol. Chem. Vol 280, pp 40583–40588.

Pilon G, Dallaire P, Marette A. Inhibition of Inducible Nitric-oxide Synthase by Activators of AMP-activated Protein Kinase: A New mechanism of action of insulin of insulin-sensitizing drugs. J. Biol. Chem. 2004 279: 20767-20774.

Pittner, J., Liu, R., Brown, R., Wolgast, M., Persson, A.E.G. (2003) Visualization of nitric oxide production and intracellular calcium in juxtamedullary afferent arteriolar endothelial cells. Acta Physiol Scand, Vol 179, No 3, pp 309-17.

Quaresima, V., Takehara, H., Tsushima, K., Ferrari, M., Utsumi, H. (1996) In vivo detection of mouse liver nitric oxide generation by spin trapping electron paramagnetic resonance spectroscopy. Biochem. Biophys. Res. Commun. Vol. 221, pp 729–734.

Raman, C. S., Li, H., Martasek, P., Kral, V., Masters, B. S. and Poulos, T. L. (1998) Crystal structure of constitutive endothelial nitric oxide synthase : a paradigm for pterin function involving a novel metal center. Cell (Cambridge, Mass.) *95*, pp 939-950.

Rast, S., Borel, A., Helm, L., Belorizky, E., Fries, P.H. et al.(2001) EPR spectroscopy of MRI-related Gd(III) complexes: simultaneous analysis of multiple frequency and temperature spectra, including static and transient crystal field effects. J Am Chem Soc, Vol 123, No 11, pp 2637-44.

Ratovitski, E.A., Alam, M.R., Quick, R.A., McMillan, A., Bao, C.,Kozlovsky, C.,Hand,T.A., Johnson, R.C., Mains, R.E., Eippers, B.A.(1999) Kalirin inhibition of inducible nitric oxide synthase. J.Biol. Chem. Vol. 274, No. 2, Issue of January 8, pp. 993–999.

Rees, D. D., Monkhouse, J. E., Cambridge, D. and Moncada, S. (1998) Nitric oxide and the haemodynamic pro®le of endotoxin shock in the conscious mouse. Br. J. Pharmacol. *124*, pp 540-546.

Regehr, W.G., Connor, J.A., Tank, D.W. (1989) Optical imaging of calcium accumulation in hippocampal pyramidal cells during synaptic activation. Nature, Vol 341, No 6242, pp 533-6.

Reif, A., Jacob, C.P., Rujescu, D., Herterich, S., Lang, S., Gutknecht, L., Baehne, C.G., Strobel, A., Freitag, C.M., Giegling, I., Romanos, M., Hartmann, A., Rösler, M., Renner, T.J., Fallgatter, A.J., Retz, W., Ehlis, A.C., Lesch, K.P. (2009) Influence of functional variant of neuronal nitric oxide synthase on impulsive behaviors in humans. Arch Gen Psychiatry. Vol.66, No 1, pp 41-50.

Richards, D.A., T.V. Bliss, and C.D. Richards, Differential modulation of NMDA-induced calcium transients by arachidonic acid and nitric oxide in cultured hippocampal neurons. Eur J Neurosci, 2003; 17(11): 2323-8.

Robinson, J. K.; Bollinger, M. J.; Birks, J. W. (1999) Luminol/H_2O_2 chemiluminescence detector for the analysis of nitric oxide in exhaled breath. Anal. Chem. Vol 71, pp 5131–5136.

Salerno, L., Sorrenti, V., Giacomo, C., Romeo, G., Siracusa, M.A. (2002) Progress in the development of selective nitric oxide synthase (NOS) inhibitors. Curr Pharm Des, Vol 8, No 3, pp177-200.

Samouilov, A., Woldman, Y.Y., Zweier, J.L., Khramtsov, V.V. (2007) Magnetic resonance study of the transmembrane nitrite diffusion.Nitric Oxide. Vol 16, No 3, pp 362-70.

Sari-Sarraf, F., Pomposiello, S., Laurent, D. (2008) Acute impairment of rat renal function by L -NAME as measured using dynamic MRI. MAGMA. Vol 21, No 4, pp 291-7.

Schuppe, H., Cutte, M., Chad, J.E., Newland, P.L. (2002) 4,5-diaminofluoroscein imaging of nitric oxide synthesis in crayfish terminal ganglia. J Neurobiol, Vol 53, No 3, pp 361-9.

Sennequier, N., Wolan, D. and Stuehr, D. J. (1999) Antifungal imidazoles block assembly of inducible NO synthase into an active dimer. J. Biol. Chem. Vol *274*, pp 930-938.

Sergeant, G.P., Craven, M., Hollywood, M.A., McHale, N.G., Thornbury, K.D.(2009) Spontaneous Ca^{2+} waves in rabbit corpus cavernosum: modulation by nitric oxide and cGMP.J Sex Med. Vol 6, No 4, pp 958-66.

Sirmatel O, Sert C, Tümer C, Oztürk A, Bilgin M, Ziylan Z. Change of nitric oxide concentration in men exposed to a 1.5 T constant magnetic field. Bioelectromagnetics. 2007;28(2):152-4.

Southan, G.J., Szabo,C.(1996) Selective pharmacological inhibition of distinct nitric oxide synthase isoforms. Biochem Pharmacol, Vol 51, No 4, pp 383-94.

St Croix, C. M.; Bauer, E. M. Use of spectral fluorescence resonance energy transfer to detect nitric oxide-based signaling events in isolated perfused lung. Curr. Protoc. Cytom. Chap. 12 (Unit12):13; 2008.

Stuehr, D. J. (2005) Visualizing inducible nitric-oxide synthase in living cells with a hemebinding fluorescent inhibitor. Proc. Natl. Acad. Sci. USA 102:10117–10122; 2005.

Suzuki, N., Kojima, H., Urano, Y., Kikuchi, K., Hirata, Y., Nagano, T. (2002) Orthogonality of calcium concentration and ability of 4,5-diaminofluorescein to detect NO. J Biol Chem, Vol 277, No 1, pp 47-49.

Swartz, H. M., Khan, N., Khramtsov, V. V. (2007) Use of electron paramagnetic resonance spectroscopy to evaluate the redox state in vivo. Antioxid. Redox Signal. Vol. 9, pp 1757–1771.

Taha, Z. H. (2003) Nitric oxide measurements in biological samples. Talanta Vol. 61, pp 3–10.

Terashima M, Ehara S, Yang E, Kosuge H, Tsao PS, Quertermous T, Contag CH, McConnell MV. In Vivo bioluminescence imaging of inducible nitric oxide synthase gene expression in vascular inflammation. Mol Imaging Biol. 2010 Nov 6.

Thatte, H.S., He, X.D., Goyal, R.K. (2009) Imaging of nitric oxide in nitrergic neuromuscular neurotransmission in the gut.PLoS ONE. Vol 4, No 4, pp 4990.

Townsend, D. W., Beyer, T. (2002) A combined PET/CT scanner: the path to true image fusion. Br. J. Radiol. Vol 75 Spec. No., pp S24–S30.

Tsuchiya, K., Yoshizumi, M., Houchi, H., Mason, R. P. (2000) Nitric oxide-forming reaction between the iron-N-methyl-D-glucamine dithiocarbamate complex and nitrite. J. Biol. Chem. Vol. 275, pp 1551–1556.

Ueno, T., Suzuki, Y., Fujii, S., Vanin, A.F., Yoshimara, T. (2002) In vivo nitric oxide transfer of a physiological NO carrier, dinitrosyl dithiolato iron complex, to target complex. Biochemical Pharmacol.Vol 63, No 485-493.

Vandsburger, M.H., French, B.A., Helm, P.A., Roy, R.J., Kramer, C.M., Young, A.A., Epstein, F.H. (2007) Multi-parameter in vivo cardiac magnetic resonance imaging demonstrates normal perfusion reserve despite severely attenuated beta-adrenergic functional response in neuronal nitric oxide synthase knockout mice. Eur Heart J. Vol 28, No 22, pp 2792-8.

Vanin, A. F., Bevers, L. M., Mikoyan, V. D., Poltorakov, A. P., Kubrina, L. N., van Faassen, E. (2007) Reduction enhances yields of nitric oxide trapping by irondiethyldithiocarbamate complex in biological systems. Nitric Oxide Vol. 16, pp 71–81.

Vila Petroff M.G., Kim, S.H., Pepe, S., Dessy, C., Marban, E., Balligand, J.L., Sollott, S.J.(2001) Endogenous nitric oxide mechanisms mediate the stretch dependence of Ca++ release in cardiomyocytes. Nature Cell Biol. Vol 3, pp 867-873..

Vodovotz, Y., Lucia, M.S., Flanders, K.C., Chesler, L., Xie, Q.Q., Smith,W.W.,Weidner, J., Mumford, R.,Webber, R.,Nathan, C., Roberts, A.B., Lippa, C.F., Sporn, M.B. (1996) Inducible nitric oxide synthase in tangle-bearing neurons of patients with Alzheimer's disease. J Exp Med Vol 184, pp 1425–1433.

von Bohlen, U., Halbach, O.(2003) Nitric oxide imaging in living neuronal tissues using fluorescent probes. Nitric Oxide, Vol 9, No 4, pp 217-28.

von Bohlen, U., Halbach, O., Albrecht, D., Heinemann, U., Schuchmann, S. (2002) Spatial nitric oxide imaging using 1,2-diaminoanthraquinone to investigate the involvement of nitric oxide in long-term potentiation in rat brain slices. Neuroimage, Vol 15, No 3, pp 633-9.

Waller, C., Hiller, K.H., Rüdiger, T., Kraus, G., Konietzko, C., Hardt, N., Ertl, G., Bauer, W.R. (2005) Noninvasive imaging of angiogenesis inhibition following nitric oxide synthase blockade in the ischemic rat heart in vivo. Microcirculation. Vol 12, No 4, pp 339-47.

Wingrove, J.A., O'Farrell, P.H. (1999) Nitric oxide contributes to behavioral, cellular, and developmental responses to low oxygen in Drosophila. Cell, Vol 98, No 1, pp 105-14.

Xu, Y. C., Cao, Y. L., Guo, P., Tao, Y., Zhao, B. L. (2004) Detection of nitric oxide in plants by electron spin resonance. Phytopathology. Vol. 94, pp 402–407.

Yermolaieva, O., Brot, N., Weissbach, H., Heinemann, H. T. (2000) Reactive oxygen species and nitric oxide mediate plasticity of neuronal calcium signaling. Proc Natl Acad Sci U S A, Vol 97, No 1, pp 448-53.

Yokoyama, H., Fujii, S., Yoshimura, T., Ohya-Nishiguchi, H., Kamada, H. (1997) In vivo ESR-CT imaging of the liver in mice receiving subcutaneous injection of nitric oxide-bound iron complex. Magn. Reson. Imaging Vol 15, pp 249–253.

Yoshimura, T., Yokoyama, H., Fujii, S., Takayama, F. (1996) In vivo EPR detection and imaging of endogenous nitric oxide in lipopolysaccharide-treated mice. Nat Biotechnol, Vol 14, No 8, pp 992-4.

Young, R. J., Beams, R. M., Carter, K., Clark, H. A., Coe, D. M., Chambers, C. L., Davies, P. I., Dawson, J., Drysdale, M. J., Franzman, K. W. et al. (2000) Inhibition of inducible nitric oxide synthase by acetamidine derivatives of hetero-substituted lysine and homolysine. Bioorg. Med. Chem. Lett. Vol 10, pp 597-600.

Zhang, J., Xu, M., Dence, C. S., Sherman, E. L., McCarthy, T. J., Welch, M. J.(1997) Synthesis, in vivo evaluation and PET study of a carbon-11-labeled neuronal nitric oxide synthase (nNOS) inhibitor S-methyl-L-thiocitrulline. J. Nucl. Med. Vol 38, pp 1273–1278.

Zharikov, S.I., Sigova, A.A., Chen, S., Bubb, M.R., Block, E.R. (2001) Cytoskeletal regulation of the L-arginine/NO pathway in pulmonary artery endothelial cells. Am J Physiol Lung Cell Mol Physiol, Vol 280, No 3, pp 465-73.

Zhou, D., Lee, H., Rothfuss, J.M., Chen, D.L., Ponde, D.E., Welch, M.J., Mach, R.H. (2009) Design and synthesis of 2-amino-4-methylpyridine analogues as inhibitors for inducible nitric oxide synthase and in vivo evaluation of [^{18}F]6-(2-fluoropropyl)-4-methyl-pyridin-2-amine as a potential PET tracer for inducible nitric oxide synthase.J Med Chem. Vol 52, No 8, pp 2443-53.

Ziaja, M., Pyka, J., Machowska, A., Maslanka, A., Plonka, P. M. (2007) Nitric oxide spin-trapping and NADPH-diaphorase activity in mature rat brain after injury.J. Neurotrauma Vol. 24, pp 1845–1854.

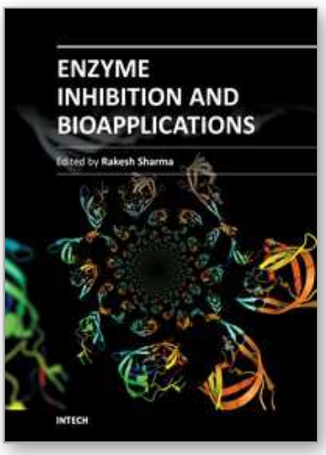

Enzyme Inhibition and Bioapplications

Edited by Prof. Rakesh Sharma

ISBN 978-953-51-0585-5
Hard cover, 314 pages
Publisher InTech
Published online 09, May, 2012
Published in print edition May, 2012

Enzyme Inhibition and Bioapplications is a concise book on applied methods of enzymes used in drug testing. The present volume will serve the purpose of applied drug evaluation methods in research projects, as well as relatively experienced enzyme scientists who might wish to develop their experiments further. Chapters are arranged in the order of basic concepts of enzyme inhibition and physiological basis of cytochromes followed by new concepts of applied drug therapy; reliability analysis; and new enzyme applications from mechanistic point of view.

How to reference

In order to correctly reference this scholarly work, feel free to copy and paste the following:

Rakesh Sharma (2012). Inhibition of Nitric Oxide Synthase Gene Expression: In vivo Imaging Approaches of Nitric Oxide with Multimodal Imaging, Enzyme Inhibition and Bioapplications, Prof. Rakesh Sharma (Ed.), ISBN: 978-953-51-0585-5, InTech, Available from: http://www.intechopen.com/books/enzyme-inhibition-and-bioapplications/inhibition-of-nitric-oxide-synthase-gene-expression-in-vivo-imaging-approaches-of-nitric-oxide-with-

INTECH
open science | open minds

InTech Europe
University Campus STeP Ri
Slavka Krautzeka 83/A
51000 Rijeka, Croatia
Phone: +385 (51) 770 447
Fax: +385 (51) 686 166
www.intechopen.com

InTech China
Unit 405, Office Block, Hotel Equatorial Shanghai
No.65, Yan An Road (West), Shanghai, 200040, China
中国上海市延安西路65号上海国际贵都大饭店办公楼405单元
Phone: +86-21-62489820
Fax: +86-21-62489821

IntechOpen